Wave chaos in acoustics and elasticity

2007 J. Phys. A: Math. Theor. 40 R443

(http://iopscience.iop.org/1751-8121/40/50/R01)

J. Phys. A: Math. Theor. **40** (2007) R443–R509 doi:10.1088/1751-8113/40/50/R01

TOPICAL REVIEW

Wave chaos in acoustics and elasticity

Gregor Tanner[1] **and Niels Søndergaard**[2]

[1] School of Mathematics, University of Nottingham, University Park, UK
[2] Division of Mathematical Physics, LTH, Sweden

E-mail: niels.sondergaard@matfys.lth.se

Received , in final form 8 October 2007
Published 28 November 2007
Online at stacks.iop.org/JPhysA/40/R443

Abstract

Interpreting wave phenomena in terms of an underlying ray dynamics adds a new dimension to the analysis of linear wave equations. Forming explicit connections between spectra and wavefunctions on the one hand and the properties of a related ray dynamics on the other hand is a comparatively new research area, especially in elasticity and acoustics. The theory has indeed been developed primarily in a quantum context; it is increasingly becoming clear, however, that important applications lie in the field of mechanical vibrations and acoustics. We provide an overview over basic concepts in this emerging field of *wave chaos*. This ranges from ray approximations of the Green function to periodic orbit trace formulae and random matrix theory and summarizes the state of the art in applying these ideas in acoustics—both experimentally and from a theoretical/numerical point of view.

PACS numbers: 05.45.Mt, 02.10.Yn, 42.25.−p, 43.20.+g, 43.30.+m, 46.05.+b

(Some figures in this article are in colour only in the electronic version)

Contents

1. Introduction

1.1. General remarks

We will in this review focus on the solutions of linear wave equations describing acoustic or vibrational phenomena; we will relate these solutions to an underlying ray dynamics generated by, in general, nonlinear ordinary differential equations or maps. We approach the field from two main directions: we first consider explicit connections between ray and wave dynamics on the level of individual system. In a second approach, universal behaviour of wave solutions are considered from a statistical point of view. We will in the following work in the continuum approximation disregarding the underlying discreteness of materials in terms of atoms and molecules. We will thus *not* consider the quantum limit of elasticity, that is, the existence of quantized lattice vibrations or phonons.

The theory describing linear wave equations in the form of ray solutions is well established using Eikonal or WKB techniques, and the limitations of such approximations are understood in principle. In the last few decades, the interest shifted towards relating the solutions of linear wave equations to the *dynamical properties* of the underlying ray dynamics. It could be shown that dynamical features ranging from regular to purely chaotic behaviour leave distinct fingerprints in the solutions of associated wave equations. The theory has mainly advanced in a quantum context giving rise to the name *quantum chaos*. Schrödinger's equation is a scalar, linear wave equation and is in that respect not very different from other physically relevant wave equations such as in optics or linear elasticity. The 'weirder' properties of quantum mechanics, as for example, the measurement process or the violation of Bell's inequalities are in fact not considered in semiclassical approaches to quantum mechanics. In that sense, techniques and insights from quantum chaos can and have been applied to classical wave equations such as in optics, elastodynamics or acoustics giving rise to a much broader field often referred to as *wave chaos*. In fact, many of the methods and concepts used and developed in quantum chaos have been considered independently in the optics and engineering community, and developments have run in parallel often with little cross fertilization.

The main goal of this review is to bring the different approaches and communities together and to discuss progress in the theory of elasticity and acoustics where it has a distinct wave chaos component. To keep the review at a manageable length, we will not consider developments in optics such as the studies on flat microwave cavities reviewed by, for example, Stöckmann (1999) and Kuhl *et al* (2005) or wave chaos applications to micro cavity lasers by Nöckel and Stone (1997). Likewise, we shall only briefly discuss diffraction in section 4.1 which may lead to randomness and disorder and thus wave chaos effects (Efetov 1997). Indeed, we will in general consider wave scattering on obstacles large compared

to typical wavelengths; 'randomness' is thus introduced through the chaoticity of the ray dynamics alone and is independent of the wavelength in contrast to diffractive wave-scattering effects.

The name quantum or wave chaos has led to a considerable amount of confusion, prompting Michael Berry to promote the name *quantum chaology* instead (Berry 1987, 1989). It is thus important to stress that

(a) we do only consider properties of linear wave equations; we are not concerned with nonlinear wave effects becoming important when going beyond the linear approximations in acoustics and elasticity theory as considered by Lauterborn and Cramer (1981), Lauterborn and Holzfuss (1991), Hamilton and Bladstock (1998) and Dong *et al* (2001);
(b) we are not primarily interested in possible chaotic behaviour of the solutions of the linear wave equations which can only exist as a transient effect due to the linearity of the underlying partial differential equation (PDE), and
(c) we do not study the 'classical' limit, that is, the transition from a wave dynamics to a deterministic ray dynamics; this limit lies in fact outside a semiclassical approach considering $k \to \infty$ with k being a typical wave number in the system.

We will instead adopt the now generally accepted definition of wave or quantum chaos: *we consider the wave properties of systems described by linear wave equations which have an associated ray or classical dynamics being chaotic*.

The research field can roughly be divided into two areas: firstly, one can express wave operators such as Green functions in terms of the ray dynamics using semiclassical or large wave number asymptotics which will be considered in section 2. Secondly, there is a connection between statistical properties of spectra and eigenfunctions (or modes) of wave systems on the one hand and random matrix theory (RMT) on the other hand. Here, the random matrix ensembles in question depend on properties of the underlying ray dynamics and symmetries of the problem and will be reviewed in section 3. From a quantum chaos perspective, both these areas have been covered in a series of textbooks (Gutzwiller 1990, Brack and Bhaduri 1997, Stöckmann 1999, Haake 2001, Cvitanović *et al* 2006) and review articles (Guhr *et al* 1998, Tanner *et al* 2000, Kuhl *et al* 2005) and will thus only be considered in as far as links between wave chaos and elasticity exist. We would like to also mention the article collections edited by Sebbah (2001) and Fink *et al* (2002) which may serve as an ideal starting point for a more in-depth introduction into this research area from an acoustics point of view.

Our emphasis will be on a ray analysis of wave phenomena in the presence of multiple scattering events and ray chaos. A ray description is common in elasticity especially when considering scattering of elastic waves at interface boundaries. The interpretation of seismographs in terms of wave pulses moving on curved rays in the earth, for example, is one of the basic applications of ray methods. Especially, the ray conversion between longitudinal and transversal wave components and the excitation of surface waves giving rise to earthquakes such as Rayleigh waves on solid–air interfaces or Lamb waves at the sea bottom have been studied in great detail (Brechovskich 1980). Processes entailing only a few scattering events such as reflection on multi-layered surfaces (Brechovskich 1980) or scattering of obstacles such as cracks (Achenbach *et al* 1982) are often studied in a WKB-type approach along rays obeying Fermat's principle of shortest travel time. Effects related to the boundary conditions such as surface waves or diffraction can be treated by considering ray dynamics in the complex plane (Keller and Karal 1960, 1964, Rulf 1969). These studies are important in the geophysical domain as well as for non-destructive evaluation using ultrasound to investigate materials for cracks and defects.

In the examples above, wave signals are often treated in terms of only a few ray paths where interference effects play no or only a minor role. This changes drastically when extending a ray analysis to long-time wave dynamics including multiple scattering; examples are wave propagation in reverberant bodies of finite size undergoing multiple reflections on the boundary or open systems containing many, disordered scatterers. The number of ray paths reaching a point $\mathbf{r}$ from a source point $\mathbf{r}_0$ will then grow quickly with the travel time due to scattering off boundaries. Not including mode conversion, the proliferation of possible paths with time is a power law for systems associated with an integrable ray dynamics. For chaotic behaviour, the effect is even more drastic leading to an exponential increase of ray trajectories connecting $\mathbf{r}_0$ and $\mathbf{r}$ in time t (Gutzwiller 1990). The possibility of mode conversion at boundaries gives additional contributions as discussed in sections 2.2.3 and 2.3.

Waves travelling along different paths will interfere leading to complicated wave patterns. A ray analysis may thus indeed seem hopeless here. We will demonstrate that this is not necessarily the case and review quantum chaos techniques and their modifications to an elastodynamics setting in section 2.1. The vectorial nature of the wave equations and the phenomenon of wave splitting due to mode-dependent wave speeds leads to a multi-component classical ray dynamics. This gives rise to new dynamical features not possible in ordinary Hamiltonian dynamics as discussed in section 2.2. Applications of ray chaos effects in wave-splitting billiards, section 2.3, time-reversal imaging (TRI), section 2.4, and its connection to fidelity decay, section 2.5, as well as underwater acoustics in section 2.6 will be reviewed.

Statistical considerations will be treated in section 3. Some of the aspects of RMT and wave chaos have been reviewed recently by Kuhl *et al* (2005) in the context of chaotic wave scattering. A partly complementary overview will be given in section 3.1; it includes a short overview on RMT as well as key results from experiments on elastic bodies. We will point out how wavefunction statistics and cross-correlation functions are related to the Green function in section 3.1.4 and discuss weak localization effects in section 3.1.5. In practical applications, absorption and other dissipative channels always play a large role in acoustic problems; a realistic treatment thus needs to take into account losses of wave energy, that is, the openness of the wave problem. In section 3.2 we focus on a statistical approach towards transport of wave energy in dissipative wave systems leading to an RMT treatment of correlation functions and higher moments of the Green function. We conclude this section by discussing the relation between wave chaos and a method widely used in engineering applications for estimating the flow of vibrational energy in large structures, *statistical energy analysis* (SEA) in section 3.3.

We close the review by giving an outlook on possible further applications of wave chaos methods in elasticity. We highlight some of the areas where there are still plenty of unresolved problems; these are in particular diffraction effects, the influence of curved surfaces, or the impact on the wave dynamics due to anisotropy of the material. These topics are discussed in section 4.

1.2. Basic wave equations

We start by introducing the linear wave equations discussed in more detail in this review. We will restrict ourselves to wave propagation in solids, fluids and gases in the continuum approximations and for small deformations. Similar wave equations appear frequently in the context of electromagnetism or quantum mechanics, however, often in a different setting; we will thus focus on applications to acoustics and elasticity throughout.

Linear elastodynamics has applications ranging from acoustic and structural engineering to seismology. Typical time scales are much larger than in the optical or quantum regime with sound speeds and frequencies allowing for time-resolved measurements of wave signals. We

will in the following assume that the wave equations are not explicitly time dependent due to, for example, time-dependent variations in material densities, and we work in the frequency domain if not stated otherwise.

Wave equations in continuum mechanics are only linearized approximations and the applicability of the equations are limited by nonlinear terms and dissipation. Including these nonlinearities can lead to chaotic effects due to nonlinear interactions between acoustic waves, also referred to as 'Acoustic Chaos' in the literature (Lauterborn and Cramer 1981), Lauterborn and Holzfuss (1991), Hamilton and Bladstock (1998) and Dong *et al* (2001). These effects are beyond the scope of this review and are negligible in many applications. 'Wave Chaos', as we understand it here, refers solely to linear wave problems where chaos is introduced through the underlying ray dynamics.

1.2.1. The Helmholtz equation. One of the most important wave equations in the context of continuum mechanics is the scalar Helmholtz equation describing, for example, acoustic pressure waves in fluids and gases, vibrations of thin membranes, shallow water waves, electromagnetic waves in thin cavities and a free quantum particle in a finite domain, a so-called quantum billiard.

The Helmholtz equation can be derived from a linearization of the Navier–Stokes equation in the adiabatic approximation and has the form (for constant density ρ)

$$c^2 \Delta \Phi(\mathbf{r}) + \omega^2 \Phi(\mathbf{r}) = 0. \tag{1}$$

Here, Φ is a scalar function such as the variation in pressure P (in dimensionless units) and $c^2 = (\partial P/\partial \rho)_S$ denotes the wave velocity (where the derivatives are taken in the adiabatic limit at constant entropy S). The latter is, for example, $c = \sqrt{T/\rho}$ for vibrating membranes with T, the tension applied at the boundary. In the more general case of inhomogeneous fluids (Brechovskich 1980), the equation for the pressure variation P becomes

$$\nabla \cdot \left(\frac{1}{\rho(r)} \nabla P \right) + \kappa(r) \omega^2 P = 0, \tag{2}$$

where $\kappa(r)$ is the adiabatic compressibility. The general form, equation (1), is recovered when switching to $\psi = P/\sqrt{\rho}$ with a new effective wave number ω/c depending on position $\mathbf{r}$.

In acoustics, damping caused by viscous or non-adiabatic effects plays an important role where the latter are due to the finite thermo-conductivity of the medium. In addition losses at interfaces and boundaries can be quite substantial; typical boundary conditions are Dirichlet, Neumann or Robin boundary conditions. More complicated conditions may apply if energy transfer at interfaces such as at fluid/solid boundaries becomes important as discussed by Temkin (1981) and Kinsler *et al* (1999).

Going from a wave to a ray pictures, one writes the wavefunction in the form

$$\Phi(\mathbf{r}) = A(\mathbf{r})\, \mathrm{e}^{\mathrm{i}S(\mathbf{r})};$$

After inserting Φ into (1) and neglecting terms of the form $\Delta A/A \ll (\omega/c)^2$, this leads to the Eikonal equation for the phase S, that is,

$$c^2(\mathbf{r})(\nabla S)^2 = \omega^2. \tag{3}$$

The PDE (3) is a Hamilton–Jacobi equation which can be solved by the method of characteristics. After defining the wave number $\mathbf{k} \equiv \nabla S$ (referred to as *momentum* $\mathbf{p}$ in the context of classical mechanics) and the Hamilton function

$$H(\mathbf{k}, \mathbf{r}) = c^2(\mathbf{r})\mathbf{k}^2 = \omega^2, \tag{4}$$

one obtains the ray trajectories $(\mathbf{r}(\tau)), \mathbf{k}(\tau))$ from Hamilton's equations

$$\frac{\mathrm{d}}{\mathrm{d}\tau}\mathbf{r} = \nabla_k H = 2c^2\mathbf{k}; \qquad \frac{\mathrm{d}}{\mathrm{d}\tau}\mathbf{k} = -\nabla_r H = -2c\mathbf{k}^2\nabla c. \tag{5}$$

Here, τ is a fictitious time conjugate to the energy $E = \omega^2$ which is related to the real time by $t = 2\omega\tau$. This translates into the more common equations of motion

$$\dot{\mathbf{r}} = c\hat{\mathbf{k}}; \qquad \dot{\mathbf{k}} = -\frac{\omega}{c}\nabla c. \tag{6}$$

The dimensionless *action* S is given as

$$S(\mathbf{r}, \mathbf{r}_0) = \int \mathrm{d}\mathbf{r}' \cdot \mathbf{k}(\mathbf{r}'), \tag{7}$$

where the integration is taken along a ray from $\mathbf{r}_0$ to $\mathbf{r}$. An $\mathbf{r}$ dependence of the 'mass' term $m = 1/2c^2$ gives rise to bending of ray trajectories. The ray equations (5) may also be obtained by a principle of least action, referred to as Fermat's principle in optics. This principle leads to an effect often observed for example in seismology; the apparent wave velocity, that is, the ratio of the distance L between source and receiver point and the pulse travel time, increases with L. Following Fermat's principle in inhomogeneous media, it is easier to find an optimal path avoiding regions with high density and slow local velocities for longer ray trajectories than for short rays. The theory including scaling laws and the onset of saturation has been worked out in (Tworzydlo and Beenakker 2000) using methods from structure optimizations for polymers.

1.2.2. The biharmonic equation. The flexural motion of a plate of constant thickness and without curvature is well described by the biharmonic wave equation (Landau and Lifshitz 1959)

$$\frac{D}{\rho h}\Delta^2\Phi - \omega^2\Phi = 0, \tag{8}$$

where the scalar 'wavefunction' $\Phi(x, y)$ now corresponds to the displacement amplitude normal to the plate. The *flexural rigidity* D is given as

$$D = \frac{Eh^3}{12(1-\sigma^2)} \tag{9}$$

with material constants referring to Young's modulus of extension, E, and the Poisson ratio, σ; h is the thickness of the plate. The biharmonic equation can be derived from the basic equations of elastodynamics, see (14) below, by assuming a vanishing component of the stress tensor normal to the plate; this approximation is called the Kirchhoff–Love model (Love 1944, Achenbach *et al* 1982). If the assumption of no curvature is relaxed one arrives at the more general shell theories discussed in section 4.2.

Common boundary conditions are *clamped*

$$\Phi = 0, \qquad \partial\Phi/\partial n = 0, \tag{10}$$

simply supported

$$\Phi = 0, \qquad \frac{\partial^2\Phi}{\partial n^2} + \sigma\frac{d\theta}{dt}\frac{\partial\Phi}{\partial n} = 0, \tag{11}$$

or *free* boundary conditions

$$\begin{aligned} &-\frac{\partial\Delta\Phi}{\partial n} + (1-\sigma)\frac{\partial}{\partial t}\left[\cos\theta\sin\theta\left(\frac{\partial^2\Phi}{\partial x^2} - \frac{\partial^2\Phi}{\partial y^2}\right) + (\sin^2\theta - \cos^2\theta)\frac{\partial^2\Phi}{\partial x\partial y}\right] = 0 \\ &\Delta\Phi + (1-\sigma)\left(2\sin\theta\cos\theta\frac{\partial^2\Phi}{\partial x\partial y} - \sin^2\theta\frac{\partial^2\Phi}{\partial x^2} - \cos^2\theta\frac{\partial^2\Phi}{\partial y^2}\right) = 0, \end{aligned} \tag{12}$$

where n and t refer to the normal and tangential direction at the boundary in the plane of the plate and $\theta = \angle(\mathbf{r}, \mathbf{n})$ (Landau and Lifshitz 1959). Note that plates also support wave modes related to deformations in the plane of the plate. These in-plane deformations are discussed in the following paragraph and, in the context of shell theory, in section 4.2.

The wave equation (8) factorizes in the form

$$(\Delta - k^2)(\Delta + k^2)\Phi = 0 \qquad \text{with} \qquad k^4 = \frac{\rho h}{D}\omega^2 \tag{13}$$

giving rise to strong dispersion and propagating and decaying solutions. The latter exist near boundaries, whereas the former obey the Helmholtz equation with conventional ray dynamics. The boundary conditions lead to mixing between propagating and decaying modes resulting in non-trivial phase shifts for the propagating wave field far from the boundaries, see section 2.2.2.

1.2.3. Wave equation for isotropic elastic bodies. The propagation of elastic deformations in a three dimensional, isotropic body written in terms of the forces acting on volume elements has the form

$$\nabla \cdot \boldsymbol{\sigma}(\mathbf{u}) = \rho \frac{\partial^2}{\partial t^2}\mathbf{u}. \tag{14}$$

Here $\mathbf{u}(\mathbf{r})$ describes the displacement from the equilibrium position $\mathbf{r}$ and

$$\sigma_{ij} = \lambda \partial_k u_k \delta_{ij} + \mu(\partial_i u_j + \partial_j u_i) \tag{15}$$

is the isotropic stress tensor representing the force F_i acting on the surface dA_j where, the summation convention is used. The wave equation (14) can be written in terms of the Navier–Cauchy equation which in the frequency domain has the form

$$\mu \Delta \mathbf{u} + (\lambda + \mu)\nabla(\nabla \cdot \mathbf{u}) + \rho\omega^2 \mathbf{u} = 0, \tag{16}$$

with material constants λ, μ, the so-called Lamé coefficients; see Landau and Lifshitz (1959), Bedford and Drumheller (1994) as well as a review by Weaver (2001) for an introduction.

Introducing elastic potentials Φ and Ψ by using standard Helmholtz decomposition of the displacement field $\mathbf{u}$, that is,

$$\mathbf{u} = \mathbf{u}_p + \mathbf{u}_s \qquad \text{with} \qquad \mathbf{u}_p = \nabla\Phi, \qquad \mathbf{u}_s = \nabla \times \Psi, \tag{17}$$

the Navier–Cauchy equation reduces to two Helmholtz equations, that is,

$$\left(\Delta + k_p^2\right)\Phi = 0; \qquad \left(\Delta + k_s^2\right)\Psi = 0 \qquad \text{with} \qquad k_{p,s} = \omega/c_{p,s}, \tag{18}$$

where $k_{p,s}$ stands for the wave numbers for pressure (longitudinal) and shear (transversal) wave components, respectively. The wave velocities are different for the two different polarizations, that is,

$$c_p = \sqrt{\frac{\lambda + 2\mu}{\rho}} = \sqrt{\frac{E(1-\sigma)}{\rho(1+\sigma)(1-2\sigma)}}; \qquad c_s = \sqrt{\frac{\mu}{\rho}} = \sqrt{\frac{E}{2\rho(1+\sigma)}}. \tag{19}$$

Note, that pressure waves are always faster than shear waves.

By setting $\Psi = (0, 0, \Psi)^t$, one obtains the wave equation (16) in two dimensions describing in-plane deformations in plates (plane stress) or wave propagation in bodies extending to infinity along one axis (plane strain). In the case of plane stress, the longitudinal wave speed is given as

$$c_p = \sqrt{\frac{E}{\rho(1-\sigma^2)}}. \tag{20}$$

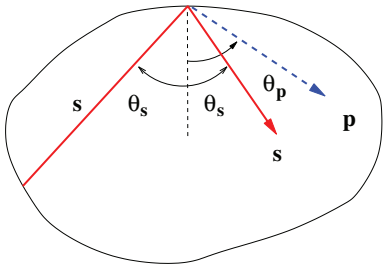

Figure 1. Wave splitting for in-plane waves at the boundary; here, conversion from an incoming *s* wave to an *s* and *p* wave are shown.

A more careful treatment of in-plane and flexural modes in plates solving explicitly the infinite plate problem leads to the Rayleigh–Lamb dispersion relations. These contain the plate and bulk dispersion relations in equations (13) and (18) only in the limit of ω small compared to the cut-off frequency; the next-to-leading order terms in a expansion in ω have been given by Bertelsen *et al* (2000).

The wave equations (18) couple at boundaries for typical boundary conditions. For example, if no forces act on the boundary, that is, free boundary conditions apply, one obtains

$$\mathbf{t}(\mathbf{u}) = \sigma(\mathbf{u}) \cdot \mathbf{n} = \mathbf{0}, \tag{21}$$

Here, $\mathbf{t}$ is called the traction and $\mathbf{n}$ denotes the normal to the boundary. For a free boundary there are still non-vanishing tangential stresses as discussed in (Pao and Mow 1971, Achenbach *et al* 1982); one has: $\sigma_{tt} \neq 0$, whereas $\sigma_{nn} = \sigma_{nt} = \sigma_{tn} = 0$ with t denoting the directions tangential to the boundary.

The ray dynamics related to the vectorial PDE (16) consists of longitudinal and transversal components propagating according to (4) with different velocities. Formally, this can be derived via a WKB-ansatz, see Achenbach *et al* (1982) or from the free Green function in the limit of large wave numbers (Musgrave 1970). For inhomogeneous media, a WKB treatment can be found in (Cervený 1985, Brechovskich 1980) taking into account variations in the density. In isotropic bodies, the two polarizations are decoupled in the interior giving rise to independent ray paths. Fermat's principle leads to a modified Snell's law at impact with boundaries according to

$$\frac{c_p}{c_s} = \frac{\sin\theta_\mathrm{p}}{\sin\theta_\mathrm{s}}, \tag{22}$$

where $\theta_\mathrm{p}, \theta_\mathrm{s}$ denote the angle of incident or reflection of the pressure and shear wave, respectively, measured with respect to the normal to the surface, see figure 1. This leads to mode conversion and ray splitting at boundaries with reflection coefficients obtained asymptotically from solving the wave equation (16) for plane waves impacting on a straight boundary; for free boundary conditions one obtains (Landau and Lifshitz 1959, Couchman *et al* 1991, 1992)

$$\begin{aligned} \alpha_{pp} &= \frac{\sin 2\theta_\mathrm{s} \sin 2\theta_\mathrm{p} - \kappa^2 \cos^2 2\theta_\mathrm{s}}{\sin 2\theta_\mathrm{s} \sin 2\theta_\mathrm{p} + \kappa^2 \cos^2 2\theta_\mathrm{s}} \\ \alpha_{ss} &= \alpha_{pp} \\ \alpha_{ps} &= -\alpha_{sp} \qquad \text{and} \qquad \alpha_{pp}^2 + \alpha_{sp}^2 = 1, \end{aligned} \tag{23}$$

where $\alpha_{\pi\pi'}$ relates components *normal* to the boundary of incoming waves of polarization $\pi' \in \{p, s\}$ to outgoing waves of polarization π and $\kappa = c_p/c_s \geqslant 1$. Defining $|a_{\pi\pi'}|^2$ as the proportion of the energy density of the wave undergoing transition from $\pi' \to \pi$, one obtains

$$a_{\pi\pi'} = \sqrt{\frac{c_\pi \cos\theta_\pi}{c_{\pi'} \cos\theta_{\pi'}}}\alpha_{\pi\pi'}, \tag{24}$$

with $|\alpha_{\pi\pi'}|^2$, the ratio of the corresponding energy fluxes normal to the boundary (with normal velocity $c_\pi \cos\theta_\pi$). The unitarity of $\boldsymbol{\alpha}$ implies flux conservation normal to the boundary.

When taking into account boundaries, solutions for problems such as scattering from the infinite half plane or the interior/exterior wave problem for a circular plate/hole can be treated analytically, see for example Landau and Lifshitz (1959), Keller and Karal (1964), Søndergaard and Tanner (2002) and Wirzba *et al* (2005). Apart from these simple geometries, numerical or approximative techniques need to be employed for solving wave problems in elasticity. Such an analysis is complicated by the fact, that for the Navier–Cauchy equation, the solutions for corners are not known in a closed form. In the following section, we will review asymptotic methods covering the high-frequency regime and connecting wave problems to a ray dynamics.

2. Wave dynamics—a ray perspective

The idea of wave energy travelling along rays is a useful guiding principle in wave propagation problems in acoustics and elastodynamics, especially in areas such as underwater acoustics, seismology or acoustic microscopy (Briggs 1992). The connection between wave problems and the details of an underlying long term ray dynamics has been considered very early in room acoustics (Joyce 1975), more systematic studies started, however, only in the late 1980s. In many applications, it is indeed only the early arrival times of acoustic signals which are considered important. This part of the signal is related to short ray paths with relatively simple dynamics. For earthquakes, for example, it is the early signal which causes most of the destruction at well-defined arrival times from the epicentre; the seismic signal arriving at later times, the so-called seismic coda, is in general incoherent and has received attention only recently in the context of reconstructing the Green function from cross-correlated data, see section 3.1.4. Acoustic signals undergoing multiple scattering such as the propagation through a disordered media, in room acoustics or in determining the distribution of vibrational energy in large build-up structures, often show seemingly random fluctuations. Statistical methods are favoured, here, which imply certain assumptions on the underlying ray dynamics such as ergodic or diffusive behaviour. These methods disregard the actual ray dynamics completely and can describe generic, universal features of wave systems; the techniques will be discussed in more detail in section 3 in the context of random matrix theory.

The relation between wave and ray dynamics became a focus in quantum mechanics in the early 1990s. Gutzwiller's progress on small wavelength approximations of the Green function in the time and frequency domain (Gutzwiller 1990) as well as uncovering the duality between eigenfrequencies and periodic rays in the asymptotic regime offered a new way forward for studying the imprint of regular or chaotic ray dynamics on the associated wave problem. In the acoustics community, this way of thinking has been picked up in the early to mid 1990s (Weaver 1989a, 1989b, Ellegaard *et al* 1995, 1996, Fink 1997, Tappert and Brown 1996) and is receiving increasing attention in an engineering context.

We will focus in this section on the interplay between wave and ray dynamics. We start by briefly reviewing short wavelength approximations of Green functions and related

operators derived in a quantum context. This is followed by a survey of wave versus ray chaos aspects in acoustics and elastodynamics including a discussion on trace formulae for elastic, isotropic bodies in section 2.2 and ray-splitting billiards in section 2.3. We will then introduce the concepts of time-reversal imaging in section 2.4 based on the time-reversal invariance of both the ray and wave dynamics and finally discuss wave chaos aspects in ocean acoustics in section 2.6.

We will in the following assume that absorption can be neglected and that the problems considered are not explicitly time dependent. We will avoid references to quantum mechanics. The high-frequency or semiclassical limit is thus understood in the sense that the wavelength is small compared to typical dimensions such as the size of the resonator. This limit is formal as ultimately the wavelength becomes as small as the inter-atomic distances in the medium and the continuum approximation breaks down. In the case of a single-crystal resonator, for example, the actual phonon dispersion relation should then be used. We will not consider such complications, but merely note that ballistic effects have been observed experimentally also for phonons by Hensel and Dynes (1977) and Northrop and Wolfe (1979). For isotropic media, often produced through fusion thus destroying the crystal structure, there is a minimum grain size at which the continuum approximation breaks down Weaver (2001). Likewise, cut-off effects may become important for wave propagation in plates or membranes when the thickness becomes comparable to the wavelength and nonlinear terms enter the wave equation for large excitations, which will, however, not be our primary concern here.

We end this introductory part with a general note. In acoustics, a distinction is often made between a ray, wave or modal picture. In the terminology of semiclassics, rays correspond to the classical limit, wave dynamics refers to wave packet propagation and modes are related to the eigenfunctions or wavefunctions of the system, respectively. The main emphasis in this section is thus on describing eigenfrequencies and eigenfunctions in terms of an underlying classical, long-term ray dynamics; this is in contrast to traditional approaches in acoustics classifying arrival times for wave packets or impulses in terms of a ray picture for short times.

2.1. A brief review of quantum chaos

Quantum spectra and wavefunctions are influenced by the underlying classical ray dynamics in an intricate way. While the wave equations are linear thus obeying the superposition principle, the often nonlinear dynamics of the ray motion manifests itself in a wide range of wave phenomena. Wave systems being integrable in the classical limit tend to be ordered and a set of integer 'quantum numbers' can be assigned to each eigenfrequency. Wavefunctions are localized on classical tori and there are no correlations between levels corresponding to series with different quantum numbers. Quite the opposite is true for wave problems related to classically chaotic systems; the eigenfrequency spectra have no obvious structure and wavefunctions are extended over the whole phase space[3]. Eigenfrequency statistics is again very different for systems with an integrable or a chaotic classical counterpart as will be discussed in more detail in section 3.

A convenient starting point for a semiclassical treatment is the Green function in the time and frequency domain solving

$$\left(-\frac{\partial^2}{\partial t^2} - \hat{H}\right)\hat{G}(\mathbf{r}, \mathbf{r}_0; t) = \delta(\mathbf{r}_0 - \mathbf{r})\delta(t); \tag{25}$$

$$(\omega^2 - H)G(\mathbf{r}, \mathbf{r}_0; \omega) = \delta(\mathbf{r}_0 - \mathbf{r}), \tag{26}$$

[3] Phase-space representations of wavefunctions can be obtained by suitable transformations such as the Wigner transformation, see Gutzwiller (1990).

where H is a time-independent wave operator such as listed in section 1.2. In the following, we will consider hyperbolic wave equations and the spectral parameter is thus not $E/\hbar$ but the square of the frequency. Note that $\hat{G}(t)$ and $G(\omega)$ are related by Laplace transformation.

Gutzwiller derived a semiclassical expression for the quantum propagator $\hat{G}(\mathbf{r}, \mathbf{r}_0; t)$ starting from Feynman's path integral (Feynman and Hibbs 1965). Using stationary phase approximation, $\hat{G}$ can be written as a sum over all possible classical trajectories from $\mathbf{r}_0$ to $\mathbf{r}$ in the time t, see Gutzwiller (1990). Such a treatment is not immediately amendable to hyperbolic wave equations as listed in section 1.2 due to time-ordering problems. A formulation in terms of path integrals has been proposed by adding an additional (fictitious) time variable to the time-independent problem (26) and constructing an artificial parabolic equation (Schulman 1981, Bothelho and Vilhena 1994) or by employing parabolic approximations of the original equations (Dashen 1979, MacDonald and Kuperman 1987, Dacol 1994) such as discussed in section 2.6. For an exact treatment of arrival time problems in acoustics and elasticity see the discussion by Miklowitz (1978) and Hudson (1980). We circumvent the problem here by focusing on time-independent problems considering the Green function in the frequency domain, equation (26); it has the same structure irrespective of whether the associate time-dependent PDE is hyperbolic and parabolic and can thus be expressed in terms of the same semiclassical formulae.

The Green function exhibits poles at the eigenfrequencies or resonances; for closed systems, G may be written in terms of the real eigenfunctions (or modes) u_n which for scalar wave equations reads

$$G(\mathbf{r}, \mathbf{r}_0, \omega) = \sum_n \frac{u_n(\mathbf{r})u_n(\mathbf{r}_0)}{\omega^2 - \omega_n^2}. \tag{27}$$

In the high-frequency limit, G may be approximated using expressions derived in a quantum context. For short distances and direct paths with $|\mathbf{r} - \mathbf{r}_0|k \sim 1$, the Green function can be written in terms of the free Green function with local wave number $k = k(\mathbf{r})$. Contributions from paths long compared to the wavelength give rise to the approximate form

$$G_{\mathrm{sc}}(\mathbf{r}, \mathbf{r}_0; \omega) = \frac{\pi}{\omega} \frac{1}{(2\pi \mathrm{i})^{(d+1)/2}} \sum_{\substack{cl.tr \\ \mathbf{r}\to\mathbf{r}_0}} \sqrt{|D|} \exp\left[\mathrm{i}S(\mathbf{r}, \mathbf{r}_0; \omega) - \mathrm{i}\mu\frac{\pi}{2}\right], \tag{28}$$

where d is the dimension of the system and the sum is over all classical paths from $\mathbf{r}_0 \to \mathbf{r}$ on the energy manifold $H(\mathbf{p}, \mathbf{r}) = \omega^2$. The Hamilton function H is given for example by equation (4). The action $S(\mathbf{r}, \mathbf{r}_0; \omega)$ defined in (7) is taken along the classical path. The amplitude can be written as

$$D(\mathbf{r}, \mathbf{r}_0; \omega) = \frac{1}{|\dot{\mathbf{r}}||\dot{\mathbf{r}}'|} \det\left(\frac{\partial^2 S}{\partial r_i \partial r_j{}'}\right), \tag{29}$$

where $\dot{\mathbf{r}}', \dot{\mathbf{r}}$ are the velocities at the start and end points of the trajectory and the partial derivatives are taken in a local coordinate system perpendicular to the classical path, see Gutzwiller (1971, 1990). The integer index μ counts the number of caustics or singular points for which $D^{-1} = 0$ along the classical path on the energy manifold. The validity of (28) is so far independent of the type of the underlying classical dynamics, e.g. chaotic, integrable or mixed behaviour. Deviations from the exact Green functions due to the stationary phase approximation are most prominent at classical caustics where the amplitudes $D(\mathbf{r}, \mathbf{r}_0; \omega)$ diverge. Note that the semiclassical approximation contains wave-like elements such as the interference of paths, but can in this form not account for effects such as diffraction or tunnelling. These can be incorporated by including non-classical paths in terms of solutions of the complexified equations of motion (5) as discussed by, for example, Keller and Karal (1962) and Creagh (1996).

2.1.1. Trace formulae and spectral determinants. The information about the eigenfrequency spectrum $\{\omega_n\}$ is contained in the trace of the Green function

$$g(\omega) = \operatorname{Tr} G(\omega) = \int \mathrm{d}^d r\, G(\mathbf{r}, \mathbf{r}; \omega) \sim \sum_n \frac{1}{\omega^2 - \omega_n^2}. \tag{30}$$

For systems of finite size, the density of states is related to the trace by

$$d(\omega) = \sum_n \delta(\omega - \omega_n) = -\frac{2\omega}{\pi} \lim_{\epsilon \to 0+} \operatorname{Im} g(\omega + \mathrm{i}\epsilon). \tag{31}$$

Inserting the semiclassical approximation, (28), into (30) and evaluating the resulting integrals by stationary phase leads to unphysical singularities near bifurcation points in mixed regular and chaotic systems. Closed semiclassical expressions for the trace in its simplest form can thus be given only for integrable or completely chaotic systems. The trace can in both cases be written as a sum over classical periodic orbits of the system; this establishes a Fourier relation between the eigenfrequencies of a wave system and the set of periodic orbits of the underlying ray dynamics. Bifurcations can be taken into account using uniform approximation which leads to contributions going beyond Gutzwiller's treatment, see for example Schomerus and Sieber (1997).

Trace formulae. In integrable problems such as the ray dynamics in rectangular or spherical cavities, phase space can be foliated in terms of invariant tori and the Hamiltonian can in action-angle variables be written as a function of the actions I alone. Approximations to the eigenfrequencies can be obtained in terms of the Einstein–Brillouin–Keller (EBK) condition, the multidimensional generalization of WKB quantization in one dimension. Periodic boundary conditions on the tori demand

$$I_{m_j} = 2\pi\left(m_j + \frac{\sigma_j}{4}\right), \qquad m_j \in \mathbb{N} \qquad \text{and} \qquad j = 1, \ldots, d, \tag{32}$$

where the integer Maslov index σ_j labels the number of caustics along a 2π rotation in the angle ϕ_j conjugated to I_j. The eigenfrequencies are then obtained by Gutzwiller (1990)

$$\omega_{\mathbf{m}}^2 = H(I_{m_1}, \ldots, I_{m_d}). \tag{33}$$

The corresponding wavefunction (in Wigner representation) is localized on the torus I_m (Berry 1977a, Ozorio de Almeida and Hannay 1983). For integrable systems, the integration in (30) can be performed in angle variables giving rise to contributions from continuous families of periodic orbits on tori with rational winding numbers. The resulting periodic orbit formula is equivalent to the EBK quantization (33) (Berry and Tabor 1976, 1977a).

The other extreme case, hard chaos, is characterized by ergodic classical motion with exponential separation of neighbouring trajectories. Inserting expression (28) into (30), only those trajectories contribute which close in coordinate space. The main contributions to the trace integral come from stationary phase points giving rise to the additional condition $k = k'$, that is, the initial and final momentum coincides. The trace can thus be written as a sum over (unstable) periodic orbits of the chaotic system and the density of states takes on the form (Gutzwiller 1990),

$$d(\omega) \approx \bar{d}(\omega) + \frac{1}{\pi} \sum_{\mathrm{po}} T_{\mathrm{po}} \sum_{r=1}^{\infty} \frac{\cos(r S_{\mathrm{po}}(\omega) - r\sigma_{\mathrm{po}}\pi/2)}{\sqrt{\left|\det\left(\mathbf{M}_{\mathrm{po}}^r - \mathbf{1}\right)\right|}}. \tag{34}$$

The first sum is taken over all periodic orbits (po) of the classical ray system and the sum over r accounts for the repetitions. In a chaotic system, these orbits form a dense set of measure zero in phase space. The action S is taken along the orbit and T represents the period. The

Monodromy or stability matrix **M** is the Jacobian matrix of the full phase space flow in a reduced local phase-space coordinate system perpendicular to the trajectory and on the energy manifold. It describes the linearized dynamics in the neighbourhood of the orbit after one revolution. The stability of a periodic orbit is characterized by the eigenvalues Λ of **M**. The integer index σ, also called the Maslov index, is closely related to the number of caustics μ in (28). It is equivalent to a winding number counting twice the number of revolutions of the stable or unstable eigenvectors of **M** around the periodic trajectories as investigated in (Creagh *et al* 1990, Robbins 1991).

The smooth part $\overline{d}(\omega)$ originates from contributions of the form $\lim_{\mathbf{r}\to\mathbf{r}'} G(\mathbf{r},\mathbf{r}',\omega)$ giving rise to the mean level density, also called the Thomas–Fermi contribution in atomic physics or the Weyl term in the context of resonators, see section 2.2.1 for details. For scalar wave equations of the Helmholtz-type, one obtains in leading order

$$\overline{d}(\omega) = \frac{2\omega}{(2\pi)^d} \int\!\!\int \mathrm{d}^d r\, \mathrm{d}^d k\, \delta(\omega^2 - H(\mathbf{p},\mathbf{r})), \tag{35}$$

see for example Gutzwiller (1990).

Spectral determinants. It is sometimes advantageous to consider the so-called spectral determinant

$$D(\omega) = \det(\omega^2 - \hat{H}) = \prod_n \left(\omega^2 - \omega_n^2\right)$$

which has zeros at the position of the eigenfrequencies; it is obtained from the trace (30) via the relation $D(\omega) = \exp\left(\int 2\omega g(\omega)\,\mathrm{d}\omega\right)$. Making use of (34) valid for chaotic systems, one obtains

$$\begin{aligned} D_{\mathrm{sc}}(\omega) &\sim \mathrm{e}^{-\mathrm{i}\pi\overline{N}(\omega)} \prod_{\mathrm{po}} \exp\left[-\sum_{r=1}^{\infty} \frac{\exp\left[\mathrm{i}r\left(S_{\mathrm{po}}(\omega) - \sigma_{\mathrm{po}}\pi/2\right)\right)}{r\sqrt{\left|\det\left(\mathbf{M}_{\mathrm{po}}^r - \mathbf{1}\right)\right|}}\right] \\ &= \mathrm{e}^{-\mathrm{i}\pi\overline{N}(\omega)} \zeta_{\mathrm{sc}}^{-1}(\omega), \end{aligned} \tag{36}$$

where $\overline{N}$ denotes the smooth part of the *spectral staircase*

$$N(\omega) = \int_{0+}^{\omega} \mathrm{d}\omega' \overline{d}(\omega'). \tag{37}$$

The integration over frequency is carried out using the relation $T_{\mathrm{po}} = \partial S_{\mathrm{po}}/\partial\omega$. The last equality defines the semiclassical zeta function ζ^{-1} which for bound problems has properties reminiscent of the Riemann zeta function (Titchmarsh 1986, Berry 1986, Brack and Bhaduri 1997).

The S–matrix and periodic orbits. The periodic orbit formulae discussed in the previous sections are valid also for open systems provided the Green function has been appropriately regularized before taking the trace. In acoustics, one often considers waves scattering from walls or other obstacles in an otherwise open setting, where it is more useful to work with the scattering matrix directly. For a more in depth discussion of open systems, see section 3.2 and especially section 3.2.2.

A connection between the S-matrix and the trace of the Green function (and thus periodic orbit formulae) is provided by *Krein's formula* (Krein 1953)[4]

$$2\omega \lim_{\epsilon\to 0} \mathrm{Im}\,\mathrm{Tr}[G(\omega^2 + \mathrm{i}\epsilon) - G_0(\omega^2 + \mathrm{i}\epsilon)] = \frac{\mathrm{i}}{2}\frac{\mathrm{d}}{\mathrm{d}\omega} \log\det S(\omega). \tag{38}$$

[4] Strictly speaking, (38) is applicable only after considering the whole system in a large box to obtain a discrete spectrum for both G and G_0. The imaginary part of the traces is (up to a factor of π) the level density (31); it is properly defined only by setting $\mathrm{Im}\,\mathrm{Tr}G(\omega^2 + \mathrm{i}\epsilon) := -\frac{\mathrm{i}}{2}[\mathrm{Tr}G(\omega^2 + \mathrm{i}\epsilon) - \mathrm{Tr}G(\omega^2 - \mathrm{i}\epsilon)]$. Letting the box radius go to infinity before taking ϵ to zero provides the finite, nontrivial result.

(See also equation (80) defining a relation between the Green function and the scattering matrix in the presence of well-defined scattering channels.) The periodic orbit contributions are contained in the trace of the total Green function G, whereas the reference Green function G_0 regularizes the expressions for $r \to \infty$.

One obtains the determinant of the S-matrix in terms of semiclassical zeta functions after formally integrating and exponentiating (38) on both sides. Splitting the imaginary part into a contribution from the upper and the lower complex energy half plane, one obtains:

$$\det S(\omega) = \mathrm{e}^{-2\pi \mathrm{i}\tilde{N}(\omega)} \frac{\zeta_{\mathrm{sc}}^{-1}(\omega^*)^*}{\zeta_{\mathrm{sc}}^{-1}(\omega)}. \tag{39}$$

The zeta function $\zeta_{\mathrm{sc}}^{-1}(\omega)$ introduced here is defined in (36); the product is taken now over all classical periodic orbits trapped in the scattering system. The phase $\tilde{N}(\omega)$ is the effective phase-space volume of the scatterer (Smilansky and Ussishkin 1996); its derivative with respect to energy is directly related to the mean delay time due to the scattering process, also referred to as the Wigner–Smith time delay (Wigner 1955, Smith 1960). Equation (39) reveals the connection between the zeros of the zeta function and the poles of the S–matrix. The resonances of a scattering system are thus again intimately connected to the classical periodic orbits.

The semiclassical formulae (34), (36) and (39) establish Fourier relations between eigenfrequencies or resonances of a wave systems and the periodic orbits of the related classical or ray dynamics. The classical ingredients, such as, actions, stabilities and winding numbers of periodic orbits as well as the eigenvalues, are invariant under coordinate transformation and so are the quantum and semiclassical traces. Note, however, that both for classically chaotic as well as for integrable systems, it is the sum over *all* periodic orbits which gives rise to the poles at the eigenenergies.

2.1.2. The transfer operator and semiclassical quantization conditions. The periodic orbit formulae (34) or (36) for chaotic systems are not absolutely convergent for real energies $E = \omega^2$ as discussed in (Eckhardt and Aurell 1989); to obtain convergent expressions on the real axis, it is vital to find an efficient ordering scheme in the summation to ensure maximal cancellation between terms (Aurich *et al* 1988, Sieber and Steiner 1990, Cvitanović and Eckhardt 1989, Berry and Keating 1990, Tanner *et al* 1991). An ordering is naturally provided by the so-called transfer operator method (Bogomolny 1992) which will be briefly introduced here. Transfer operators are a generalization of boundary integral kernels; the latter find widespread use as a numerical tool to obtain eigenfrequencies in acoustics and elasticity in finite domains (Bonnet 1995). As usual, we will restrict the discussion to scalar wave equations; the generalization to elasticity will be treated in section 2.2.

We start from a classical Poincaré map defined on a $(2d-2)$-dimensional sub-manifold of the full phase space—the surface of section—by a condition $f(\mathbf{r}, \mathbf{p}) = 0$; $H(\mathbf{r}, \mathbf{p}) - \omega^2 = 0$. The mapping is given by subsequent intersections of a trajectory with the surface of section. Choosing, e.g. $f = r_d$ (which may be achieved after an appropriate coordinate transformation), one defines in analogy a quantum Poincaré map acting as a discrete-time propagator on wavefunctions

$$\psi_{m+1}(\mathbf{s}) = \int \mathrm{d}s_0^{d-1} T(\mathbf{s}, \mathbf{s}_0; \omega) \psi_m(\mathbf{s}_0)$$

with $\mathbf{s}, \mathbf{s}_0$ on the $(d-1)$-dimensional surface of section. The so-called transfer operator $T(\mathbf{s}, \mathbf{s}_0; \omega)$ is unitary reflecting the phase-space conservation of the classical map. Neither the classical Poincaré map nor the corresponding quantum transfer operators can in general be

given analytically. The classical map is usually obtained by solving the equations of motion numerically. Constructing the corresponding quantum map explicitly is a more elaborate task; quite general methods are presented in (Doron and Smilansky 1992, Dietz and Smilansky 1993, Prosen 1994, 1995, 1996, Rouvinez and Smilansky 1995). The quantum Poincaré map contains the whole information about the eigenfrequency spectrum given by the fixed point condition $\psi = T(\omega)\psi$, that is, eigenfrequencies correspond to the zeros of the function

$$\zeta^{-1}(\omega) = \det[1 - T(\omega)]. \tag{40}$$

A direct connection between (40) and the semiclassical zeta function (36) can be established for chaotic systems; by writing T in a semiclassical form, one obtains (Bogomolny 1992, Doron and Smilansky 1992)

$$T_{\rm sc}(\mathbf{s}, \mathbf{s}_0; \omega) = \frac{1}{(2\pi \mathrm{i})^{(n-1)/2}} \sum_{\substack{\text{cl.tr} \\ \mathbf{s}_0 \to \mathbf{s}}} \sqrt{\left|\det\left(\frac{\partial^2 S}{\partial s \partial s_0}\right)\right|} \exp\left(\mathrm{i}S(\mathbf{s}, \mathbf{s}_0; \omega) - \mathrm{i}\mu\frac{\pi}{2}\right), \tag{41}$$

where the sum is taken over trajectories form $\mathbf{s}_0$ to $\mathbf{s}$ without crossing the Poincaré surface of section. For chaotic systems, the trace of the transfer operator T^n is linked to the periodic orbits of length n by stationary phase approximation, i.e.

$$\operatorname{Tr} T^n_{\rm sc}(\omega) = \sum_{\rm po}^{(n)} \frac{\exp\left(\mathrm{i}S_{\rm po}(\omega) - \mathrm{i}\sigma_{\rm po}\frac{\pi}{2}\right)}{\sqrt{|\det(\mathbf{M}_{\rm po} - \mathbf{1})|}}. \tag{42}$$

Using the relation

$$\det(1 - T) = \exp[\operatorname{Tr}\log(1 - T)] = \exp\left(-\sum_{n=1}^{\infty}\frac{1}{n}\operatorname{Tr} T^n\right) = \zeta^{-1}, \tag{43}$$

one regains the semiclassical zeta function, (36). Provided the operator T has the so called trace class property (which essentially means, that the $\operatorname{Tr} T$ exists and is finite), one can show (Reed and Simon 1972a, 1972b) that the determinant (40) converges when expanded in terms of cumulants, that is,

$$\zeta^{-1}(\omega) = \det[1 - T(\omega)] = \sum_{n=0}^{\infty} c_n(\omega), \tag{44}$$

where the c_n are obtained recursively

$$c_n = -\frac{1}{n}\sum_{m=0}^{n-1} \operatorname{Tr} T^{n-m} c_m, \qquad c_0 = 1. \tag{45}$$

Writing out the first few terms in the expansion, one obtains

$$\zeta^{-1}(\omega) = 1 - \operatorname{Tr} T - \frac{1}{2}(\operatorname{Tr} T^2 - (\operatorname{Tr} T)^2) - \frac{1}{3}\left(\operatorname{Tr} T^3 - \frac{3}{2}\operatorname{Tr} T^2 \operatorname{Tr} T + \frac{1}{2}(\operatorname{Tr} T)^3\right) - \cdots. \tag{46}$$

The convergence of the cumulant expansion (44) originates from cancellations between the terms in brackets. Thus, an exponentially increasing number of periodic orbits contained in $\operatorname{Tr} T^n$ is balanced in a delicate way by products of shorter orbits leading to a rapid decay in the c_n's for large n. The so-called *cycle expansion* technique makes use of these cancellations on the level of individual periodic orbits, see Cvitanović (1988), Artuso *et al* (1990), Cvitanović *et al* (2006) and references therein. Periodic orbit quantization using cycle expansion techniques has been applied to chaotic systems ranging from the stadium billiard to the three-body Coulomb problem helium, see for example Cvitanović and Eckhardt (1989), Ezra *et al* (1991), Tanner *et al* (1991), Wirzba (1992), Tanner and Wintgen (1995) and Tanner *et al* (1996, 2000).

2.2. *Trace formulae in elastodynamics*

The general theory sketched in the last section can directly be applied to problems in linear acoustics. The two-dimensional Helmholtz equation with constant wave velocity has been studied in detail in the context of 'quantum billiards' and has been realized experimentally in flat microwave cavities. The underlying classical dynamics is here only influenced by the shape of the boundary and model systems with desired properties can easily be constructed; a detailed account of studies on quantum billiard is, for example, given by Stöckmann (1999) and Kuhl *et al* (2005). For an experimental demonstration of wave chaos effects in water-filled cavities, see Chinnery and Humphrey (1996).

In the following, we will review progress in adapting the methods introduced in section 2.1 to the more complex wave equations found in elastodynamics. The presence of longitudinal and transversal waves with different velocities leads to *ray splitting* and thus a non-deterministic ray dynamics. Ray splitting is in fact a general phenomenon of wave propagation occurring, for example, in optics at interfaces with a sudden change in the refractive index or in quantum mechanics at step-potential barriers. Its presence leads to interesting new effects when studying the relation between linear wave equations and an underlying ray dynamics. We will consider some simple geometries for elastic bodies in section 2.2.3 and ray splitting billiards in section 2.3 in more detail. We start by giving the known results for the mean density of states for plate and bulk spectra.

2.2.1. Mean density of eigenfrequencies and the Weyl expansion. The average density of eigenfrequencies of bodies of finite size can be given in terms of a series expansion in the wave number also referred to as Weyl expansion (Baltes and Hilf 1976, Safarov and Vasil'ev 1992). The mean density enters as a leading, non-oscillatory term in the trace formula (34) or in integrated form in the spectral determinant, equation (36). Weyl's original motivation for studying the mean density was to estimate thermodynamic quantities such as the heat capacity for elastic bodies (Weyl 1911); it furthermore plays an important role in energy transport problems such as SEA, see section 3.3. Systematic methods for obtaining the Weyl expansion beyond the leading order, equation (35), have been given for the Schrödinger equation by Grammaticos and Voros (1979) and for the Helmholtz equation with smooth boundaries by Stewartson and Waechter (1971) and Berry and Howls (1994). The latter demonstrate that the resulting series is asymptotic and that its divergence is controlled by 'short' periodic orbits. The theory can also be applied to the biharmonic equation, which acts in many ways as a Helmholtz equation with special (mixed) boundary conditions (Legrand *et al* 1992, Bogomolny and Hugues 1998). In isotropic elastodynamics, however, only the first two terms of the Weyl series are known at present and for shells and anisotropic media only the leading term has been derived explicitly, see sections 4.2 and 4.3.

The smooth part of the spectral staircase function (37) for wave equations in two dimensions and homogeneous and isotropic media is of the general form (Baltes and Hilf 1976, Safarov and Vasil'ev 1992, Bogomolny and Hugues 1998)

$$\overline{N}(k) = \alpha \frac{A}{4\pi} k^2 + \beta \frac{L}{4\pi} k + c_0,$$

where A and L denote the area and perimeter length of the domain, respectively, and α, β depend on the wave equation and the boundary conditions. For scalar wave equations and smooth boundaries, the constant terms is given in terms of the curvature R of the boundary

$$c_0 = \gamma \int \frac{\mathrm{d}l}{R(l)}$$

and γ depends on the boundary conditions. Extra contributions arise at sharp corners (Bogomolny and Hugues 1998). For the Helmholtz equation, one obtains $\alpha = 1, \beta = \pm 1$ for Neumann and Dirichlet boundary conditions, respectively, and $\gamma = 1/12\pi$. A general method for calculating the boundary term β is, for example, given in (Prange *et al* 1996).

The first few terms of the Weyl expansion for bending modes in plates were derived by Vasil'ev (1987), see also Safarov and Vasil'ev (1992). Common to both of these mathematical derivations is the use of Krein's formula (38). Bogomolny and Hugues (1998) offer a derivation in the spirit of Balian and Bloch (1970) for quantum billiards. Boundary corrections are determined by considering the free Green function as well as the half-plane Green function with appropriate boundary conditions. One obtains for *clamped edges*

$$\beta = -1 - \frac{\Gamma(3/4)}{\sqrt{\pi}\Gamma(5/4)} \tag{47}$$

and for *free edges*

$$\beta = -1 + 4(\sigma(2 - 3\sigma') + 2\sigma'\sqrt{2\sigma'^2 - 2\sigma' + 1})^{-1/4} \tag{48}$$

$$-\frac{4}{\pi}\int_0^1 \mathrm{d}t \arctan\left[\sqrt{\frac{1-t^2}{1+t^2}}\left(\frac{1+\sigma' t^2}{1-\sigma' t^2}\right)^2\right], \tag{49}$$

with modified Poisson ratio $\sigma' = 1 - \sigma$ and k is the flexural wave number as given in (13). The constant term c_0 is also discussed by Bogomolny and Hugues (1998).

We finally turn to the Navier–Cauchy equation in two spatial dimensions describing plane strain in bulk elasticity or in-plane modes in plates. The leading term is now given by the 'phase-space' volume of shear and pressure modes separately and one obtains the expansion (Vasil'ev 1987, Safarov and Vasil'ev 1992)

$$\overline{N}(k_s) = \frac{(1+\kappa^{-2})A}{4\pi}k_s^2 + \frac{\beta L}{4\pi}k_s + o(k_s), \tag{50}$$

with

$$\beta = -1 - \frac{1}{\kappa} - \frac{4}{\pi}\int_{1/\kappa}^1 \mathrm{d}\xi \arctan\sqrt{(1-(\kappa\xi)^{-2})(\xi^{-2}-1)} \tag{51}$$

for a clamped boundary and

$$\beta = 4/\gamma - 3 + \frac{1}{\kappa} + \frac{4}{\pi}\int_{1/\kappa}^1 \mathrm{d}\xi \arctan\frac{(2-\xi^{-2})^2}{\sqrt{(1-(\kappa\xi)^{-2})(\xi^{-2}-1)}} \tag{52}$$

for free boundaries. Here, $\kappa = c_p/c_s$ where the pressure wave speed is given by equations (19) for bulk waves and (20) for plates. The term containing γ in (52) originates from Rayleigh surface wave contributions; see section 4 with $\gamma \in (0, 1)$ given by the equation

$$\gamma^6 - 8\gamma^4 + 8(3 - 2\kappa^{-2})\gamma^2 - 16(1 - \kappa^{-2}) = 0, \tag{53}$$

the so-called Rayleigh equation (Ewing *et al* 1957, Landau and Lifshitz 1959). It determines the wave number of surface Rayleigh waves as $k_\mathrm{R} = \gamma k_s$.

The explicit form of β has first been discussed by Lotfi (1995); an improved version has been published by Bertelsen *et al* (2000). The boundary corrections in three dimensions have been derived by Dupuis *et al* (1960), see also Prange *et al* (1996). Weaver (1989a) obtained experimentally a large set of eigenfrequencies for aluminium blocks and tested Weyl's law for the elastic wave equation. Later experiments by Schaadt *et al* (2003a) provided an accurate

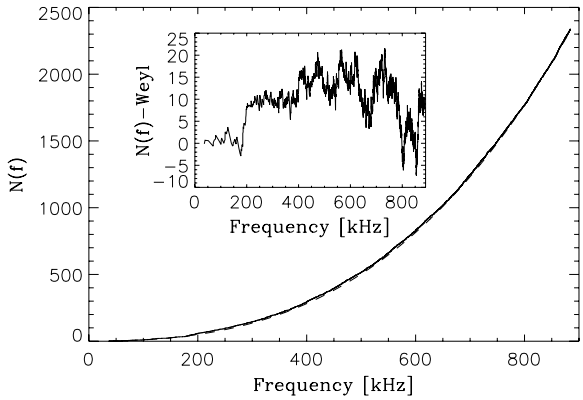

Figure 2. Experimental staircase function measured for a rectangular fused-quartz block by (Schaadt *et al* 2003a). Inlet shows fluctuations around the mean.

confirmation of (50) using up to 2500 eigenfrequencies of a three-dimensional quartz block, see figure 2.

For anisotropic, homogeneous media, only the leading term of the Weyl expansion is known and has been worked out explicitly by Søndergaard *et al* (2004). It can again be interpreted in terms of the available phase-space volume albeit with an anisotropic set of momentum surfaces; see 4.3 for more details.

In an interesting experiment by Lobkis and Weaver (2001a), the spectral density of aluminium *foam* was determined. Somewhat surprisingly, it was found that the mean density is independent of the frequency; this indicates that the metal foam in the wavelength regimes considered behaves very much like a 'quasi' one-dimensional system similar to quantum graphs or lattice models studied by Kottos and Smilansky (1997, 1999).

2.2.2. Trace formulae for bending modes in plates. By factorizing the biharmonic equation in the form (13), one recovers the Helmholtz equation as the wave part of the PDE. The other factor, $(\Delta - k^2)$, gives rise to exponentially decaying modes; they contribute only in a strip of size $1/k$ near the boundary. A semiclassical description of the wave dynamics in the interior of the plate is thus identical for both plates and membranes. Especially, rays contributing to the approximate Green function (28) or trace formulae such as (34) are governed by Hamiltonian equation of motion of the from (4). The decaying modes act effectively as a modified boundary condition. Semiclassically, this enters in the form of extra phases at ray-impact with the boundary.

Legrand *et al* (1992) were the first to consider wave chaos in the context of plates by studying numerically the solutions of the biharmonic equation in a stadium-shaped domain with clamped boundary conditions. Good agreement could be achieved comparing their results with solutions of the Helmholtz equation with a special type of mixed boundary conditions. By investigating the wavefunctions, signs of *scarring*, that is, enhanced intensities along periodic orbits have been found; for references on scarring see McDonald and Kaufman (1979, 1988) and Heller (1984) and the more recent review by Kaplan (1999). Scarring effects have also been seen experimentally by Teitsworth (2000). A semiclassical theory for the biharmonic equation was finally worked out by Bogomolny and Hugues (1998). By employing single-layer potential theory on the boundary both for the propagating and decaying modes and working out the large k asymptotics, a transfer operator kernel of the form (41) has been

derived. Those components of T describing transitions from propagating to decaying modes at the boundary vanish in the semiclassical limit and one obtains in leading order

$$T_b(s, s_0; k) = \mathrm{e}^{\mathrm{i}\phi(\theta,k)} T_h(s, s_0; k), \qquad \text{with} \qquad s, s_0 \text{ on the boundary}$$

and where T_h refers to the semiclassical expression (41) for the Helmholtz equation with Neumann boundary conditions and θ is the angle with respect to the normal at the boundary point s_0. The phase ϕ coincides with the phase shift obtained by solving the infinite half-plane problem and is given as (Vasil'ev 1987, Safarov and Vasil'ev 1992)

$$\begin{aligned} \phi &= -2 \arctan \left[\frac{\cos\theta}{\sqrt{1+\sin^2\theta}} \right] \quad \text{clamped;} \\ \phi &= -2 \arctan \left[\frac{\cos\theta}{\sqrt{1+\sin^2\theta}} \left(\frac{1+\sigma' \sin^2\theta}{1-\sigma' \sin^2\theta} \right)^2 \right] \quad \text{free} \end{aligned} \tag{54}$$

with $\sigma' = 1 - \sigma$.

Periodic orbit trace formulae of the form (42) have been derived by Bogomolny and Hugues (1998); the periodic orbit contributions contain extra phases here due to the phase jumps, equation (54), at impact with the boundary. Spectra for a disk and a stadium-shaped plate have been obtained numerically. By comparing the Fourier transform of the trace with periodic orbit contributions, excellent agreement with the semiclassical expressions was obtained. Note that for the integrable disc geometry, a modified trace formula applies and periodic orbit families contribute with weights proportional to $\sqrt{k}$, see Bogomolny and Hugues (1998) for details.

Experimental verification for periodic orbit contributions in plate spectra has been obtained by Neicu *et al* (2001) and Neicu and Kudrolli (2002) using a clover-shaped fused-quartz plate. The validity of semiclassical trace formulae is not immediately evident given that the biharmonic equation is itself an approximation of the true plate dynamics. Unambiguous result could only be obtained by Neicu and Kudrolli (2002) after including higher order corrections to the dispersion relation as given by Bertelsen *et al* (2000) and carefully tracing individual peaks in the Fourier transformed spectrum by making small changes to the shape of the plate. An overall scaling factor in the frequency remained unaccounted for.

An interesting application of wave chaos effects to the radiation patterns of plates and membranes has been suggested by Delande and Sornette (1997). It is pointed out that acoustic radiation is linked via Rayleigh's formula to the Fourier transformed eigenmodes of the plate, that is, the wavefunction in momentum representation. In particular, it is demonstrated that a high degree of directionality of the sound emission is achieved along scars in momentum space, see figure 3. Such scaring effects have been studied also by Bäcker and Schubert (1999). Directionality due to dynamical ray effects have found widespread interest in the optics community in the context of micro-lasers (Nöckel and Stone 1997).

2.2.3. Bulk elasticity—wave dynamics and mode mixing. The ray dynamics associated with waves in isotropic elastic media is fundamentally different from the type of classically deterministic dynamics considered so far. While the elastic potentials still obey Helmholtz equations, the two modes have different wave speeds leading to ray splitting at the boundary with conversion coefficients depending on the boundary conditions, see section 1.2.3. (We will not distinguish between bulk elasticity and in-plane modes in plates in what follows.) Thus, a new feature enters, not normally considered in dynamical systems theory: trajectories can convert from one mode type to another on impact with the boundary which leads to a change of the momentum component normal to the boundary. The conversion rates are given

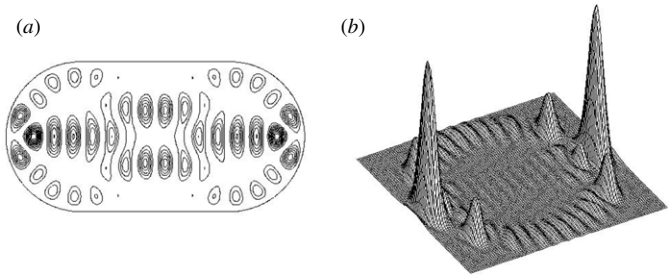

Figure 3. (*a*) Scar in the stadium billiard at $k = 12.918$ and (*b*) the corresponding radiation diagram (essentially the square of the Fourier transform of the wavefunction). The latter shows large directivity in the direction of periodic orbits (Delande and Sornette 1997).

by the modulus square of the coefficients (23), thus adding a probabilistic component to the dynamics. This has interesting consequences for semiclassical expressions as well as the notation of 'chaos' of the underlying ray dynamics.

Periodic orbit formulae. While the evolution of wave impulses along elastic rays has been studied in detail in a wave-scattering context such as seismology, Couchman *et al* (1991, 1992) were the first to consider seriously the influence of mode mixing on the ray dynamics in a closed elastic cavity. The authors showed in classical trajectory simulations that ray splitting leads to an enhancement of chaos in so-called Benettin–Strelcyn ovals (Benettin and Strelcyn 1978), a class of billiards, whose boundaries interpolate between a circle and a stadium billiard. By comparing phase-space plots with and without mode conversion, it is demonstrated that ray splitting tends to destroy invariant tori and stable islands and to increase the ergodic component of the dynamics. Exceptions are phase-space regions where ray splitting is suppressed such as for *s*-rays hitting the boundary at angles $\theta > \theta_{\rm cr}$ with $\theta_{\rm cr} = \arcsin(1/\kappa)$, the critical angle for $s \to p$ conversion. Likewise, two-bounce orbits with normal impact at the boundary at both ends have $\alpha_{ps} = \alpha_{sp} = 0$, and thus do not mode convert, see (23).

Couchman *et al* (1991, 1992) also give a trace formula for elastic media in analogy to Gutzwiller's original work for quantum systems as presented in section 2.1. The resulting formula for completely chaotic resonators (here given in the notation used throughout the paper) is

$$d_{\rm osc}(\omega) = \frac{1}{\pi}\sum_{\rm po}\sum_{r=1}^{\infty}\frac{T_{\rm po}|\alpha_{\rm po}|^r}{|{\rm Det}(\mathbf{M}_{\rm po}^r) - \mathbf{1})|^{1/2}}\cos\left[r\left(\omega T_{\rm po} + \Phi_{\rm po} - \mu_{\rm po}\frac{\pi}{2}\right)\right]. \tag{55}$$

The sum is over all periodic orbits (including rays undergoing mode conversion) which are assumed to be isolated and unstable here. The index r denotes repetitions and $T_{\rm po}$ is the accumulated time over the various shear (s) or pressure (p) segments when traversing the orbit. The amplitude consists of a geometric and a ray splitting contribution. Denoting the segments along an n-bounce orbit as $\{v_1, \ldots v_n\}$ with $v_i = p$ or s, mode conversion enters through $\alpha_{\rm po} = \prod_{i=1}^{n}\alpha_{v_i v_{i+1}}$ with mode conversion factors given in (23). The Monodromy matrix $\mathbf{M}_{\rm po}$ is calculated as the accumulated product of stability matrices including extra contributions whenever refraction takes place. Note that the dynamics including ray splitting is still symplectic—Safarov and Vasil'ev (1992) refer to it as 'a branching Hamiltonian flow'. The phase $\mu_{\rm po}$ is the Maslov index keeping track of passages through caustics (Gutzwiller 1990) and $\Phi_{\rm po} = \arg(\alpha_{\rm po})$.

The short wavelength asymptotics of a boundary integral kernel has been postulated by Søndergaard and Tanner (2002) and explicitly derived from the governing equations (16) by

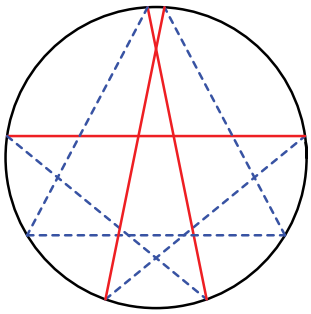

Figure 4. Example of a periodic orbit undergoing ray splitting (in a disc with $c_p/c_s = 3.61$); solid line (red): s-wave, dashed line (blue): p-wave. The orbit shown here has eight bounces and winds around three times.

Tanner and Søndergaard (2007) employing methods similar to those used in (Bogomolny and Hugues 1998). The resulting transfer operator is now a matrix kernel, but otherwise similar to the scalar case (41). In two dimensions, it takes on the form

$$\boldsymbol{T}(s, s_0) = \frac{1}{\sqrt{2\pi \mathrm{i}}}\sqrt{\left|\frac{\partial^2 L}{\partial s \partial s_0}\right|}\boldsymbol{\alpha}(s, s_0) \cdot \begin{pmatrix} \sqrt{k_p}\,\mathrm{e}^{\mathrm{i}k_p L} & 0 \\ 0 & \sqrt{k_s}\,\mathrm{e}^{\mathrm{i}k_s L} \end{pmatrix}, \tag{56}$$

where $L(s, s_0)$ is the length of a ray segment from boundary points $s_0 \to s$ and α is the 2×2 matrix of reflection coefficients (23) for free boundary conditions. The trace formula (55) can then be derived by stationary phase approximation.

A serious discussion on the interplay between eigensolutions of the Navier–Cauchy equation in finite elastic bodies and the underlying classical ray dynamics including ray splitting is still in its infancy. Two geometries considered in more detail are circular boundaries in two dimensions and rectangular bodies in two or three dimensions.

Circular geometries. For a circular disc, the wave equation is still separable in cylindrical coordinates (Søndergaard and Tanner 2002); from a ray dynamics point of view, this means that the angular momentum is a conserved quantity also under mode conversion. The dynamics is thus integrable in each component; transitions between a shear and pressure torus having the same angular momentum occur at impact with the boundary at a rate given by the square of the coefficients (23). The dynamics is equivalent to that of a simple two-leg quantum graph (Kottos and Smilansky 1997, 1999) with classical limit given in terms of a purely probabilistic two level Markov chain.

A trace formula for the elastic disc has been derived by Søndergaard and Tanner (2002) starting from the scattering matrix and using the so-called inside–outside duality (Smilansky 1994), that is, the scattering matrix $S(\omega)$ describing wave scattering from the exterior has a unit eigenvalue at an eigenfrequency ω of the interior problem. The oscillatory part of the density of states for this integrable problem reads

$$d_{\mathrm{osc}}(\omega) = \sqrt{\frac{a\omega}{\pi}}\sum_{\mathrm{po}}\frac{T_{\mathrm{po}}}{\sqrt{\frac{n_{\mathrm{p}}c_p}{\cos\theta_p^{po}} + \frac{n_{\mathrm{s}}c_s}{\cos\theta_s^{po}}}}\sum_{r=1}^{\infty}\frac{\alpha_{\mathrm{po}}^r}{r^{3/2}}\cos[r(\omega T_{\mathrm{po}} - n_{\mathrm{po}}\pi/2) + \pi/4], \tag{57}$$

where n denotes the number of bounces of a periodic ray which contains n_{p} segments of pressure polarized rays and n_{s} segments of shear polarized rays with $n = n_{\mathrm{p}} + n_{\mathrm{s}}$ and T_{po} is the period of a periodic ray. For an example of such an orbit see figure 4. The fluctuations are enhanced by a factor of $\sqrt{\omega}$ here, compared to semiclassical periodic orbit contributions for

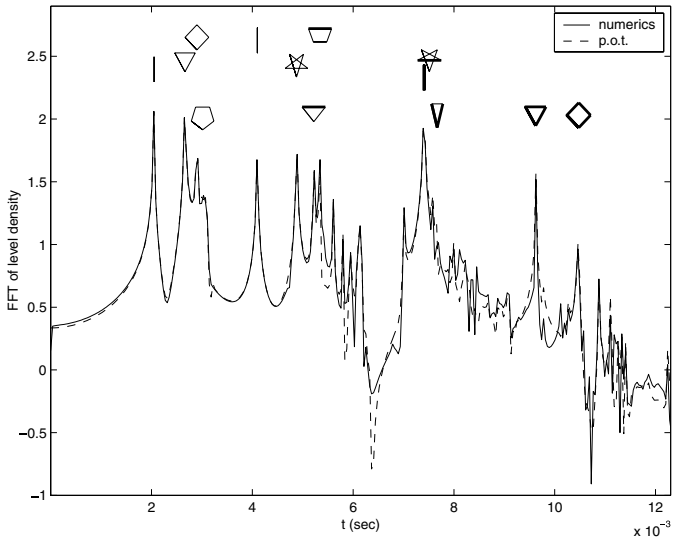

Figure 5. Fourier transform of spectral fluctuations in an elastic disc (Søndergaard and Tanner 2002). Thin/thick lines: longitudinal/transverse polarization. Peaks corresponding to ray-splitting orbits can be identified.

fully chaotic systems, (55); this is in accordance with the trace formula given by Berry and Tabor (1976, 1977a) for quantum systems with integrable classical limit. The total amplitude in (57) can again be decomposed into a geometric factor depending on the angles of incidence θ_p, θ_s and a mode conversion factor α_{po} similar to (55). The Fourier transformed density of states is depicted in figure 5 showing pronounced peaks at periodic rays including those undergoing mode conversion.

The N-disc scattering problem discussed in detail by Wirzba (1999) for the Helmholtz equation has been adapted for elasticity by Søndergaard (2001) and Wirzba *et al* (2005). In this context, the wave dynamics is that of an infinite plate with N circular holes governed by the vectorial PDE (16). The determinant of the scattering matrix for the full system can be given in a form similar to (39); the poles of the S matrix are expressed in terms of the zeros of a zeta function given here as the determinant of an inter-disc scattering matrix. It can be written in semiclassical approximation as a product over periodic orbits of the scattering problem. Søndergaard (2001) and Wirzba *et al* (2005) studied the two-disc problem in more detail, both numerically and semiclassically. In this system, there is only one geometric periodic orbit supporting both polarizations. In addition, there are diffractive or creeping waves, also called Franz resonances, (Franz 1954, Keller and Karal 1964) which also exist in the Helmholtz case (Vattay *et al* 1994) giving rise to an exponentially decaying surface contribution. More importantly, weakly attenuated Rayleigh surface waves enter in the case of free boundary conditions giving rise to additional periodic orbit contributions consisting of segments of geometric and Rayleigh rays. The interplay between shear, pressure and Rayleigh contributions leads to a rather complicated resonance pattern for this simple problem (Wirzba *et al* 2005), especially when compared to the two-disc Helmholtz spectrum (Wirzba 1999). Further details on diffractive orbits are given in section 4.

Rectangular geometries. The coupling between shear and pressure modes lifts the translational symmetry in rectangular plates and blocks, and the wave equation (16) is no longer separable in Cartesian coordinates. Still, the periodic orbits of the ray dynamics are not geometrically

hyperbolic, that is, nearby trajectories of the same mode type separate at most algebraically. Rectangular bodies thus represent an interesting intermediate geometry where all the wave chaos (if it exists) must originate from mode conversion effects. Bohigas *et al* (1991) pointed out that finding RMT statistics in Weaver's early experiment (Weaver 1989a) is surprising in that sense; Weaver used aluminium blocks with slits cut into them for which the geometric ray-dynamics is at most pseudo-integrable (Richens and Berry 1981) and deviations from GOE[5] are to be expected (Bogomolny *et al* 1999, Bogomolny and Schmitt 2004). A more careful reanalysis of Weaver's original data (Delande *et al* 1994) showed good agreement with GOE as well as periodic orbit contributions on large spectral scales in agreement with semiclassical theories. This finding has furthermore been confirmed by more recent experiments on rectangular, fused-quartz plates (Schaadt *et al* 2001) and blocks (Schaadt *et al* 2003a); due to the enhanced number of resolved eigenfrequencies in the experiment, it could be verified that the spectral statistics coincides with a superposition of several independent GOE spectra (due to the discrete symmetries of the objects) and not a Poisson distribution as suggested in an earlier experiment by Ellegaard *et al* (1995). This is a clear indication of wave chaos behaviour. The result was surprising as the ray dynamics (including ray splitting) in rectangular geometries is not ergodic, that is, for all $\kappa > 1$ only a finite number of directions are explored by a given trajectory (Biswas 1996, Schaadt *et al* 2001, 2003a). Such a behaviour is typical for pseudo-integrable systems (Richens and Berry 1981). However, it has also been shown numerically, that the number of periodic rays increases exponentially (Biswas 1996), a phenomenon known only from classically chaotic systems.

The intermediate character of rectangular bodies is also revealed in the nodal line patterns measured by Schaadt *et al* (2001), Ellegaard *et al* (2001) and Schaadt *et al* (2003a) for in-plane modes of rectangular plates. A large number of wavefunctions show ergodic nodal line patterns such as the wave pattern at 556.5 kHz, 592.1 kHz, 599.0 kHz or 645.9 kHz in figure 6; they appear very similar to wavefunctions in fully chaotic geometries such as for quantum billiards with Sinai or stadium-shaped boundaries or flexural eigenmodes in stadium-shaped plates such as shown in figure 16 (Ellegaard *et al* 2001, Schaadt *et al* 2003b). Besides, one finds regular patterns in figure 6 similar to the chequer-board patterns observed for flexural modes in rectangular plates such as shown in figure 17. Note, that the biharmonic equation (8) is separable for rectangular geometries having clamped boundaries, but that when all edges are free, the solution cannot be given in closed form but only as an infinite series expansion (Gorman 1978, 1982). Wavefunctions of the type shown in the first and the last row in figure 6 are reminiscent of so-called bouncing ball (bb) modes observed for, for example, the stadium Helmholtz billiard (Sieber *et al* 1993). The first row in figure 6 has indeed been identified mainly as shear type bb-mode whereas the last two rows have characteristics typical for pure pressure waves.

It is, however, not clear whether the ratio of regular to irregular modes vanishes asymptotically in elastic rectangles as it does in the stadium (Tanner 1997). This question is closely related to an extension of Shnirelman's theorem (Shnirelman 1974) to elastic wave equations (Weaver 1982, Akolzin and Weaver 2004). The precise nature of the wave chaos aspects found in rectangular elastic bodies is still an open question.

2.3. Ray-splitting billiards

Inspired by the theoretical study on ray propagation in elastic media by Couchman *et al* (1991, 1992), Prange *et al* (1996) and Blümel *et al* (1996a, 1996b) started to consider

[5] GOE statistics applies to eigenvalues of random, symmetric matrices reflecting the underlying time-reversal symmetry; for more details, see section 3.1.

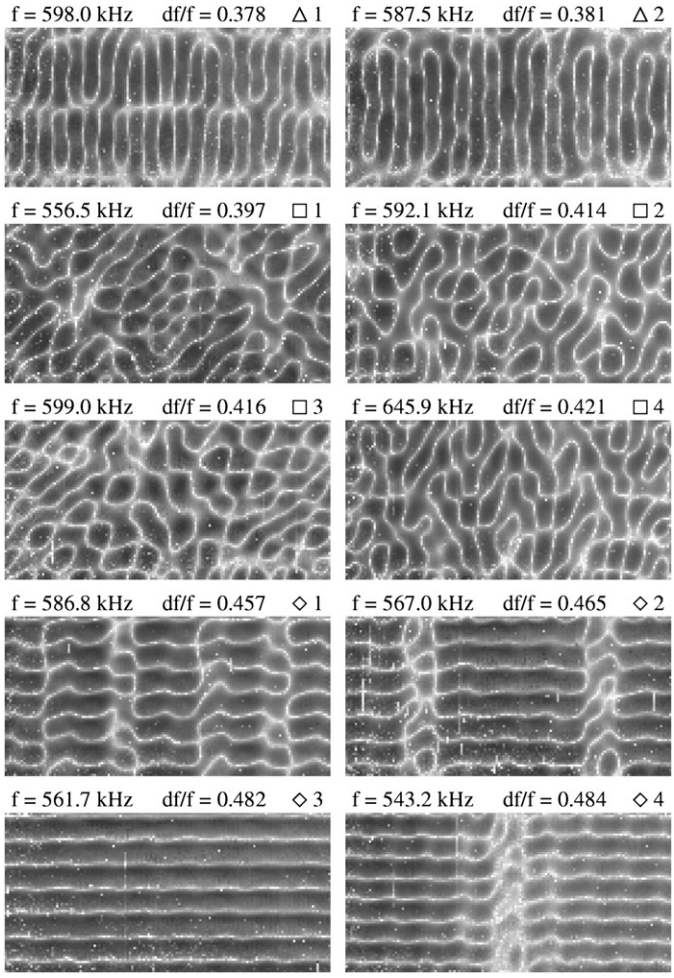

Figure 6. In plane modes for a rectangular plate of fused quartz; (the notation df/f refers to a frequency shift with respect to variations in temperature being different for longitudinal and transversal waves) (Schaadt *et al* 2001).

dynamical systems with ray splitting associated with scalar wave equations. Ray splitting occurs generally at interfaces at which the wave velocity $c(r)$ changes discontinuously (that is, fast on the scale of the wavelength considered). Possible realizations are quantum billiards with step potentials, see figure 7, or thin microwave cavities with abrupt changes in height or in the index of refraction. Thus, ray splitting does not require the underlying wave equation to be of vectorial nature.

The next-to-leading order terms in the Weyl expansion for ray splitting billiards have been derived by Prange *et al* (1996) and Kohler and Blümel (1998b) and experimentally verified by Vaa *et al* (2003). A systematic way to calculate higher order terms similar to the approach by Berry and Howls (1994) for the Helmholtz equation was discussed by Décanini and Folacci (2003). Blümel *et al* (1996a, 1996b) showed that ray splitting typically enhances the degree of chaos in the system; in their example, a circle billiard with a change in wave speed along the diameter was considered. The classical phase space is mostly chaotic which is reflected in the spectral statistics being close to GOE, see also Oertner *et al* (1996). A

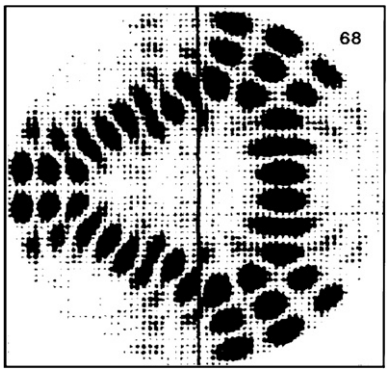

Figure 7. The 68th wavefunction in a disc billiard with potential step exhibiting ray splitting (Blümel *et al* 1996a, 1996b).

modified transfer operator of the form (41) including ray splitting amplitudes was derived by Blümel *et al* (1996a, 1996b) and generalized trace formulae were deduced and applied to the circular billiard. Diffractive contributions along the wave-splitting boundary (lateral orbits) were considered and discussed in more detail by Kohler and Blümel (1998a). A numerical test of the semiclassical formulae has been performed in (Kohler and Blümel 1999). An experimental realization of a ray splitting billiard was first presented by Sirko *et al* (1997) and Bauch *et al* (1998); the eigenfrequencies of thin microwave cavities of stadium and rectangular shape were measured using dielectric (Teflon) and metal bars as ray-splitting interfaces. Periodic orbits introduced through ray splitting could be identified in the Fourier transformed spectrum. In a similar experiment, Schäfer *et al* (2001) measured both the eigenfrequencies and wavefunctions in a rectangular cavity with a circular Teflon scatterer—a ray-splitting Sinai billiard. Scars along ray-splitting orbits have been observed, see figure 8.

Kohler *et al* (1997) considered the influence of a ray splitting barrier on the dynamics of a class of triangular billiards. They demonstrated that the dynamics, which is integrable or pseudo-integrable without ray splitting, becomes completely chaotic. This provided for the first time an example of strong chaos induced by ray splitting alone. Similar observations were made for rectangular elastic bodies, see section 2.2.3. The equivalence between one-dimensional ray-splitting billiards and two-state quantum graphs were pointed out by Dabaghian *et al* (2001); this is in analogy to the connection between in-plane modes of circular elastic plates and quantum graphs as discussed by Søndergaard and Tanner (2002), see section 2.2.3.

2.4. Time-reversal imaging

Time-reversal invariance together with the linearity of the wave equations gives rise to remarkable effects of which weak localization, discussed in more detail in section 3.1.5, and *time-reversal imaging* (TRI) are the most prominent once. We will briefly summarize the ideas behind TR techniques here and highlight some of the main results; for a more comprehensive overview, see the review papers by Fink (1997) and Fink *et al* (2000).

In a time-reversal experiment, a medium is typically excited by a short pulse at a source point $\mathbf{r}_0$ at time $t = 0$ and the resulting wave field is measured at one or several receiver points $\mathbf{r}$, see figure 9. It is important that the time dependence of the signal is fully resolved, that is, that both the intensity and the phase is recorded. For acoustic signals with frequencies in

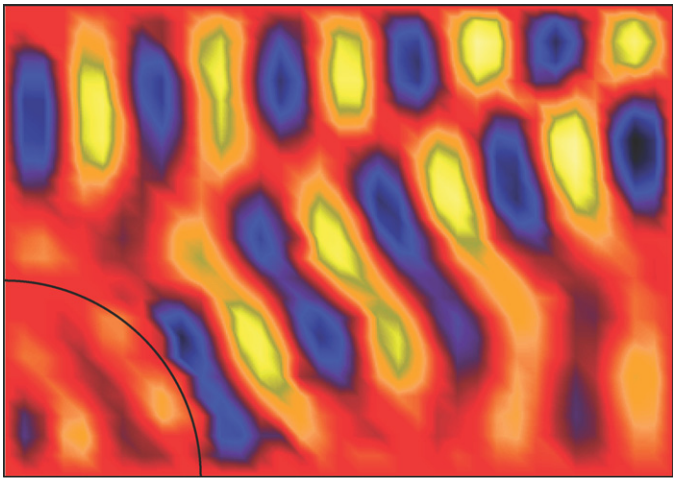

Figure 8. Wavefunction in a Sinai-type microwave billiard with circular Teflon scatterer. Teflon acts as a potential step producing ray splitting; scarring and transmission into the Teflon disc can be observed (Schäfer *et al* 2001).

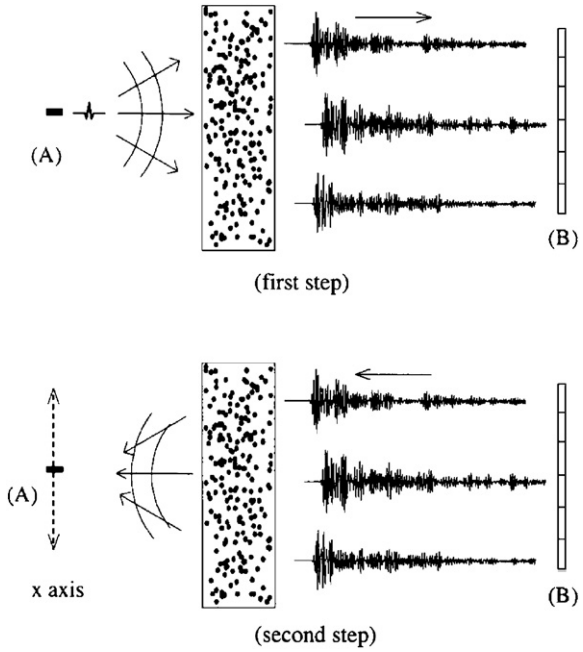

Figure 9. Typical setup for a time-reversal experiment; in a first step the source (A) transmits a short pulse that propagates through the rods. The scattered waves are recorded on a 128-element array (B). In the second step, the 128 elements retransmit the time-reversed signals through the rods. The piezoelectric element (A) is now used as a detector and can be translated along the x direction (Fink *et al* 2000).

the MHz range, standard transducers can achieve this easily; the same is non-trivial for, for example, optical signals. (A technique similar to TRI used in optics is *phase conjugation*, where a time-reversal effect is achieved by reversing the sign of the phase; for similarities

and differences of both techniques, see the discussion by Fink *et al* (2000) and Derode *et al* (2001).) A stretch of the signal in a time interval $[t_0, t_1]$ is then time reversed electronically and fed back into the system, typically at the receiver point. Starting the time measurement at $-t_1$, the resulting wave field combines and forms a localized peak of high intensity at the source point at $t = 0$.

Interpreting the effect in a ray picture, wave energy is transported along classical rays from $\mathbf{r}_0 \to \mathbf{r}$ and the signal at the receiver position $\mathbf{r}$ is a coherent superposition of waves having the same arrival time. The time-reversed signal thus produces wave fronts which travel back along the ray paths from $\mathbf{r} \to \mathbf{r}_0$ and interfere constructively at the source point $\mathbf{r}_0$ at time $t = 0$. In an ideal TR experiment, the signal is recorded over a closed surface surrounding the source thus retaining the full information of the wave field. But even if only parts of the wave field are recorded by for example, an array of receivers—a time-reversal mirror (TRM)—there is always a coherent part of the time-reversed field which will refocus at the source point. In addition, there is now a reproducible background field due to wave fronts launched at angles not reversing the original ray path from source to receiver.

Derode *et al* (1995, 1998) demonstrated experimentally the robustness of the effect in the presence of multiple scattering by sending an acoustic underwater pulse through a layer of 2000 randomly distributed steel rods. After recording the diffusive signal by a TRM and resending the time-reversed signal through the layer, a TR peak could be produced. Chaotic scattering leads to an effective enhancement of the aperture of the device due to ray paths reaching the source/receiver which would have been lost without the scatterers. The resolution of the peak is significantly better compared to TRI without scattering medium and is independent of the length of the time window $t_1 - t_0$ as long as the window is taken in the diffusive regime produced by multiple scattering events. When choosing a periodic array of scatterers, however, hyper-focusing is not observed (Tourin *et al* 2006) and the spatial resolution of the TR peak is the same as that without a scattering medium, limited by the size of the TRM alone. Chaos thus enhances the resolution of the signal!

It came as a surprise that wave dynamics is so stable under a time-reversal operation in a chaotic scattering environment whereas the corresponding ray dynamics is unstable and thus sensitive to small perturbations. Snieder and Scales (1998) point out that interference acts as a filter singling out the 'good' rays while other paths give rise to an incoherent background signal only. They show furthermore that the system is indeed exponentially unstable, but with respect to changing the positions of the scatterers before applying the time-reversed signal. The authors consider in fact the fidelity of the wave system (without mentioning this); their findings are in agreement with the theory outlined in section 2.5 such as the arguments given by Cerruti and Tomsovic (2002) based on Lagrangian manifold techniques and also discussed in the context of underwater acoustics in section 2.6. The overall properties of TRM have been studied in detail in (Derode *et al* 2001). It is shown experimentally, that the hyper-focusing property of the TR peak saturates and that side lobes appear when increasing the width of the scattering layer. It is suggested that the additional side peaks are caused by correlations in the arrival time distributions for paths from $\mathbf{r}_0 \to \mathbf{r}$ due to, for example, crossing of scattering paths. Such correlations have been shown to be of importance in a semiclassical description of the universality of spectral statistics (Sieber and Richter 2001, Sieber 2002, Berkolaiko *et al* 2002, 2003, Heusler *et al* 2004, Müller *et al* 2004, 2005, 2007), see section 3.1. Applying a TR process is indeed equivalent to measuring the auto-correlation functions of the Green function, that is, the signal $s(t)$ at the source point $\mathbf{r}_0$ after applying the TR signal is

$$s(t) = \sum_i \int_{-t_1}^{-t_0} \mathrm{d}\tau\, \hat{G}(\mathbf{r}_0, \mathbf{r}_i, \tau)\hat{G}(\mathbf{r}_0, \mathbf{r}_i, t + \tau), \tag{58}$$

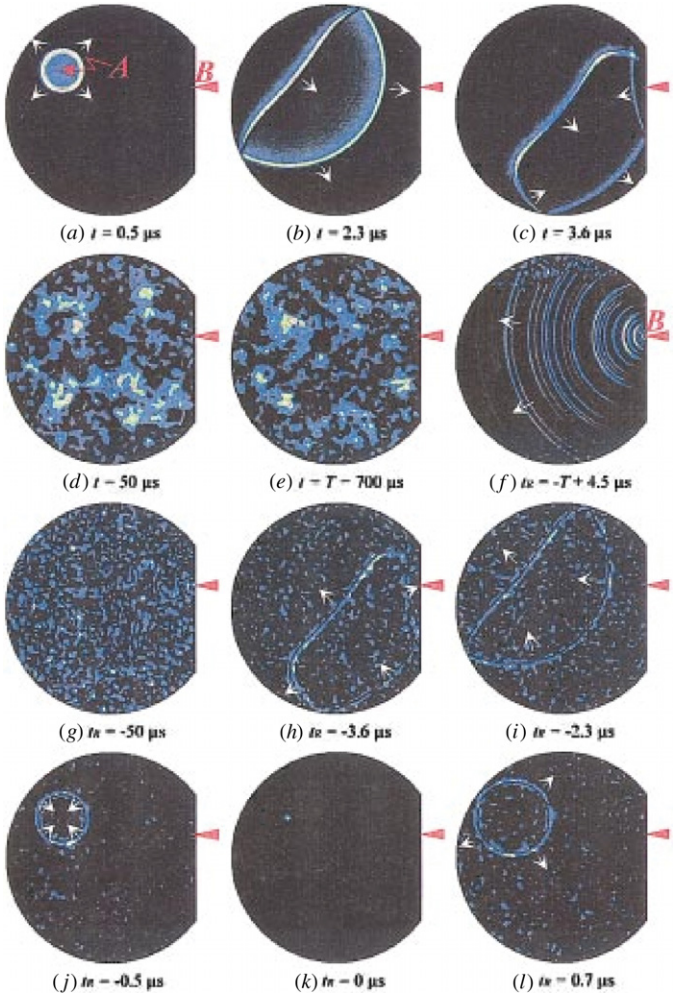

Figure 10. Numerical simulation of a one-channel time-reversal experiment; from (Draeger and Fink 1997): (*a*)–(e) injection of a short pulse in A and recording in B; (*f*)–(*l*) emission of the time-reversed signal in B and refocusing in A. Reprinted with permission from the American Physical Society.

where $\hat{G}$ denotes the time-dependent Green function defined in (25) and the summation is taken over the receiver positions i; furthermore, the symmetry $\hat{G}(\mathbf{r}_0, \mathbf{r}, t) = \hat{G}(\mathbf{r}, \mathbf{r}_0, t)$ is used. It is shown that the number of transducers does not affect the spatial resolution, but enhances the signal-to-noise ratio up to a saturation level. TRI is closely related to another wave effect, namely recovering the Green function from cross-correlation signals as discussed in section 3.1.4; this link has been worked out in detail in (Derode *et al* 2003a, 2003b).

Draeger and Fink (1997) demonstrate that TRI works also in a chaotic cavity using a single transducer. Here, the wave field in a mono-crystalline silicon wafer is excited at a source point by a short pulse and is measured at a single point on the boundary; see figure 10 for a numerical simulation. The time-reversed and re-emitted signal focuses at the source point with a signal-to-noise ratio proportional to the time window $\Delta T = t_1 - t_0$. Chaos in the underlying ray dynamics is essential as it leads to a fast equidistribution of the wave

field making single channel TRI possible—the technique does indeed not work for rectangular cavities. The theory behind TRI in closed domains has been developed by Draeger and Fink (1999). For chaotic cavities, the so-called cavity equation holds

$$s(t) = \int_{-t_1}^{-t_0} \mathrm{d}\tau\, \hat{G}(\mathbf{r}_0, \mathbf{r}, \tau)\hat{G}(\mathbf{r}_0, \mathbf{r}, t+\tau) \tag{59}$$

$$= \int_{-t_1}^{-t_0} \mathrm{d}\tau\, \hat{G}(\mathbf{r}_0, \mathbf{r}_0, \tau)\hat{G}(\mathbf{r}, \mathbf{r}, t+\tau), \tag{60}$$

that is, the signal $\hat{G}(\mathbf{r}_0, \mathbf{r}_0, t)$ emanating from and refocusing at the source $\mathbf{r}_0$ is convoluted by the signal at the receiver position $\mathbf{r}$. Side lobes, observed also in cavity TRI, can be related to correlations between the travel times entering $\hat{G}(\mathbf{r}_0, \mathbf{r}_0, t)$ and $\hat{G}(\mathbf{r}, \mathbf{r}, t)$ which are of the order of the mean travel time between two reflections on the boundary. Information loss thus happens entirely at the receiver point due to undirected remission. In an experimental study carried out by Draeger *et al* (1999), the refocused wave field of the bending modes of a silicon plate is measured using laser interferometry. The influence of the time window ΔT on the peak to side lobes as well as peak to noise levels is studied confirming a saturation regime for the former and linear increase for the latter. Similar results are obtained in time-reversal experiments in elastic solids by Sutin *et al* (2004) using doped glass and Berea sandstone. Neither strong mode conversion leading from a pressure dominated early signal to a shear wave dominated coda, nor the large difference in the attenuation properties of the two material influences the time-reversal properties significantly confirming theoretical considerations by Draeger *et al* (1997).

In a conventional TRI experiment, the time-reversal symmetry is actually broken as the energy inserted at time $t = 0$ is not taken out of the system after refocusing. This limits the resolution of the refocused peak to half a wavelength λ as the TR signal still consists of an incoming and outgoing wave at $t = 0$. de Rosny and Fink (2002) demonstrate that by applying a time-reversed pulse at $t = 0$, the size of the focus can indeed be decreased further; the pulse interferes destructively with the outgoing wave thus producing a sharp peak with focal spot size $\lambda/14$, see figure 11.

Just retaining the qualitative features of the phase of the time-reversed signal seems sufficient for TRI: in (Derode *et al* 1999), the signal was time reversed and only its sign was kept. This one-bit-digitized signal was then used instead and produced even sharper peaks with a signal-to-noise ratio lowered by 1.2 dB.

In a recent study by de Rosny *et al* (2004), it has been pointed out that an enhancement of the peak signal by a factor of 2 is observed when performing a TR experiment where source and receiver position coincide; signals travel back along two distinct paths from $\mathbf{r} \to \mathbf{r}$, namely the original ray and its time-reversed partner. This effect is reminiscent of coherent backscattering enhancement as discussed in section 3.1.5. de Rosny *et al* 2005 show, however, that there is a subtle, but important difference between these two effects. When performing an experiment in a rotating cylinder filled with water, coherent backscattering enhancement vanishes as the rotation frequency is increased from zero. The TR signal vanishes, however, only for $\mathbf{r} \neq \mathbf{r}_0$, but approaches a constant, but finite value for $\mathbf{r} = \mathbf{r}_0$. The enhancement of the TR signal at the source is here due to waves travelling along rays which return to the source point; these rays exist even when time-reversal invariance is broken making refocusing possible if $\mathbf{r}$ and $\mathbf{r}_0$ coincide.

The possibility of the detection of a noise source using TRI is discussed theoretically and studied experimentally by Ribay *et al* (2005). The time-dependent field amplitude produced by a noisy signal localized in space, but not in time, is recorded and time reversed. The TR

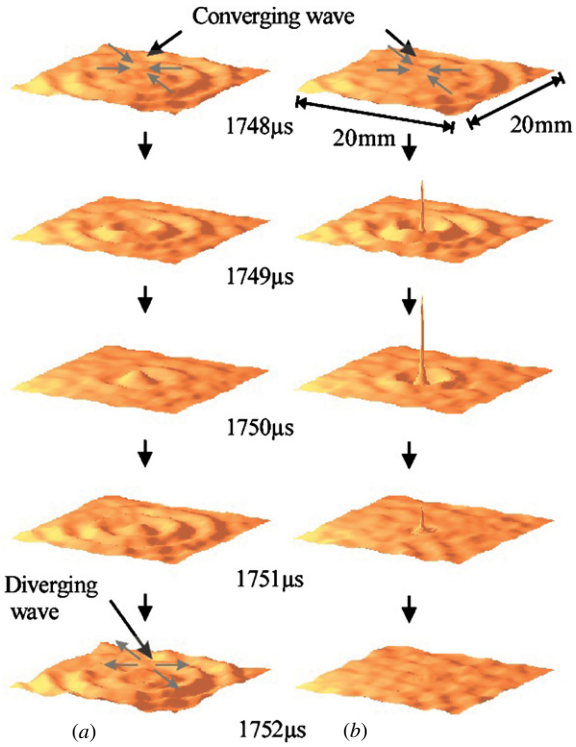

Figure 11. TRI experiment without (*a*) respective with (*b*) an acoustic sink (de Rosny and Fink 2002).

wave field shows an enhanced amplitude at the source point with a focus size $\lambda/2$. The signal-to-noise ratio depends only on the number of transducers used in the TRM. The possibility of separating two nearby noise sources is discussed. Applying TRI for acoustic communication has been explored by Heinemann *et al* (2002) and Derode *et al* (2003c); Heinemann *et al* (2002) use TRI to efficiently communicate a signal to a desired spot within a reverberant acoustic enclosure. Derode *et al* (2003c) showed that contrary to intuition, the capacity to transport information in form of acoustic signals is enhanced in a chaotic scattering medium compared to a ballistic channel due to the hyper-focusing property of TRI. Likewise TRI has been demonstrated with radio waves (Strohmer *et al* 2004, Popovski *et al* 2007).

2.5. Fidelity studies in elastodynamics

In recent years, studies of the stability of linear wave propagation under changes of the system parameters (in contrast to changes in the initial conditions) have found renewed interest in quantum mechanics in the context of quantum computation. A useful measure is here the *fidelity* (also referred to as Loschmidt echo) defined as (Peres 1984)

$$F(t) = |f(t)|^2; \qquad f(t) = \langle\psi|\hat{G}'(-t)\hat{G}(t)|\psi\rangle,$$

with $\hat{G}(t)$, $\hat{G}'(t)$ being the Green functions for two slightly different systems and $|\psi\rangle$ refers to the initial wave excitation at time $t = 0$; we use here Dirac notation, that is,

$$\hat{G}(t)|\psi\rangle \equiv \psi(\mathbf{r}, t) = \int \mathrm{d}\mathbf{r}_0\, \hat{G}(\mathbf{r}, \mathbf{r}_0; t)\psi(\mathbf{r_0}, 0).$$

Fidelity is obviously relevant for the applicability of TRI giving an estimate for how much the system can change between recording and re-emitting the signal.

Various time regimes have been identified: a perturbative regime with Gaussian decay for very short times is followed by an exponential decay with exponent obtained from time-dependent perturbation theory, the so-called 'Fermi golden rule' regime and for larger times by the classical Lyapunov exponent (Jalabert and Pastawski 2001, Jacquod *et al* 2001, Cerruti and Tomsovic 2002, Prosen and Znidaric 2002), see also Prosen *et al* (2003) for an overview. These predictions have been verified experimentally in a chaotic microwave cavity by Schäfer *et al* (2005). In the experiment, the cross-correlation function of a scattering matrix, that is, the signal transmitted and received at the input and output antenna with and without changing the cavity was measured. The correlation function is directly related to the fidelity $F(t)$. The theme has recently been picked up in seismology and elastodynamics: Snieder *et al* (2002) considered the influence of changes in the position of the scatters in a multiple scattering wave system. By working in the perturbative regime, estimates for the mean displacement of the scatterers can be inferred from the cross-correlation function; this has direct applications in seismology for monitoring small scale movements due to for example temperature changes in the earth crust. In an experiment similar in spirit by Lobkis and Weaver (2003), an aluminium block was excited by a short pulse and changes in the output signal under changes in temperature were recorded. The experiment of Lobkis and Weaver (2003) has been reconsidered by Gorin *et al* (2006) in the context of fidelity theory. The cross-correlation function used in (Lobkis and Weaver 2003) was shown to coincide with the fidelity and the distortion coefficient measured is related to the exponent found in the Fermi golden rule regime. Good agreement with RMT results were found both for irregularly shaped blocks as well as a rectangular block. The latter came as a surprise, again underlining the 'chaotic' nature of rectangular geometries in elasticity, see section 2.2.3.

2.6. Wave chaos in underwater acoustics

The influence of wave chaos effects in acoustics has been discussed in some detail in the context of sound transmission in oceans, see Brown *et al* (2003), Beron-Vera *et al* (2003) for comprehensive overviews. In 1948, Ewing and Worzel (1948) discovered the existence of a sound channel in mid-latitudes at an ocean depth of about 1 km; this channel guides sound waves over ranges of several thousands of kilometres. It arises from the depth dependence of the wave velocity which decreases in the upper ocean layers due to typical changes in temperature and salinity, but increases again in the deep ocean region where the rising water pressure becomes the dominant factor. Sound rays bend towards smaller wave velocities, see equation (5), and rays emanating in forward direction start to oscillate around the sound speed minimum without touching the strongly attenuating sea bed or the ocean surface (acting as a random scatterer). For a detailed account of the physics behind wave velocity profiles in oceans, see Flatté *et al* (1979) or Kuperman and Jackson (2002). Recent experimental results on acoustic wave transport over a 3250-km range can be found in (Worcester *et al* 1999, Colosi *et al* (1999)).

By employing so-called parabolic approximations of the wave equation valid for small angle scattering, the three-dimensional Helmholtz equation describing acoustic wave propagation in water can be written in form of a one-dimensional time-dependent Schrödinger equation; here, the range r, that is the distance from source to receiver, takes on the role of a fictitious 'time' and the depth $z < 0$ below sea-level acts as the other variable, see Tappert and Brown (1996), Virovlyansky and Zaslavsky (1999) and references therein. (Castor *et al* (2004) discuss wave propagation including nonlinear terms in the wave equation). Assuming

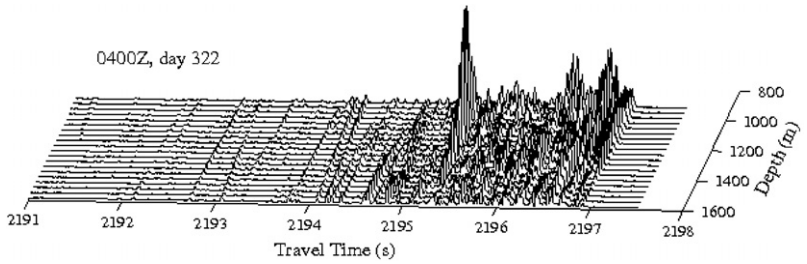

Figure 12. Time front measured at a vertical line array stationed near Hawaii. Peak intensity was obtained as function of ocean depth and travel time of the signal (Worcester *et al* 1999, Colosi *et al* (1999)).

a range-independent velocity profile, that is, setting $c(\mathbf{r}) = c_M(z)$, leads to a one-dimensional Helmholtz equation (1) and the resulting ray dynamics is integrable; a realistic c_M profile has been given by Munk, see Flatté *et al* (1979). On the other hand, Tappert and co-workers pointed out (Smith *et al* 1992) that range-dependent velocity profiles

$$c(r, z) = c_M(z) + \delta c_{\mathrm{fl}}(z, r)$$

lead to an in general chaotic ray dynamics with possible implications for the stability of an analysis of acoustic signals in terms of ray or wave travel times (Tappert and Brown 1996, Virovlyansky and Zaslavsky 1999). The fluctuations δc_{fl} are caused by, for example, water waves on scales of 10^2–10^4 m and mesoscale inhomogeneities such as synoptic eddies on scales of 10^4–10^5 m (Colosi and Brown 1998). The instability in the ray dynamics turned out to be a less serious problem than anticipated. Finding relevant ray contributions corresponds to solving a boundary value problem, that is, finding a trajectory travelling from a source point $\mathbf{r}_0$ to a receiver point $\mathbf{r}$ in time t; while individual trajectories with the same initial condition will deviate exponentially under a perturbation of the system, the same is not the case for solutions to the boundary problem. In fact, Cerruti and Tomsovic (2002) and Brown *et al* (2003) point out that the Lagrangian manifold associated with the initial conditions $\mathbf{r}_0$ fixed, $\mathbf{p}$ arbitrary, is structurally stable under perturbations. Similar observations have been made by Mazur and Gilbert (1997) using variational methods based on Fermat's principle and Collins and Kuperman (1994) using boundary value techniques. This theme has also been discussed in the context of time-reversal imaging and fidelity, see sections 2.4 and 2.5. In underwater acoustics, stability is furthermore added to the classical ray dynamics by intermittency effects and large scale dynamical structures such as can-tori near stable islands; they dominate in particular the rays contributing to early arrival times (Brown *et al* 2003).

In recent years the discussion has centred on a wave description of underwater signals. While early arrival times in the signal measured by Worcester *et al* (1999) and Colosi *et al* can be assigned to individual ray trajectories, long time signals are dominated by interference effects strongly affected by range-dependent fluctuations, see figure 12. Smith *et al* (1992) coined the term *wave chaos* in the context of underwater acoustics. The connection to quantum chaos was established in more detail in the late 1990s. Virovlyansky and Zaslavsky (1999) and Virovlyansky (2000) related the wave propagation to a ray dynamics by expanding the wave front in terms of modes (or eigenfunctions) of the unperturbed problem using classical perturbation theory and action-angle variables in the z coordinate. The onset of chaos in terms of Chirikov's criterion, see Chirikov (1979), was also discussed. Wave packet dynamics was studied in terms of Husimi-distributions by Sunaram and Zaslavsky (1999) and Smirnov *et al* (2005). (The Husimi distribution is a phase-space representation of a wavefunction frequently employed in the quantum chaos, see for example Takahashi and Saito (1985), Lee (1995)).

Mirroring the debate in quantum chaos (Sepúlveda *et al* 1992, Tomsovic and Heller 1993), the time horizon for a break-down of semiclassical approximations has been discussed; it has been suggested that the log time, that is, the time at which semiclassical expressions develop singularities due to caustics in chaotic systems, is not a limiting time scale. Wolfson and Tomsovic (2001) pointed out that interference can be well described by semiclassical expressions containing sums over classical paths. It is noted, however, that the number of contributing trajectories increases exponentially with time in chaotic systems and semiclassical approximation become impractical for long time scales (Virovlyansky 2000), see section 2.1. Mixed phase-space structures typical for ocean environments (Smirnov *et al* 2001) lead to an enhancement of stability of wave mechanical propagation. These effects explain naturally the stability of the wave patterns for early arrival times as well as the log-normal distribution seen in the late arrivals measured by Worcester *et al* (1999) and Colosi *et al* (1999), see also Brown *et al* (2003) and Beron-Vera *et al* (2003). Recently, Hegewisch *et al* (2005) pointed out that the fluctuations δc_{fl} in the wave-speed profile need to be taken only up to scales of the order of the (mean) wavelength; including higher order terms leads to enhanced ray chaos which in turn results in a higher density of caustics; these semiclassical singularities need to be smoothed out by for example uniform approximations thus leading to an effectively smoothed wave-speed potential.

In separate developments, aspects of time-reversal imaging, phase conjugation and cross-correlation functions have been discussed and experimentally tested in the underwater acoustics community. Time-reversal imaging as introduced in section 2.4 has been demonstrated experimentally and numerically in an underwater waveguide by Roux and Fink (2000). Recently, Roux and Kupermann (2005) show, that it is possible to extract information about ocean wave fronts from noisy data sets by combining TRI methods with cross-correlation function techniques as discussed in section 3.1.4. For a comprehensive overview on applications of TRI in underwater acoustics, see Kuperman and Jackson (2002). In a series of further experimental, theoretical, and numerical studies (Roux and Fink 2003, Roux *et al* 2004, Sabra *et al* 2005), the connections between cross-correlation functions and Green functions have been investigated in ocean acoustics, see section 3.1.4 for details.

3. Wave dynamics—statistical approaches

Analysing wave signals in terms of statistical measures has a long tradition in acoustics predating the developments in quantum chaos and even the discovery of quantum mechanics itself; a historical account is given in section 3.2. Recent advances in using statistical methods are largely based on applying random matrix theory (RMT) to wave problems in the presence of wave chaos and disorder. This connection was first discussed by McDonald and Kaufman (1979, 1988), Casati *et al* (1980), Berry (1981) and Bohigas *et al* (1984) in a quantum context and introduced into acoustics in a pioneering study by Weaver (1989a). We review the relation between RMT and eigenmode spectra, wavefunctions, correlation functions and weak localization phenomena in section 3.1. For open systems with energy loss through absorption or other decay channels, decay time distributions and a statistical description of power transfer are typically considered in acoustics and elastodynamics, see section 3.2. A statistical technique widely used in the engineering community to estimate vibrational energy transfer between parts of complex build-up structures, *statistical energy analysis*, will be briefly introduced in section 3.3.

3.1. Random matrix theory

Since the early work by Wishart on multivariate statistics (Wishart 1928), random matrix theory has grown into an industry with applications ranging from condensed matter physics, QCD, integrable systems, quantum and wave chaos, wireless communication, uncertainties in structural dynamics, numerical linear algebra, signal processing and information theory to number theory and free probability theory. We refer the interested reader to the excellent textbooks and review articles highlighting the mathematical (Mehta 1991, Forrester *et al* 2004), physics (Efetov 1997, Guhr *et al* 1998, Haake 2001) and electrical engineering and telecommunication (Tulino and Verdú 2004) aspects of the theory. We start by giving a brief introduction of RMT before discussing the experimental and theoretical results on spectral statistics in acoustics and elasticity. We consider in this section mostly systems for which attenuation can be neglected; we come to a statistical treatment of open systems and transport problems in section 3.2.

3.1.1. Introductory remarks. Random matrix theory deals with statistical properties of ensembles of random matrices. In the context of spectra of self-adjoint operators, one considers mostly ensembles of so-called Gaussian–Wigner matrices, that is, Hermitian $N \times N$ matrices $\mathbf{H}$ with independently Gaussian distributed variables $H_{ij}, i \geqslant j$ with unit variance. One distinguishes in particular the *Gaussian unitary ensemble* (GUE) of general hermitian matrices, the *Gaussian orthogonal ensemble* (GOE) of real symmetric matrices and the *Gaussian symplectic ensemble* (GSE) of Hermitian matrices invariant under symplectic transformations. The physically most important ensembles are the GUE associated with wave operators with broken time-reversal symmetry and GOE for systems which are time-reversal invariant. The latter is the norm for classical wave equations and will thus be considered from now on. Notable exceptions have been presented by Stoffregen *et al* (1995) and Schanze *et al* (2001), where the breaking of time-reversal symmetry has been achieved in microwave experiments by inserting ferrite into the cavity; however, at the price of strong absorption. For an overview over other matrix ensembles considered in the literature, see for example Tulino and Verdú (2004) and, in the context of vibrational dynamics, the work on uncertainties in structural dynamics by Soize (2003, 2005). Often also the ensemble of real diagonal matrices with random entries is considered which yields trivially a Poisson distribution for the eigenvalues.

For the Gaussian ensembles mentioned above, the joint probability distribution for the eigenvalues can be given explicitly and from there, many statistical properties can be deduced analytically. We mention here only two popular statistical measures: these are the two-point correlation function $R_2(x)$ measuring spectral correlations over a distance x and the nearest neighbour spacing (NNS) distribution $P(s)$ expressing the probability distribution for the distance between two adjacent eigenvalues of the ordered spectrum. After rescaling the spectrum to a mean eigenvalue density one, one obtains for the GOE ensemble

$$\begin{aligned} R_2(x) &= 1 - s^2(x) - \left(\int_x^\infty s(x')\,\mathrm{d}x'\right)\left(\frac{\mathrm{d}}{\mathrm{d}x}s(x)\right) \\ &= \frac{\pi^2}{6}x - \frac{\pi^4}{60}x^3 \cdots \qquad \text{for} \quad x \ll 1 \end{aligned} \tag{61}$$

with

$$s(x) = \frac{\sin \pi x}{\pi x}.$$

The correlation function vanishes linearly for $x \to 0$ indicating linear repulsion between nearby eigenvalues. Also the Fourier transformed $\hat{Y}(\tau)$ of the level cluster function

$Y(x) = 1 - R_2(x)$, the so-called form factor, is considered, often written in the form (here for GOE):

$$K(\tau) = 1 - \hat{Y}(\tau) = \begin{cases} 2\tau - \tau \ln(1+2\tau) & \text{for} \quad 0 \leqslant \tau \leqslant 1 \\ 2 - \tau \ln \frac{1+2\tau}{1-2\tau} & \text{for} \quad 1 < \tau. \end{cases} \tag{62}$$

Note that $K(\tau) \sim 2\tau$ for $\tau \ll 1$ and approaches one for large τ. The NNS distribution, popular for comparing experimental and numerical results with theory, can not easily be written down in closed form (Mehta 1991). For the GOE case, it is well approximated by a Rayleigh distribution with variance $\sqrt{2/\pi}$, that is,

$$P(s) \approx \frac{\pi}{2} s \, \mathrm{e}^{-\frac{\pi}{4}s^2}. \tag{63}$$

Wigner obtained this as well as the results for the unitary and symplectic ensemble by carrying out the calculations for 2×2 matrices. The remarkable level of coincidence with the true distribution in all three cases gave rise to the name 'Wigner surmise' for this kind of approximation. Note that the level repulsion is again linear for small s. For comparison, a randomly distributed spectrum following a Poisson process yields

$$R_2(x) = 1; \qquad K(\tau) = 1; \qquad P(s) = \mathrm{e}^{-s}. \tag{64}$$

Main parts of the theory were worked out in the 1950s and 1960s by Wigner, Dyson, Gaudin, Mehta and others, see Forrester *et al* (2004) for a brief historical overview and relevant references. In its early stages, it was mainly motivated by modelling properties of excited states of atomic nuclei, then perceived as an intractable, complex many-body system with largely unknown forces. It emerged in the early 1980s, that it is the complexity of the underlying classical dynamics and not the many-particle aspect alone, which is captured by random matrix ensembles (McDonald and Kaufman 1979, 1988, Casati *et al* 1980, Berry 1981); this was expressed explicitly by Bohigas *et al* (1984) conjecturing that the spectra of quantum systems whose underlying classical dynamics is chaotic generically have statistical properties following RMT. A couple of years earlier, it was argued by Berry and Tabor (1977b) that quantum systems with integrable classical limit behave generically like a Poisson process. Hannay and Ozorio de Almeida (1984) and Berry (1985) obtained the asymptotics of the form factor for individual wave chaotic systems coinciding with the RMT result (62) by starting from Gutzwiller's semiclassical periodic orbit formula (34). Recently, the power series expansion of the form factor could be reproduced using periodic orbit correlations in fully chaotic systems. Starting from the τ^2 term (Sieber and Richter 2001, Sieber 2002), the full expansion for $K(\tau)$ first for $\tau < 1$ (Heusler *et al* 2004, Müller *et al* 2004, 2005) and later also for all τ (Heusler *et al* 2007) has been worked out. Equivalent results for quantum graphs as introduced by Kottos and Smilansky (1997, 1999) have been obtained by Berkolaiko *et al* (2002, 2003) which in addition provide bounds for the border of the universal regime, see also Tanner (2001). For quantum graphs, the random matrix conjecture could be confirmed using super-symmetric techniques (Gnutzmann and Altland 2004, 2005).

Statistical measures related to parametric changes in the eigenfrequency spectrum have been discussed at some length in the context of elastodynamics. Changing the properties of an elastic or reverberant body as a function of a parameter t describing for example changes in the volume, the shape or the elastic parameters of the body leads to variations in the eigenfrequencies; an example is shown in figure 13 for a plate where one of the sides was shortened and the relevant parameter $t \equiv X$ is the mass of the total plate (Schaadt and Kudrolli 1999). After rescaling the spectrum to mean level density one (for each t) and normalizing the parameter according to $\tau = \sigma t$ with $\sigma^2 = \langle (\mathrm{d}x/\mathrm{d}t)^2 \rangle$ with x, the rescaled eigenfrequencies, one considers the velocity and curvature distributions $P(v)$ and $P(k)$ with $v_n = \mathrm{d}x_n/\mathrm{d}\tau$ and

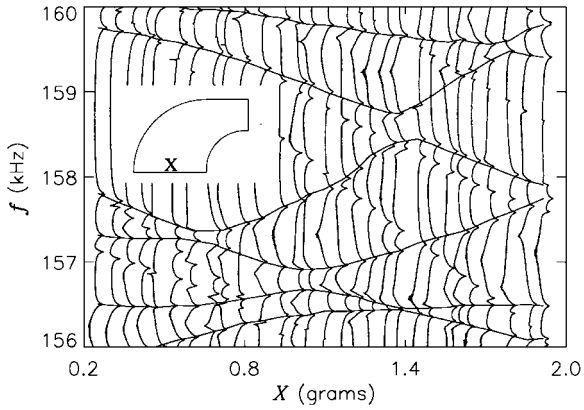

Figure 13. The transmission amplitude as a function of the frequency in steps of the parameter X. The flexural modes are joined by a solid curve to guide the eye. Other modes pass through the diagram without any interaction with the flexural modes. These are the in-plane modes, which are not included in the data analysis (see text). Inset: the shape of the Sinai–Stadium plate. The side which is polished to effect a parametric change is indicated by X (Schaadt and Kudrolli 1999).

$k_n = \pi^{-1}\,\mathrm{d}^2x_n/\mathrm{d}^2\tau$ of the parameterized eigenvalues x_n. RMT predicts a standard Gaussian distribution for $P(v)$ (Simons and Altshuler 1993) and

$$P(k) = \frac{1}{2}\frac{1}{(1+k^2)^{3/2}} \tag{65}$$

for the GOE ensemble (Zakrzewski and Delande 1993, von Oppen 1994, 1995 and Fyodorov and Sommer 1995). Another popular measure is the velocity autocorrelation function

$$c(\tau) = \left\langle \frac{\mathrm{d}x}{\mathrm{d}\tau_0}(\tau_0)\frac{\mathrm{d}x}{\mathrm{d}\tau_0}(\tau_0+\tau)\right\rangle \tag{66}$$

for which asymptotic results have been given by Szafer and Altshuler (1993), see also Bruus *et al* (1996). The results above apply to parametric changes under global perturbations; the case of localized perturbing potentials and the crossover regime is discussed in Marchetti *et al* (2003).

3.1.2. Spectral statistics in elastodynamics.

Spacing statistics. Eigenvalue spacing statistics has been considered in acoustic as early as 1946 (Bolt 1946a, 1946b, Schröder 1954a); actual experiments have been carried out by Schröder (1954b) measuring the spacing distribution for rectangular cavities and comparing the results with theoretical calculations predicting a Poisson process. In 1969, Lyon took up the subject in the context of the then emerging SEA theory and briefly discussed the Wigner surmise (63). However, based on the results of Schröder (1954b) and early data from spacing distributions in nuclei, he concluded that level repulsion may lead to a depletion of the distribution for small s, but that an exponential tail in $P(s)$ is generic—in contrast to the GOE result (63).[6] This point of view has dominated the acoustics literature until

[6] Such a behaviour is typical for pseudo-integrable systems (Bogomolny *et al* 1999, Bogomolny and Schmitt 2004); plates or other structures carrying waves in an engineering context often contain straight edges meeting at rational angles and may thus well be of pseudo-integrable type. The Poisson tail is easily destroyed, however, by e.g. wave-splitting effects (Kohler *et al* 1997).

recently, see for example (Fujisaka and Tohyama 2003). A systematic study of spectral statistics in acoustics and elastodynamics started with Weaver (1989a), who measured the eigenfrequency spectra of rectangular aluminium blocks using ultrasound detecting several hundred spacings. The discrete symmetries of the blocks were broken by cutting slits into the surface. Good agreement with GOE statistics was obtained, a result which was surprising at first; in the light of the RMT conjecture (Bohigas *et al* 1984), one may expect that a regular geometry such as an isotropic and homogeneous rectangular block would show deviations from GOE and tend towards a Poisson distribution. It was thus suggested by Bohigas *et al* (1991) and Delande *et al* (1994), that the slits act as defocusing elements effectively introducing ray and thus wave chaos. Indeed, early experiments on aluminium blocks without slits by Ellegaard *et al* (1995) seemed to indicate a Poisson spacing distribution. Subsequent measurements on eigenmodes in rectangular blocks (Schaadt *et al* 2003a) and for in-plane modes of rectangular plates (Schaadt *et al* 2001) revealed that the distributions are more in line with a superposition of k-independent GOE spectra; here, k counts the number of discrete symmetries with $k = 4$ for plates and $k = 8$ for blocks. The enhanced statistics in these experiments was achieved by using plates and blocks made of fused quartz with a Q value[7] of the order 10^5–10^6 compared to about 5×10^3 for the experiments by Ellegaard *et al* (1995) using aluminium. It is thus likely that the mixing between shear and pressure modes at the boundaries or likewise the ray-splitting dynamics alone introduces enough 'wave chaos' to ensure RMT statistics. The exact nature of the statistics of rectangular elastic bodies is still an open questions; it is linked to the features of the underlying ray-dynamics when including ray splitting as discussed in section 2.2.3.

Introducing a series of experimental innovations, the Copenhagen group led by Ellegaard managed to obtain spectra and wavefunctions of eigenmodes of elastic bodies with unprecedented accuracy. Details about the experimental set-up can be found in (Schaadt 2001). Effects due to symmetry breaking were considered, first in an aluminium block (Ellegaard *et al* 1995) and later in a block of anisotropic quartz (Ellegaard *et al* 1996). In both cases, an octant of a sphere was gradually removed from one of the corners of the blocks and a transition towards a single-GOE spectrum was observed. In the experiment by Ellegaard *et al* (1996) using anisotropic quartz, the original quartz block was cut such as to possess a single two-fold symmetry. By breaking this symmetry, details of the transition from two to one GOE could be studied. They were found by Leitner (1997) to be in good agreement with the theoretical predictions by Guhr and Weidenmüller (1990). Experiments with Sinai-shaped (aluminium) plates were conducted by Bertelsen *et al* (2000) and a transition from two to one GOE distributions was found after coupling in-plane and flexural modes by making cuts (of half the thickness of the plate) into the surface; the mean density for both mode types (as discussed in section 2.2.1) is approximately equal in the frequency range considered which explains the two to one transition. The two mode types can be distinguished in the spectrum by making use of the enhanced damping of flexural modes compared to in-plane modes under an increase in air pressure from vacuum ($<10^2$ Torr) to atmospheric pressure (Schaadt and Kudrolli 1999). Andersen *et al* (2001) varied the thickness of the plate slightly (by removing material from the surface with sandpaper) which led to a variation in the position of the resonance peaks; this made it possible to detect nearly degenerate eigenfrequencies and to obtain the full spectrum for both mode types without missing levels. By gradually making a single cut into the plate, the transition from two independent sub-spectra to one GOE spectrum was measured and reproduced in an RMT model. The flexural modes of a clover-shaped plate with C_{4v} were measured by Neicu *et al* (2001) and computed numerically (Brodier *et al*

[7] The Q value is defined as $Q = f/\Delta f$ where Δf is the mean width of a measured resonance.

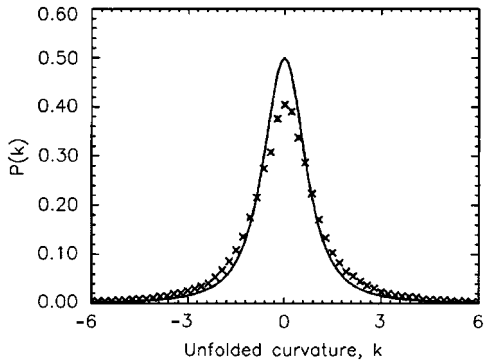

Figure 14. Experimentally obtained curvature distribution $P(k)$, (65), shown as crosses, and the analytical GOE result as a solid line. There is a deviation in the centre, whereas the tails agree well (Bertelsen *et al* 1999).

2001); the symmetry induces an exact degeneracy in the spectrum. A transition from an NNS distribution strongly peaked at $s = 0$, a so-called Shnirelman peak, to full GOE is observed when breaking the symmetry of the plate.

The statistical properties of the flexural modes of a stadium-shaped plates were modelled numerically using the biharmonic equation (8) (Legrand *et al* 1992, Bogomolny and Hugues 1998, Neicu *et al* 2001); irregularly shaped membranes including damping were considered by Burkhardt and Weaver (1996c). In all cases, good agreement with GOE was observed.

Parametric level variation. In 1999, the Copenhagen group presented two measurements of parametric correlations on elastic bodies, which showed significant deviations from RMT. Bertelsen *et al* (1999) measured the spectrum of a mono-crystalline quartz block having the shape of a 3D Sinai billiard as a function of an external parameter, in this case the temperature. The flexural eigenmodes of an aluminium plate were measured by Schaadt and Kudrolli (1999) while changing the length of one side of the plate. In both cases, deviations from the velocity and curvature distribution function (65) and velocity correlation function (66) were found, see figure 14 and figure 15. The NNS distributions coincided well with the GOE result in both cases. Statistical measures of parametric changes are known to be very sensitive to non-chaotic features in the underlying dynamics resulting in deviations from RMT. Non-universal curvature distributions were found for the Helmholtz equation by Takami and Hasegawa (1992) and Sieber *et al* (1995) and could be attributed to the bouncing-ball orbits in the stadium billiard. They vanished after eliminating this effect from the spectrum. Deviations from RMT found in microwave experiments (Barth *et al* 1999b) have been related to the locality of the perturbation introduced, see also Marchetti *et al* (2003). Such effects can, however, not explain the deviations from RMT in the Copenhagen experiments. The perturbations applied in both experiments act globally and bouncing ball contributions do either not exist (Schaadt and Kudrolli 1999) or have been accounted for (Bertelsen *et al* 1999). This is in contrast to the experiments on a clover-shaped fused-quartz plate by Neicu and Kudrolli (2002), where deviations in $c(\tau)$ for the flexural spectrum may be due to stable periodic orbits present in the system. Two further studies on ray-splitting billiards as discussed in section 2.3 tried to shed light on this issue. For two of the billiard problems considered, namely a ray-splitting annulus (Hlushchuk *et al* 2000) and a triangular billiard (Savytskyy *et al* 2000), strong deviations from RMT have been recorded. However, it is expected that in both cases, regions of stability exist which may account for the non-universal features.

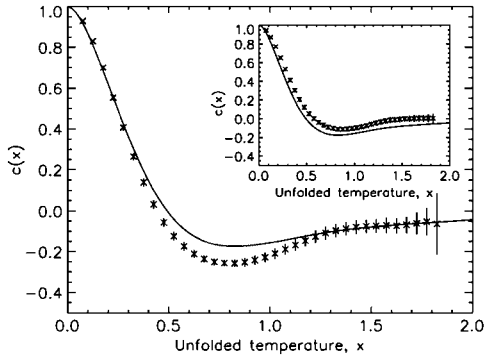

Figure 15. (Bertelsen *et al* 1999): Experimentally obtained velocity correlator $c(x)$ as crosses versus unfolded temperature x, compared with the numerical GOE result (Bruus *et al* 1996). There is a considerable deviation for medium values of x. As an inset, the experimental result for $c(x)$ is shown for the spectra from which the bouncing-ball-like modes have not been removed.

It was proposed that a hidden approximate symmetry may be responsible for the deviations from RMT in the elastic body measured by Bertelsen *et al* (1999); this could be due to non-complete coupling between transversal and longitudinal modes at the boundaries. In two theoretical studies, the effect of symmetry breaking on the curvature distribution $P(k)$ was studied; Hussein *et al* (2002) obtained the transition from two to one GOE numerically from a model Hamiltonian, while for a similar scenario the distributions were calculated analytically by Ergün and Fyodorov (2003). In the latter study, the tendency of having a higher probability for large curvatures when introducing symmetry—as displayed in figure 14—could be reproduced. However, the exact nature of the deviations from RMT in the experiments remains an open question.

3.1.3. Wavefunction statistics. The notion of random or diffusive wave fields in irregularly shaped reverberant bodies has played an important role both in acoustics and elastodynamics (Morse and Bolt 1944, Schröder 1959, Schröder 1962, Lyon 1969) and forms an integral part of statistical transport theories as discussed in section 3.3. In these theories, an equilibrium configuration is considered having its wave energy equipartitioned over the available (phase-space) volume. This principle has been shown to hold rigorously by Shnirelman (1974) stating that a generic eigenmode is equidistributed over ergodic components of the underlying ray-dynamics in the limit $\omega \to \infty$; see also de Verdière (1985) and Zelditch (1987). Weaver (1982) points out that the wave energy of a diffusive field in an elastic solid is distributed over the different modes according to the relative density of eigenfrequencies for each mode-type and thus, from Weyl's law, relative to the phase-space volume available for each component of the wave field. Equipartition in seismic signals confirming this expectation have been reported by Hennino *et al* (2001).

A connection between random wave fields and the underlying ray dynamics has been established by Berry (1977b). He conjectured that in the presence of ray chaos, individual eigenfunctions of the scalar Schrödinger equation behave in the asymptotic limit on small scales like a superposition of plane waves with fixed wave number k sampled randomly over the wave direction $\mathbf{k}/k$ and phases. A proof of this conjecture for ballistic systems (performing averages by adding a random potential) has recently been given by Gonyi and Mirlin (2002). It follows immediately that the wavefunction amplitudes u are Gaussian distributed and that

the intensities obey a one-dimensional χ^2 distribution, that is,

$$P(|u|^2) = \sqrt{\frac{1}{2\pi|u|^2}}\,\mathrm{e}^{-|u|^2/2}. \tag{67}$$

Relation (67) has originally been considered in the context of resonance-width distributions in nuclei and is often referred to as *Porter–Thomas* distribution (Porter and Thomas 1956, Porter 1965), see also section 3.2.3. Scalar random waves show correlations on length scales of the wavelength, that is,

$$C(\mathbf{r};\mathbf{x}) = \langle u(\mathbf{r})u(\mathbf{r}+\mathbf{x})\rangle = \Gamma\left(\frac{d}{2}\right)\left(\frac{2}{kx}\right)^{\frac{d}{2}-1} J_{\frac{d}{2}-1}(kx), \tag{68}$$

where $\Gamma(x)$ is the Gamma function, J_ν denotes Bessel functions and d is the dimension of the system; one thus finds $C(\mathbf{x}) \sim J_0(kx)$ and $C(\mathbf{x}) \sim \sin(kx)/kx$ in two and three dimensions. For the intensity correlation function, one obtains assuming a Gaussian random process

$$C_I(\mathbf{r};\mathbf{x}) = \langle u^2(\mathbf{r})u^2(\mathbf{r}+\mathbf{x})\rangle = 1 + 2C^2(\mathbf{r},\mathbf{x}), \tag{69}$$

where the relation on the RHS is again valid only on scales of a few wavelengths; it is assumed that the wavefunctions are normalized such that $\langle u^2(\mathbf{r})\rangle = 1$. The so-called *inverse participation ratio* is given as

$$I_\mathrm{p} = C_I(\mathbf{r};0) = \frac{\langle u^4(\mathbf{r})\rangle}{\langle u^2(\mathbf{r})\rangle^2}. \tag{70}$$

One thus obtains $I_\mathrm{p} = 3$ from RMT. Equations (68) and (69) are indeed valid only on short scales of the order of a wavelength and correspond to a zeroth-order approximation. Corrections due to the presence of boundaries in billiards have been discussed by Berry (2002), Bies *et al* (2003), Wheeler (2005) and others. A more systematic way for expressing deviations from the random wave approximation has been presented by Hortikar and Srednicki (1998a, 1998b) and Urbina and Richter (2003, 2004, 2006); the authors point out that the correlation function (68) can be written in terms of the Green function, that is,

$$C(\mathbf{r};\mathbf{x}) = \frac{2\omega}{\pi}\langle \mathrm{Im}\, G(\mathbf{r},\mathbf{r}+\mathbf{x};k)\rangle, \tag{71}$$

where the average is taken over a small frequency range. After inserting semiclassical expressions of the form (28), one obtains the Bessel function contributions in (68) to leading order with corrections given by classical orbits. Akolzin and Weaver (2004) generalize (71) to vector wave equations such as the Navier–Cauchy equation (16) using the Green function in tensorial form. The correlation functions for vectorial eigenfunctions are in analogy to (68) given by the free tensor Green function of the wave equation. Result (71) is also valid for open systems in equilibrium with a diffusive environment (Weaver and Lobkis 2004); here, the field is considered locally in a volume V produced by an incoherent superposition of incoming random waves. The Green function is in this case obtained inside V.

Wavefunction intensities for both flexural and in-plane eigenmodes were measured experimentally by the Copenhagen group for aluminium plates being Sinai and stadium-type shaped as well as for rectangular plates (Schaadt *et al* 2001, Ellegaard *et al* 2001, Schaadt *et al* 2003b). Examples of measured wavefunctions are displayed in figures 16 and 17 as well as in figure 6 taken from (Ellegaard *et al* 2001, Schaadt *et al* 2001). The difference between regular and chaotic geometries becomes clear by inspection, see figures 16 and 17. Note, however, that the biharmonic equation (8) is not separable for rectangular geometries other than for clamped boundaries (Gorman 1978, Gorman 1982). The separability observed in the experiments, figure 17, is thus only approximate, but is well fulfilled sufficiently far from

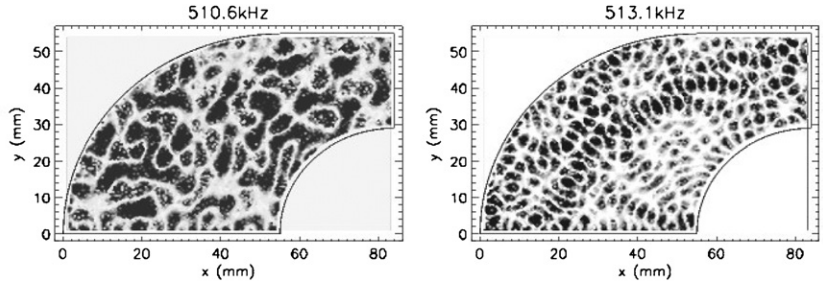

Figure 16. Measurement of wavefunction in the chaotic Sinai billiard: in-plane mode (on the left) versus flexural mode (on the right); note the difference in wavelength at comparable frequencies (Ellegaard *et al* 2001).

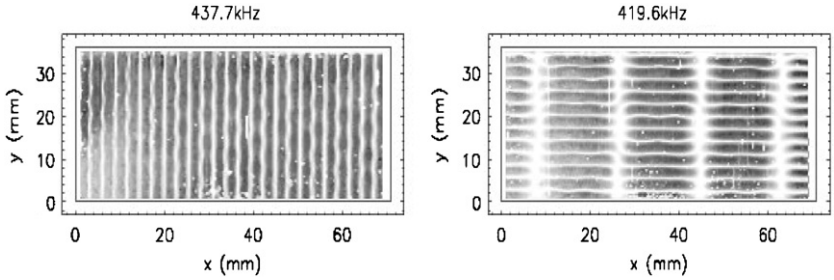

Figure 17. Rectangular plate of fused quartz: regular wavefunctions of flexural-type from (Ellegaard *et al* 2001, 2003).

the boundary where the wavefunctions are in good approximation solutions of the Helmholtz equation with modified boundary conditions, see section 2.2.2.

The validity of the Porter–Thomas distribution was confirmed both for bending and in-plane eigenmodes; this was also found in numerical studies for the biharmonic equation in chaotic cavities (Brodier *et al* 2001). Further, Schaadt *et al* (2003b) demonstrated, that for bending modes the intensity correlation functions follow the scalar Gaussian wave model (68). For in-plane modes carrying two polarizations with different wave speeds, the correlations show significant deviations from the scalar case revealing the vectorial nature of the wave equations. Possible theoretical treatments were discussed in (Schaadt *et al* 2003b, Akolzin and Weaver 2004); a related study on three-dimensional microwave cavities was carried out by Eckhardt *et al* (1999) showing good agreement between theory and experiment.

3.1.4. Recovering the Green function from cross correlations. Lobkis and Weaver (2001b, 2003) and Weaver and Lobkis (2001, 2002, 2003) point out, that the cross-correlation function for a chaotic wave field can be written in the form

$$\hat{C}(\mathbf{r}, \mathbf{r}_0, t) = \int \mathrm{d}t\, u(\mathbf{r}, \tau) u(\mathbf{r}_0, t + \tau) \sim \frac{\mathrm{d}}{\mathrm{d}t}[\hat{G}(\mathbf{r}, \mathbf{r}_0, t) - \hat{G}(\mathbf{r}, \mathbf{r}_0, -t)], \quad (72)$$

where $\hat{G}(t)$ is the Green function in the time domain, equation (25), describing wave propagation form a source point $\mathbf{r}_0$ to $\mathbf{r}$ in time t. Equation (72) follows immediately from (71) when going from the frequency domain to the time domain. The relation holds for random (diffusive) fields in the regime where there is no net current into or out of a region containing both $\mathbf{r}$ and $\mathbf{r}_0$. It implies, that information about the Green-function, that is, the response of the

system at point $\mathbf{r}$ to an excitation at $\mathbf{r}_0$, can be obtained by measuring a 'noisy' signal at $\mathbf{r}_0$ and $\mathbf{r}$ simultaneously. The diffusive field may be produced at some other point $\mathbf{r}'$ (such as by an earthquake) or may be due to thermal phonons or some other form of random excitation. This makes it possible to perform ultrasonic measurements without a source (Weaver and Lobkis 2001, 2003) which is of particular importance to seismology and underwater acoustics. Note, that the cross-correlation function is symmetric about $t = 0$ due to time-reversal symmetry which is reflected in the terms $\hat{G}(t)$ and $\hat{G}(-t)$ on the LHS in (72); recall that $\hat{G}(t)$ is non-zero for $t > 0$ only.

This idea was in fact presented earlier in helioseismology by Duvall *et al* (1993), Gough *et al* (1996) and Ricket and Claerbout (1999). Its full potential started to emerge only after the theoretical and experimental work by Weaver and Lobkis (2001, 2003). They demonstrated that the autocorrelation function obtained from thermal noise in a cylindrical aluminium body coincides with the signal obtained from a pulse-echo experiment and thereby managed to reconstruct $\hat{G}(\mathbf{r}, \mathbf{r}, t)$ for short times. In a similar experiment, the same authors studied the cross-correlation function $\hat{C}(\mathbf{r}, \mathbf{r}_0, t)$ of an experimental signal obtained from a single-source excitation (Lobkis and Weaver 2001b, Weaver and Lobkis 2002). The results were less convincing prompting a series of papers on the influence of absorption and the extension of the idea to open systems (Derode *et al* 2003a, 2003b, Weaver and Lobkis 2004). It was pointed out that relation (72) holds for open systems as long as there is a random distribution of sources or more generally, the local wave field is in equilibrium with a global random field and there is no net flux. There is a close relationship between cross-correlated signals and time-reversal imaging as discussed in section 2.4. Cross correlation and convolution with a time-reversed signal are identical operations; using a generalization of the cavity equation (59), the cross-correlation function (72) can be obtained by applying a pulse at $\mathbf{r}_0$ and recording at some point $\mathbf{r}'$ (Derode *et al* 2003a, 2003b). Exciting the medium with the time-reversed signal again at $\mathbf{r}'$ leads to refocusing of the wave field at $\mathbf{r}_0$; this implies, that the signal measured at the point $\mathbf{r}$ is equivalent to $\hat{C}(\mathbf{r}, \mathbf{r}_0, t)$ (up to a convolution with the Green function $\hat{G}(\mathbf{r}', \mathbf{r}', t)$).

van Tiggelen (2003) re-derive (72) in terms of a diffusion equation obtained from multiple scattering theory. The asymmetry around the point $t = 0$ often observed in experimental data is related to deviations from equipartition of the wave field (Malcolm *et al* 2004). Weaver and Lobkis (2005a, 2005b) give estimates for the variance of the reconstructed Green function both for open and closed systems. It is established that the variance scales like

$$\operatorname{var} \hat{C}(t) \sim (t_{\mathrm{H}}/t)^2(1 - \exp(-2t_{\mathrm{H}}/t)),$$

where t_{H} is the Heisenberg time and t is the sampling time. Here, the variance is large for small sampling time t at high frequencies as $t_{\mathrm{H}} \sim \omega^2$. The theoretical studies mentioned above are mostly based on a modal picture expressing the Green function in terms of the eigenfunctions strictly valid only for closed systems. A theoretical analysis relating the cross-correlation function to the time-dependent Green function written in terms of ray paths has been presented by Snieder (2004) and Roux *et al* (2005) for the ballistic case and by Sabra *et al* (2005) in the presence of multiple scattering in an ocean wave guide. Recently, de Verdiére (2006) picked up this theme giving a rigourous mathematical description in terms of pseudo-differential operators and random fields.

The effect can be used most efficiently in analysing ambient noise data in seismology. Campillo and Paul (2003) considered the late seismic coda, that is, the diffusive signal following an earthquake, for 110 earthquake events measured simultaneously at two different locations in central Mexico. The cross-correlated signal clearly exhibited peaks at travel times of the corresponding Rayleigh and Love surface wave between the two locations. In a further large-scale study by Shapiro and Campillo (2004) and Shapiro *et al* (2005), surface wave

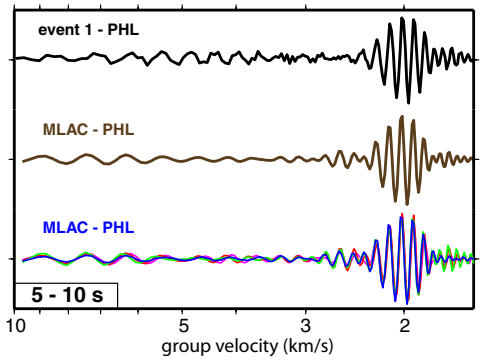

Figure 18. Signals measured between two seismological stations in California (PHL versus MLAC). Top: earthquake pulse. Middle: cross correlations of ambient seismic noise over one year. Bottom: four samplings over three months of ambient noise. The earthquake signal was normalized to the noise signal from Shapiro *et al* 2005. Reprinted with permssion from AAAS.

speeds could be mapped with an unprecedented resolution by measuring ambient seismic noise on a grid of stations in California, see figure 18. The results depend, however, on the time window chosen reflecting the fact that the seismic wave field is not fully diffusive. This allows for a depth-dependent analysis. The connection between cross-correlation functions, TRI and seismology has recently been reviewed by Larose *et al* (2006).

Coherent wave signals could also be extracted from noisy data sets in ocean acoustic waveguides as discussed in section 2.6. This was demonstrated in numerical simulations (Roux and Fink 2003, Sabra *et al* 2005) as well as using experimental data taken from an array of hydro-phones (Roux *et al* 2004). It was shown that the dominant contribution to the signal comes from noise sources aligned with the two receivers producing the cross-correlated signal. Roux and Kupermann (2005) went a step further by producing a time-reversal mirror as discussed in section 2.4 using the cross-correlation function obtained from passive noise measurements thereby *mimicking* a true, that is, active point source! The coherent backscattering effect, discussed in the next section, has been demonstrated using cross-correlation functions (Larose *et al* 2006) allowing for an enhanced spatial resolution for small (virtual) source and receiver distances.

3.1.5. Weak localization and the modal echo. Weak localization, more commonly known as *coherent backscattering* in the acoustics literature, has first been discussed in the context of electronic transport through disordered media and Anderson localization; see Bergmann (1984) and references therein. The effect amounts to an enhancement of the backscattered field at the source. In a typical experiment, the field is excited by a localized pulse at a source point $\mathbf{r}_0$ and returns to that point after undergoing multiple, chaotic scattering in some medium. The ensemble averaged intensity distribution for times larger than some characteristic scattering time is considered. For open scattering systems, the field intensity at $\mathbf{r}_0$ is enhanced by a factor of 2 compared to the far-field intensities. For closed systems such as cavities, one observes an enhancement rising from two to three for times larger than the Heisenberg time (Weaver and Burkhardt 1994); this increase has been called *modal echo* by Weaver and Lobkis (2000a).

The factor 2 can be easily explained in a ray picture; due to time-reversal invariance, every path from $\mathbf{r}_0 \rightarrow \mathbf{r}_0$ has a time-reversed partner with which it interferes constructively. In closed systems with an underlying classically chaotic dynamics, there is an extra contribution;

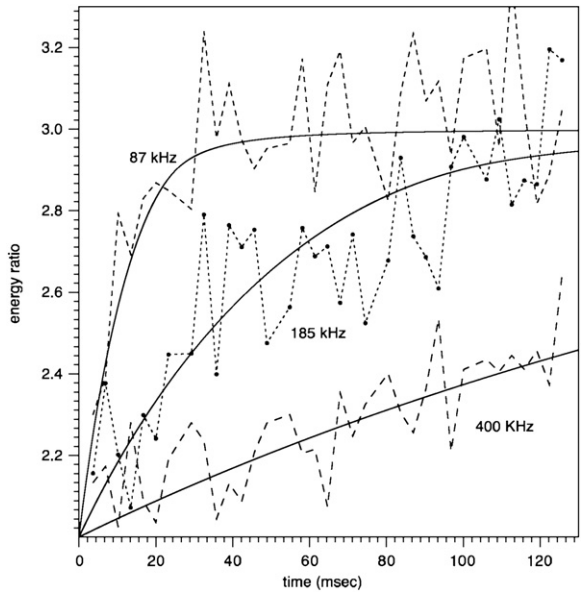

Figure 19. (Weaver and Lobkis 2000a): experimental observation of the modal echo, that is, the enhancement of the coherent backscattering peak from a factor 2 to 3; different curves correspond to different frequencies and thus different T_{H}.

the initial impulse leads to a random wave field which can be expressed in terms of a random superposition of the eigenfunctions of the cavity. The time dependence of the intensity of the wave field at point $\mathbf{r}$ excited initially at $\mathbf{r}_0$ can for times $t > t_{\mathrm{Ehrenfest}}$ [8] be written in terms of the correlation function $C(\mathbf{r}_0, \mathbf{r})$ (69) (Weaver and Burkhardt 1994, Weaver and Lobkis 2000a, de Rosny *et al* 2000, Langley and Cotoni 2005). Including correlations due to RMT, one obtains in particular

$$\langle |u(\mathbf{r}_0, \mathbf{r}; t)|^2 \rangle = 1 + [1 + K(t/t_{\mathrm{H}})]\, C^2(\mathbf{r}_0, \mathbf{r}), \tag{73}$$

where $K(t)$ denotes the form factor defined in (62) and t_{H} is the Heisenberg time. (t_{H} is proportional to the mean level density, and may thus be regarded infinitely large for open systems.)

Coherent backscattering peaks were first observed in optics in the 80s by Tsang and Ishimaru (1984), Van Albada and Lagendijk (1985) and Wolf and Maret (1985). Experiments in acoustics started in the 90s recording the backscattered signal from a random media immersed in water (Bayer and Niederdränk 1993, Sakai *et al* 1997, Tourin *et al* 1997). In particular, Tourin *et al* (1997) used the time dependence of the pulse width to extract information about dynamic transport properties of the medium such as the diffusion constant.

Weak localization in closed systems was first considered in the context of quantum dots by Prigodin *et al* (1994) and then derived in terms of an eigenfunction expansion of the propagator (Weaver and Burkhardt 1994). A first experimental verification of the transition from 2 to 3 was given by Weaver and Lobkis (2000a) using a 3D irregular shaped aluminium block, see figure 19. Recently, Larose *et al* (2006) measured coherent backscattering signals passively using cross-correlation methods as discussed in the previous section. Both active (laser) and passive (thermal phonons) sources have been considered; deviations from the enhancement

[8] The Ehrenfest time is the time at which classical and quantum evolution deviate and is for chaotic systems of the order $t_{\mathrm{Ehrenfest}} \propto \log k$.

factor 3 in the passive experiment was attributed to losses. Excitation by polarized sources was considered experimentally using silicon plates by de Rosny *et al* (2001) and numerically by Margerin *et al* (2001), van Tiggelen et al (2001). Polarized sources are particularly important in seismology as earthquakes emanating from dislocations often have a large bipolar component. Weak localization has been observed in an experiment with seismic waves in (Larose *et al* 2004).

Weak localization is often discussed in the context of Anderson localization, that is, the regime where wave solutions are localized in extended systems due to the presence of disorder. Strong localization is a phenomenon linked to multiple scattering, interference and classical diffusion; it depends crucially on the dimension of the system and its interpretation in terms of an underlying ray dynamics and wave chaos is still an open problem. This review focuses on the interplay between wave and ray dynamics and no attempt will be made here to cover the extensive literature on Anderson localization in general and in acoustics and elasticity in particular.

We refer the reader with particular interest in localization phenomena to the reviews by Guhr *et al* (1998) focusing on concepts from random matrix theory, (Beenakker 1997) with special emphasis on wave transport and Hodge and Woodhouse (1984) covering localization in elastic media. Some more recent studies on localization and its influence on the description of wave transport through elasto-mechanical systems can be found in Weaver and Burkhardt (2000), Weaver and Lobkis (2000b) and Grönqvist and Guhr (2005). For time resolved studies considering pulse transmission through disorder, quasi-one-dimensional microwave guides, see for example Titov and Beenakker (2000), Schomerus *et al* (2000, 2001), Chabanov and Genack (2001), Chabanov *et al* (2004) and references therein. The dynamics of localized wave fields in three-dimensional, open systems has been considered by Skipetrov and van Tiggelen (2006).

3.2. Transport and decay in dissipative systems

Signals in acoustics are often dominated by dissipation due to, for example, wall absorption of acoustic waves, energy loss caused by internal friction in elastic bodies or damping due to coupling at boundaries. From a wave perspective this leads to finite width resonances and wavefunctions coupled to decay channels. The study of signal decay, energy transfer through open systems and the statistics of their fluctuations has a remarkable history in acoustics and goes back more than a century; it ranges from early attempts to measure and predict decay times in reverberation rooms such as concert halls in the late 19th century to a general theory of vibrational energy flow in large build up structures (such as cars or buildings) and recent studies describing fluctuations in the Green function within the framework of RMT using super-symmetric methods.

3.2.1. Decay times—early considerations. Sabine (1992, 1964) found experimentally that the exponential decay of acoustic signals often does not depend on the shape of the room, but is given by a simple universal expression for the decay time T_S, that is,

$$T_S = \frac{4V}{S}\frac{1}{v\alpha}, \tag{74}$$

where V and S are the volume and surface of the room, respectively, v is the speed of sound and $0 \leqslant \alpha \leqslant 1$ is the mean surface absorptivity. The expression $4V/S$ can be interpreted as the mean distance between two points on the surface of a three-dimensional convex body. The latter result dates back at least to Czuber (1884) and Clausius (1889). (In two dimensions,

$4V/S$ is replaced by $\pi S/P$, where S is the area and P the perimeter). Relation (74) is valid only for small absorptivity α, extension to intermediate α values yields

$$T_{NE} = -\frac{4V}{S}\frac{1}{v\ln(1-\alpha)}, \tag{75}$$

often referred to as Norris–Eyring time (Fokker 1924, Schuster and Waetzmann 1929, Eyring 1930), see also Morse and Bolt (1944). The universality of Sabine's formula (74) or equation (75) was soon questioned leading to a discussion on the relation between decay times and the underlying (acoustic) ray dynamics. It was found that Sabine's formula does not hold for rectangular rooms without dispersing elements such as for example an audience (Fokker 1924). The confusion was lifted only in the 1970s when the connection between the validity of Sabine's law and ergodicity of the corresponding ray dynamics became clear, see Joyce (1975) and references therein. Joyce (1975) points out in particular that universality holds only if the correlation time T_c measuring the decay of correlations in the ray dynamics obeys the relation $T_c \ll T_{NE}$. The inequality ensures that phase space is sufficiently explored before absorption takes over[9]. Legrand and Sornette (1990) test Sabine's law numerically for the classical ray dynamics in enclosures such as stadium or Sinai billiards. Good agreement with equation (75) is found for small absorption, but deviations occur due to non-exponential decay of correlation in these systems caused by bouncing ball orbits (Mortessagne *et al* 1992, 1993). Corrections to the Norris–Eyring law due to fluctuations in the mean free path length between bounces with the billiard boundaries have been considered by Mortessagne *et al* (1992, 1993), see also Kuttruff (1970, 1971).

With the arrival of dynamical systems theory in the 1980s, it became clear that the above mentioned decay times are approximations of the so-called classical escape time T_e (Kadanoff and Tang 1984, Blümel and Smilansky 1988, Doron *et al* 1990, 1991, Lewenkopf and Weidenmüller 1991). In open chaotic systems, T_e measures the exponential decay of the probability $P(t) \sim \exp(-t/T_e)$ for a particle to stay in the reverberation or reaction region; absorption is treated here as an escape channel. The escape rate $\gamma_e = 1/T_e$ is the leading eigenvalue of a linear phase-space propagator, the Perron–Frobenius operator (Cvitanović and Eckhardt 1991); effective methods for calculating these eigenvalues can be found in (Cvitanović *et al* 2006) and references therein.

The above analysis is entirely based on the classical ray dynamics and gives the mean decay of acoustic or elastic signals neglecting fluctuations due to wave interference. Different approaches are favoured in different communities when dealing with the full wave problem. In quantum systems, the excitation of a system due to particles such as photons, electrons or neutrons has a strong influence on the systems as a whole and the process is best treated as a scattering problem with well-defined entrance and exit channels. This is in contrast to acoustics and elastodynamics, where the main source of dissipation is due to absorption in the interior or on boundaries whereas the influence of the source or the receiver on the system is often negligible. A Green function approach including absorptive channels is thus favoured here. Both approaches are of course closely related, see Kuhl *et al* (2005) for a discussion of this topic.

3.2.2. The Green function approach and the scattering matrix. The wave equation with absorption can be written in an operator form as

$$H = H_0 - \mathrm{i}WW^T, \tag{76}$$

[9] Joyce talks about a mixing time; Legrand and Sornette (1990) point out the importance of the correlation time as the relevant time scale.

where H_0 is the linear operator for the isolated system without absorption and W represents the coupling to dissipative channels such as contacts, friction or absorption at boundaries. For the wave equations considered here, H_0 can be chosen real symmetric reflecting the time-reversal symmetry of the problem; the real matrix elements W_{ij} represent the coupling of the ith wavefunction to the jth channel. It is assumed that the coupling is independent of frequency. This is assumption is generally valid in the high-frequency limit and for chaotic wave fields where the coupling elements are roughly constant over frequency ranges large compared to the mean separation of resonances. Note that the actual number of channels does not enter into (76); absorption acts as a multitude of dissipative channels and it is often easier to work with the symmetric operator WW^T instead, whose matrix elements may be deduced from experiments or taken randomly from appropriate matrix ensembles.

In a typical experimental situation, a force F is applied to the system at a source point $\mathbf{r}_0$ with frequency ω and the signal is detected by a receiver at $\mathbf{r}$. The stationary wave field $u(\mathbf{r})$ induced by a localized source is a solution of the inhomogeneous equation

$$(\omega^2 - H)u(\mathbf{r}) = F\delta(\mathbf{r} - \mathbf{r}_0)$$

with appropriate boundary conditions. The wave amplitude at the receiver is then proportional to the Green function including dissipation, that is,

$$G(\omega) = \frac{1}{\omega^2 - (H_0 - \mathrm{i}WW^T)}. \tag{77}$$

It is assumed here, that source and receiver do not act as dissipative channels themselves and thus do not influence the pole distribution of G. The acoustic energy absorbed by the source or receiver can in general be kept small when injecting or detecting signals through point contacts; this is in contrast to quantum systems or microwave cavities where source and receiver generally act as scattering channels.

The operator H is complex symmetric with complex eigenvalues $(\omega_n - \mathrm{i}\gamma_n)^2$ and eigenfunctions $u_n(\mathbf{r})$. For a typical system, the eigenvalues of H will be distinct, and one can write the Green function in spectral form as

$$G(\mathbf{r}, \mathbf{r}_0, \omega) = \sum_n \frac{u_n(\mathbf{r})u_n(\mathbf{r}_0)}{\omega^2 - (\omega_n - \mathrm{i}\gamma_n)^2}. \tag{78}$$

where one uses the fact that

$$\int \mathrm{d}\mathbf{r}\, u_n(\mathbf{r})u_m(\mathbf{r}) = \delta_{n,m} \tag{79}$$

for the square-integrable, in general complex eigenfunctions u_n. Note, however, that H in contrast to H_0 is not necessarily diagonalizable as (79) does not induce a norm, i.e. $\int \mathrm{d}\mathbf{r}\, u^2(\mathbf{r}) = 0$ does not imply $u \equiv 0$ for complex wavefunctions.

The Green function (78) or its modulus, the power transmission function $T(\mathbf{r}, \mathbf{r}_0, \omega) = |G(\mathbf{r}, \mathbf{r}_0, \omega)|^2$, are of special importance in elasticity and acoustics; they describe the transport of wave energy through a system. The Green function is closely related to the scattering matrix through

$$S = 1 - 2\mathrm{i}W^T \frac{1}{\omega^2 - H} W = 1 - 2\mathrm{i}W^T G W, \tag{80}$$

describing the transition between well-defined scattering channels.

Schröder (1962) first coined the term *statistical wave acoustics* for analysing the seemingly random response signals obtained from typical reverberation chambers. The connection to RMT was established only in the late 1980s by Weaver (1989a). Recent progress in analysing scattering processes in the framework of random matrix theory has led to a wealth of results

in a quantum context, see for example the review articles by Fjodorov *et al* (2005) on the application of super-symmetric techniques in RMT as well as by Stöckmann (1999) and Kuhl *et al* (2005) focusing on experimental verification of the results in microwave billiards. A statistical treatment of dissipative systems in acoustics and elastodynamics has focused on correlations in the Green function $G(\omega)$ and the variance of the power transmission function $T^2(\omega)$ which will be reviewed below. The power variance is of interest to an SEA treatment as presented in section 3.3 and has so far defied a full random matrix analysis.

3.2.3. Correlations in the Green function. Starting from (78), Schröder (1962) considered the Green function in the time domain, (25), that is,

$$\hat{G}(\mathbf{r}, \mathbf{r}_0; t) = \sum_n \frac{u_n(\mathbf{r})u_n(\mathbf{r}_0)}{2\mathrm{i}(\omega_n - \mathrm{i}\gamma_n)} \mathrm{e}^{-\mathrm{i}\omega_n t - \gamma_n t}. \tag{81}$$

Approximating the decay rates by their mean value $\langle\gamma_n\rangle = \bar{\gamma}$ and treating the wavefunctions u_n's as Gaussian random fields, one obtains

$$\hat{C}(t) = \frac{\langle|\hat{G}(t)|^2\rangle}{\langle|\hat{G}(0)|^2\rangle} \approx \mathrm{e}^{-\bar{\gamma}t} \tag{82}$$

after averaging over source and receiver positions. The exponential decay immediately leads to a Lorentzian shape of the auto-correlation function, that is,

$$C(\omega) = \frac{\langle G(\omega_0 + \omega/2)G^*(\omega_0 - \omega/2)\rangle}{\langle|G(\omega_0)|^2\rangle} = \int \mathrm{d}t\, \hat{C}\, \mathrm{e}^{\mathrm{i}\omega t} \approx \frac{1}{1 + \bar{\gamma}^2\omega^2}. \tag{83}$$

Schröder associated $1/\bar{\gamma}$ with Sabine's decay time (74). The connection to the classical decay time becomes apparent when writing $\hat{C}(t)$ in (82) in terms of semiclassical approximations for $\hat{G}(t)$ similar to (28); the dominant contributions to the resulting double sum over trajectories from $\mathbf{r}_0$ to $\mathbf{r}$ stems from diagonal terms and one obtains

$$\hat{C}(\mathbf{r}, \mathbf{r}_0, t) \approx \sum_{\mathbf{r}_0 \to \mathbf{r}} \left|A_{r_0 \to r}\right|^2 = \mathcal{L}(\mathbf{r}, \mathbf{r}_0, t) \sim \mathrm{e}^{-\gamma_\mathrm{e} t}, \tag{84}$$

where $A_{r_0 \to r}$ is the semiclassical amplitude and $\mathcal{L}$ is the Frobenius–Perron operator, a classical propagator acting on phase-space densities (Cvitanović *et al* 2006). The decay pattern is thus determined by the eigenvalue spectrum of $\mathcal{L}$; the eigenvalue closest to the real axis gives the escape rate γ_e (Cvitanović and Eckhardt 1991) which dominates decay of the correlation function for large t (Blümel and Smilansky 1988, Doron *et al* 1990, 1991, Lewenkopf and Weidenmüller 1991, Lai *et al* 1992). Eigenvalues of the Frobenius–Perron operator other than γ_e give rise to fast decay on short time scales which has been verified in microwave experiments by Pance *et al* (2000).

Remarkably, Schröder (1962) derived (83) for room acoustics independently and at about the same time as Ericson working in nuclear scattering (Ericson 1960, 1963). It took another 30 years until acoustics fully embraced the usefulness of random matrix theory in a statistical description of wave phenomena.

Schröder (1965) also noted that exponential decay is only valid in the limit of uniform damping or a large number of dissipative channels. Defining the number of dissipative channels ν as the rank of W, we may write the decay width as

$$\gamma_n = \frac{1}{\omega_n} \sum_{i=1}^{\nu} \eta_i \left|u_n^i\right|^2,$$

where u_n^i is the projection of u_n on the ith channel and η_i are (real) coupling constants. The decay widths are distributed according to sums over squares of Gaussian random variables if

the wavefunctions $u_n(\mathbf{r})$ behave like Gaussian random functions, as is generally assumed in section 3.1.3. If the $u_n(\mathbf{r})$ are furthermore approximately real (Burkhardt and Weaver 1996b) and the η_i are independent of n, one obtains a χ^2 - distribution with ν degrees of freedom, that is,

$$P_\nu(\gamma) = \frac{\nu}{(2\bar{\gamma})^{\nu/2}} \frac{\gamma^{\nu/2-1}\, \mathrm{e}^{-\frac{\nu}{2\bar{\gamma}}\gamma}}{\Gamma(\nu/2)}, \tag{85}$$

where $\Gamma(x)$ is the Gamma function. Decay then becomes algebraic, that is,

$$\hat{C} \sim \left(1 + \frac{2t\bar{\gamma}}{\nu}\right)^{-\frac{\nu}{2}} \tag{86}$$

approaching the exponential distribution (82) only in the limit $\nu \to \infty$. These results, well known from nuclear physics (Porter and Thomas 1956, Porter 1965), have been introduced by Schröder (1965) and later by Burkhardt and Weaver (1996b) and Burkhardt (1997) into the acoustics community. However, absorption in reverberation rooms or elastic media tends to be uniformly distributed leading to $WW^T \sim \bar{\Gamma} I$ with I the identity, and thus exponential decay. Algebraic tails in response signals (often referred to as 'decay curvature', that is, deviations from purely exponential decay) have been reported in acoustic reverberation chambers (Kawakami and Yamiguchi 1986, Bodlund 1987) and in experiments on aluminium blocks (Burkhardt 1998, Lobkis *et al* 2000), where ν and $\bar{\gamma}$ were treated as fit-parameters. Burkhardt (1997) suggested to use this information as a measure for non-destructive characterization of micro structural damages in materials; dislocations contribute indeed to a large part to the friction and thus dissipation in elastic bodies. Experiments performed on aluminium blocks for which localized areas of increased friction were simulated by adding water-filled plunge cut slots on top of the block were reported by Burkhardt (1998). Information about the area of enhanced friction could be extracted.

For a more sophisticated treatment of the correlation functions (82) and (83), one averages over an ensemble of Hamiltonians H_0 in (77); the ensemble average can be carried out using super-symmetric techniques, see (Verbaarschot *et al* 1985, Fjodorov and Sommers 1997). A controlled experiment comparing (86) with super-symmetric results is difficult in the presence of absorption as the channel number ν is usually not well defined. Lobkis *et al* (2003) circumvented this problem by attaching a wire to an aluminium block. The wire was immersed in water acting as a sink with a well-defined number of channels. By subtracting the decay signals with and without wire, an algebraic decay curve could be extracted with fitted channel numbers ν in agreement with expectations. The experimental curves were compared to both (86) and the full super-symmetric result; small but significant differences at high frequencies and thus large resonance overlap could be detected clearly favouring the full RMT result. It is remarkable that after a century of studying response decay signals, acoustics and ultrasonics provide the most sensitive tests of a statistical theory originally developed in a quantum setting.

3.2.4. Variance of the power transmission function. The mean energy density induced in a given part of the system by a source at some point $\mathbf{r}_0$ (as used in an SEA treatment) can be obtained from

$$E(\omega) \sim \langle T(\mathbf{r}, \mathbf{r}_0; \omega)\rangle, \tag{87}$$

where $T = |G|^2$ is the transmission function and the averages are carried out over receiver and source positions. As pointed out in Lyon (1969), a proper analysis of the range of applicability of SEA needs information about the fluctuations in the energy density. This requires the evaluation of quantities not normally considered in quantum scattering theory such as the 4th moment $\langle |G|^4\rangle \sim \langle |T|^2\rangle$ discussed in more detail below.

Lyon (1969) and Davy (1981, 1987) noted that the 2-point correlation function $R_2(x)$ measuring correlations between the real parts of the resonances, ω_n, plays a role in evaluating $\langle T^2(\mathbf{r}, \mathbf{r}_0; \omega)\rangle$. The energy density $E(\omega)$, on the other hand, is independent of these correlations (assuming real u_n); including decay rate distributions according to equation (85), Burkhardt and Weaver (1996a) obtained

$$E(\omega) \sim \langle |G|^2 \rangle \sim \frac{\overline{d}\pi}{\bar{\gamma}} \frac{1}{1-\sigma} \tag{88}$$

with $\sigma = 2/\nu$, the relative variance of the χ^2 distributions $P_\nu(\gamma)$. Here, $\overline{d}$ denotes the mean density of resonances in the same way as Weyl's law gives the mean density of eigenmodes in a closed system. (The concept of a mean density is somewhat vague for a dissipative system and is here in general understood as the density of eigenfrequencies of the corresponding isolated system.)

Assuming constant decay rates γ_n, Legrand *et al* (1995) showed that the Fourier transformed averaged input impedance has, in contrast to the correlation function (82), the form

$$\hat{C}_I(t) = \frac{\langle |\mathrm{Tr}\, \hat{G}(t)|^2 \rangle}{\langle |\mathrm{Tr}\, \hat{G}(0)|^2 \rangle} \approx \mathrm{e}^{-\bar{\gamma}t} K(t/\overline{d}) \approx \frac{t}{\overline{d}} \mathrm{e}^{-\bar{\gamma}t}, \tag{89}$$

where $K(t/\overline{d})$ denotes the spectral form factor (62). The auto-correlation function for $\mathrm{Tr}\, G(\omega)$ thus becomes the derivative of a Lorentzian.

The relative variance of the power transmission function is a useful tool to measure deviations from the mean energy density as obtained in (88) or in an SEA analysis. It turns out that the relative variance

$$\mathrm{relvar} = \frac{\langle T^2 \rangle}{\langle T \rangle^2} - 1$$

is very sensitive to the various approximations made. Early attempts (Lyon 1969, Davy 1981, 1987, Weaver 1989b, Burkhardt and Weaver 1996a) arrived at expressions of the form

$$\mathrm{relvar} = 1 + \frac{1}{\bar{M}} \left(I_\mathrm{p}^2 - 3a + 4\sigma \left(I_\mathrm{p}^2 - a \right) \right) \tag{90}$$

where $\bar{M}$ is the so-called modal overlap factor, that is, the ratio of mean decay rate to the separation of nearby resonances $\Delta = 1/\overline{d}(\omega)$, that is,

$$M = 2\pi \overline{d}(\omega) \bar{\gamma} \sim \omega^{d-1}, \tag{91}$$

I_p is the inverse participation ratio (70) and a is a measure for the degree of level repulsion with $a = 0$ for a Poisson distribution and $a = 1$ for GOE. Equation (90) was presented in this form first by Burkhardt and Weaver (1996a) and includes decay rate variations according to (85) as well as level repulsion, albeit using a fairly crude approximation for the form factor (62) (Weaver 1989b).

Result (90) was seemingly in good agreement with experiments (Davy 1981, 1987) and numerical simulations (Burkhardt and Weaver 1996a). A more careful study by Lobkis *et al* (2000) comparing experimental data from aluminium blocks to a refined theory retaining the full GOE and χ^2 expressions led to significant discrepancies. The authors concluded that the remaining approximations, namely the assumption of real wavefunctions u and the statistical independence of real and imaginary parts of the eigenvalues are not satisfied. It was indeed shown theoretically and confirmed experimentally that by dropping the assumptions of real u, the inverse participation ratio I_p decreases from 3 to 2 as the ratio $\langle \mathrm{Im}\, u \rangle / \langle \mathrm{Re}\, u \rangle$

increases (Lobkis and Weaver 2000) bringing theory more in line with experiment. A similar study implementing GOE-statistics for the spacings, but assuming constant resonance widths has been carried out by Langley and Brown (2004a, 2004b) leading to a generalization of equation (90); agreement with numerical results is again only obtained when choosing $I_p \approx 2.75$, that is, different from the random matrix expectation $I_p = 3$. Extension of these results including spatial correlation in the ensemble averaged transmission function (68) and the modal echo (73) have been presented in (Langley and Cotoni 2005). Accompanying numerical and experimental results can be found in (Cotoni *et al* 2005).

A full treatment based on evaluating the fourth moment of the Green function (77) by averaging H_0 over an appropriate matrix ensemble and using super-symmetric techniques was carried out by Rozhkov *et al* (2003, 2004). In a first calculation, results for averaging over the physically less interesting GUE ensemble were obtained and excellent agreement with numerical simulations was found (Rozhkov *et al* 2003). The more challenging case of GOE statistics was tackled by Rozhkov *et al* (2004); however, parameters in the theoretical model can no longer be related easily to measurable quantities (such as $\bar{\gamma}$) which prevented a direct comparison between theory and experiment so far.

3.3. Statistical energy analysis (SEA)

A technique widely used for estimating the power flow of elastic wave energy in large built-up structures such as vehicles, buildings or other multi-component objects is the so-called statistical energy analysis (SEA). The theory is based on a flow model describing mean values for the energy distribution in sub-components of the structure under a set of simplifying assumptions. Testing the validity of these assumptions and getting reliable estimates for the variance of the energy distribution function naturally leads to connections with wave and ray chaos problems as discussed in section 2. It also triggered the interest in spectral statistics of reverberant bodies as discussed in section 3.1 and especially section 3.2.4. We provide here an overview over the main ideas behind SEA and discuss briefly some of the more recent developments. The textbooks by Keane and Price (1994), Lyon and DeJong (1995) and Craik (1996) provide a more in depth introduction and give practical engineering applications.

The starting point for an SEA treatment is a division of the whole system into subsystems; this will usually be along natural boundaries, such as joints between plates or walls in a building. Vibrational energy is pumped into the system from sources (such as motors, etc) and is distributed throughout the systems in terms of vibrational energy in one form or another. The goal of an SEA analysis is to get estimates for the distribution of energy between these subsystems. These estimates are subsequently converted to quantities of interest for engineering purposes such as mean-square vibrational levels, sound, pressure and noise levels, etc.

The basic idea of SEA goes back to Lyon (1969) who adopted a 'thermodynamical' approach describing the power flow between subsystems in the form

$$P_{ij} = \omega \bar{d}_i \eta_{ij} \left(\frac{E_i}{\bar{d}_i} - \frac{E_j}{\bar{d}_j} \right), \tag{92}$$

where P_{ij} is the power flowing from subsystem i to j, ω is the (mean) frequency of the source and $\bar{d}_i$ and $\bar{d}_j$ are the mean densities[10] of eigenfrequencies (or modes) of the (uncoupled) subsystems as discussed in section 2.2.1. Furthermore, η_{ij} are coupling loss factors and

[10] Modal densities are generally denoted as n_i in the engineering literature; we keep here in line with the notation adopted in section 2.

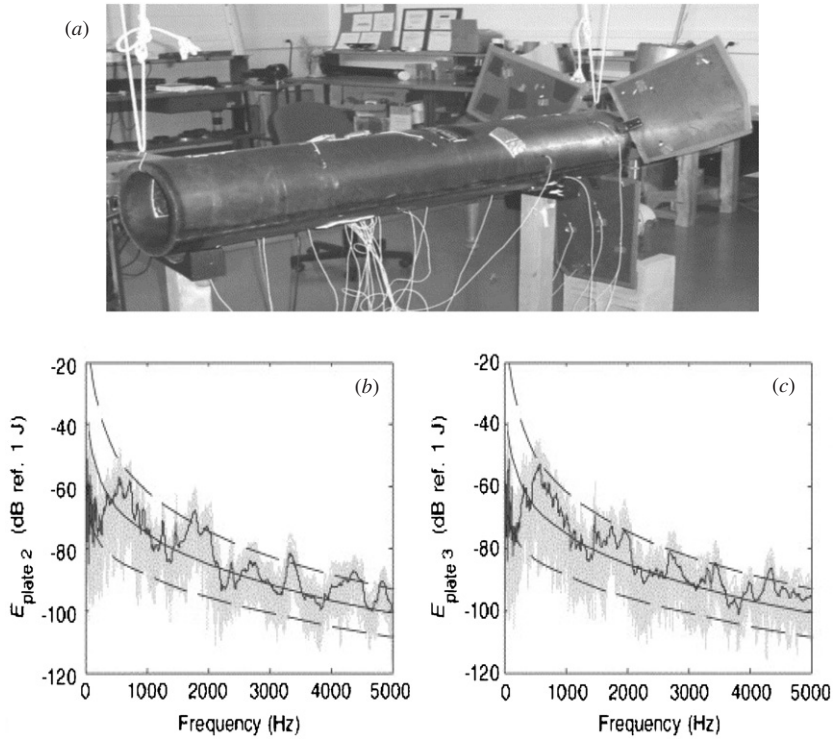

Figure 20. From (Cotoni *et al* 2005): energy frequency response of a structure consisting of a cylinder and three plates (*a*); plate 1 is driven by a point force and the response is measured in plates 2 (*b*) and 3 (*c*). Gray: different samples (extra loads, different source and receiver positions); fluctuating black: mean over all samples; smooth solid line: SEA prediction; dashed line: theoretical bounds of 99% confidence interval.

E_i, E_j are the total vibrational energies stored in the subsystems. After setting up a power balance equation for each subsystem including possible source terms as well as dissipation, one obtains a set of linear equations which can be solved for the unknown energies E_i. Estimates for the modal densities can be obtained from Weyl's law, the coupling constants η_{ij} can be estimated from experimental or numerical data (Mace and Shorter 2000, Mace 2003, 2005) or in terms of a local analysis assuming random wave fields on both sides of the boundary (Lyon and DeJong 1995). Note that the wave energies E_i per subcomponent are related to the square of the amplitude of the wave-field integrated over the subsystem. SEA gives mean values for these energies in the same way as Weyl's law gives the mean density of eigenfrequencies or the mean level staircase function such as shown in figure 2. It can not account for the fluctuations in the signal when for example viewed as a function of ω which are due to resonance or interference effects and reveal the true wave nature of the problem, see figure 20.

SEA is often regarded as a statistical theory in the sense that averaging over an ensemble of similar systems is deemed necessary; this is slightly misleading as the mean can also be defined for a single system. In practical applications, the mean is obtained by performing local frequency averaging.

The validity of an SEA treatment is based on assumptions such as the so-called *coupling power proportionality*, equation (92), stating that power flows along the energy gradient just

like thermal energy does along the temperature gradient (Lyon and DeJong 1995); furthermore, it is assumed that the systems have no memory, that is, the coupling constants η_{ij} depend only on the properties of the subsystems i and j; and thirdly, that the eigenfunctions of the (uncoupled) subsystem behave similarly and can locally be described in terms of random Gaussian fields (diffusive wave fields). Weak coupling between subsystems is often cited as a further condition (Langley 1990). In a wave chaos context, the SEA assumptions may be formulated as follows: the underlying ray dynamics in each subsystems is chaotic, the escape rates for each subsystem are small and one works in the high-frequency limit where a high modal density favours equipartition of the energy between modes. Details of the subsystems become irrelevant due to the universality of the spectral correlations and only the volume of the subsystem and the coupling mechanism enter the theory. Explicit bounds for the validity of the SEA theory have been given by Mace (2003, 2005) calculating the SEA parameters directly from an FE solution for relative simple model systems and comparing with the SEA prediction.

By the nature of the technique, only relatively rough estimates for energy distributions can be obtained. Still, for high-frequency noise sources, SEA or variants thereof are often the method of choice. 'Exact' solution tools such as finite element (FE) or boundary element methods become both too expensive computationally and unreliable, that is, small uncertainties in the systems may lead to very different outputs. One of the big challenges in mechanical engineering is the so-called *mid-frequency problem*, that is, handling the frequency range which is out of reach for 'exact' numerical methods but not yet in the high-frequency regime where a purely statistical treatment may suffice. SEA has been discussed as a starting point for penetrating the mid-frequency regime by employing hybrid methods based on combining an FE and SEA treatment (Langley and Bremner 1999, Mace and Shorter 2000, Shorter and Langley 2005). An approach similar in spirit is the so-called 'fuzzy structure theory' by Soize (1993, 2003, 2005) where randomness is directly introduced in the set of (sub-)system parameters.

Theoretical work on predicting the variance of the energies found in each subsystem for an ensemble of similar systems (or by considering a frequency interval) has provided a bridge towards spectral statistics and ultimately RMT. For such an analysis, the statistics of the eigenfrequency spectrum of the sub-systems are important, see also section 3.2.4. Whereas historically a Poissonian distribution or ad hoc model probability distributions were assumed (Lyon 1969, Davy 1981, 1987, Lyon and DeJong 1995, Langley 1999), a random matrix point of view as presented in section 3.2 is now generally accepted (Soize 2003, 2005, Langley and Brown 2004a, 2004b). Using the approximative results by Langley and Brown (2004a, 2004b) valid for single systems, Langley and Cotoni (2004) developed a reliable method for calculating the variance for multi-component systems making use of power-balance conditions between the subsystems; the method is expected to work well for systems, for which SEA gives a good approximation of the mean and the subsystems follow GOE statistics (when isolated). This has been confirmed in numerical (Langley and Cotoni 2004) and experimental studies (Cotoni *et al* 2005), see figure 20.

4. Diffraction, curvature and anisotropy

Diffraction, elastic waves on curved bodies and anisotropic materials lead to new effects which are beyond the ray versus wave chaos picture for isotropic and homogeneous media discussed so far. We will briefly summarize some know results and point out connections to wave chaos applications.

4.1. Diffraction

The simple ray theory discussed in section 1.2 breaks down or needs to be modified when considering bodies with curved surfaces, curved plates such as shells or wave solutions near corners and point/line defects. Including diffraction effects (Keller and Karal 1960) is important when modelling materials with mechanical defects (Achenbach *et al* 1982) and play a role in semiclassical expressions such as the density of states as discussed in section 2.2 in the low-to-medium frequency regime. Below we shall discuss typical diffractive phenomena such as surface waves occurring in elastodynamics. We first give an overview over surface waves in the case of no curvature and will then move on to the general case of curved boundaries. Diffractive effects at corners and wedges will be briefly reviewed at the end of this section.

4.1.1. Surface waves on flat boundaries. The general problem of determining the elastic Green function with traction free boundary conditions in an infinite half space is called the Lamb problem (Ewing *et al* 1957, Brechovskich 1980). It does not admit closed form solutions but can be written in terms of an integral representation. The asymptotic analysis reveals that besides direct geometric rays and rays involving mode conversion at impact with the boundary, there are further contributions which can be interpreted as surface waves. The most prominent one is the Rayleigh earthquake wave, see also (53), which can be associated with a pole in the reflection coefficients (23) entering the integral representation of the Green function. Another surface contribution is due to head waves which occur when an incoming transverse wave converts to a fast longitudinal wave at the critical angle where the longitudinal wave *glances* along the boundary. In the integral representation of the Green function, these wave types appear as branch cuts in k-space (Brechovskich 1980).

Thus, the infinite half-space problem supports the Rayleigh surface waves and head waves at the boundary. The surface wave that carries most energy in, for example, an earthquake is the Rayleigh wave. This wave moves without attenuation along the boundary with a velocity slightly lower than the transverse wave, decays exponentially into the medium and propagates without dispersion. Head waves moving with the wave speed of longitudinal waves are faster than Rayleigh waves and act as early warning systems for earthquakes. They decay, however algebraically along the boundary. Head wave contributions can also be observed in microwaves where these wave types are called lateral waves. Glancing rays in quantum billiards were considered by Sieber *et al* (1995). Head wave contributions have not been considered in wave chaos except in a ray splitting billiards by Blümel *et al* (1996a, 1996b), see section 2.3.

Another surface contribution is the so-called pseudo-Rayleigh wave which like the Rayleigh wave corresponds to a pole in the reflection coefficients (23). This wave is a leaky wave with a complex wave number in the direction along the boundary. It therefore looses amplitude exponentially with distance and is not considered a proper surface wave.

At the interface between two media propagating waves, so-called Stonely waves (Brechovskich 1980, Ewing *et al* 1957) may be supported. In the case of layers of finite thickness the corresponding waves are called Love waves. They are transversal waves travelling inside the layer in the limit when the wavelength becomes small compared to the thickness of the layer. Such waves occur for instance in layered regions of the earth or in thin films on top of a secondary solid half space.

4.1.2. Surface waves on curved boundaries. The effects of curvature on surface waves have been studied by Viktorov (1967) and Izbicki *et al* (1998) who investigated the specific example of scattering on a circular cavity. Viktorov (1967) focused on Rayleigh waves and

their attenuation whereas Izbicki *et al* (1998) also treated pseudo-Rayleigh waves and two kinds of so-called Franz creeping waves (Franz 1954) to be discussed in more detail below. Izbicki *et al* (1998) considered the full scattering problem and found in the limit of high wave numbers the scattering determinant (39) to be related to (53), the Rayleigh equation for the infinite half-plane problem. This and further asymptotic analysis allowed to group the scattering poles into four types: Rayleigh, pseudo-Rayleigh and transversal respective longitudinal Franz waves.

Rayleigh waves The Rayleigh and the pseudo-Rayleigh waves were originally discussed in the context of an infinite half plane but can also be found for curved boundaries at high wave numbers. In the case of cavities, curvature introduces dispersion and attenuation along the boundary. A general discussion of dispersion of Rayleigh waves was given by Gregory (1971). He also showed that Rayleigh wave packets move on geodesics on the surfaces of isotropic solids. A dispersion relation for the Rayleigh wave in the case of a circular disc was studied by Rulf (1969) and Izbicki *et al* (1998). The wave number itself has an imaginary part which becomes exponentially small with increasing frequency (Viktorov 1967). Hence, at wavelengths small compared to the radius of curvature, the Rayleigh wave can propagate with virtually no attenuation almost being a pure surface wave. Rayleigh waves are therefore less attenuated compared to pseudo-Rayleigh waves and, hence, are expected to give the most important contribution. The influence of curvature on the attenuation in dielectrics with impedance conditions was discussed by Berry (1975) in the electromagnetic case.

Besides existing as pure surface waves, it is also possible to excite Rayleigh waves from the bulk or re-radiate back from a Rayleigh wave into the bulk. The corresponding launching and excitation coefficients were given by Keller and Karal (1960, 1964). These diffraction coefficients become exponentially small for high-frequencies scaling asymptotically as $\exp(-\omega T_i)$ where the coefficients T_i may be interpreted as an imaginary travelling time (Rulf 1969, Doolittle and Überall 1968). Rulf (1969) considered cylindrical geometries; solutions to the interior and exterior problem were given and longitudinal as well as transverse line sources were studied. For the interior problem, Rulf (1969) showed that the excitation of Rayleigh waves takes place by waves with complex wave numbers. These Rayleigh waves shed waves back into the bulk being exponentially damped away from the boundary. The geometrical theory of diffraction for surface waves as outlined by Keller and Karal (1964) were found to be less accurate at intermediate frequencies, for instance with respect to dispersion (Rulf 1969). This is in contrast to, for example, the scalar Helmholtz case (Keller and Karal 1960) or electromagnetism where diffraction theory remains valid for wavelengths comparable to the radius of curvature. Doolittle and Überall (1968) studied the more complicated problem of acoustic pressure waves impinging on an elastic cylinder. The imaginary time T_i was found to be small relative to the real time for transverse waves coupling to Rayleigh waves. Therefore, at finite frequencies such rays may have a large contribution.

Besides this additional imaginary time, the diffraction coefficients also contain amplitude prefactors which decay like $\omega^{1/2}$ with frequency. This is interpreted by Keller and Karal (1964) as a fractional half derivative in the time domain.

Despite the exponential suppression, there is evidence that closed orbits containing segments of Rayleigh surface propagation contribute to semiclassical expressions, at least at intermediate frequencies. Søndergaard (2001) and Wirzba *et al* (2005) considered the exterior scattering from two cavities in an elastic medium, see also section 2.2.3. The Wigner–Smith time delay as defined in section 2.1.1 was calculated numerically in a low frequency

region. Similar to the length spectra of quantum billiards, the time delay was found to contain fluctuations corresponding to trapped orbits and some of these were of the Rayleigh type.

Franz creeping waves. The remaining scattering poles in the cavity case (Izbicki *et al* 1998) besides Rayleigh and pseudo-Rayleigh waves are similar to those discussed by Franz in the scalar Helmholtz case (Franz 1954, Keller and Karal 1960). These poles and the pseudo-Rayleigh poles are accompanied by strong exponential decay along the surface. Hence, they are only expected to show up at low frequencies. These poles can be of longitudinal and transversal polarization. Closed orbits containing creeping segments have been found in the scalar Helmholtz case in scattering from discs (Vattay *et al* 1994, Wirzba and Rosenqvist 1996, Wirzba 1999). Closed, creeping orbits were incorporated into cumulant expansions, (46), of the scattering determinant (39). This made it possible to classify strongly damped scattering resonances deeper in the complex k-plane and to improve the agreement between semiclassical and numerical calculations for small k.

4.1.3. Wedges and corners. In the scalar case, the general theory of diffraction for wedges has been developed by Keller and Karal (1960). These ideas have been pursued also in quantum chaos. For a scattering problem with only diffractive orbits, Whelan (1996) combined the zeta function formalism with that of wedge diffraction. Another example is the case of pseudo-integrable billiards, where diffractive orbits hitting the corners were found to have a significant contribution even in the semiclassical limit (Bogomolny *et al* 2000).

The free elastic wedge is a difficult problem which does not admit separation of variables in general (not even if the angle is rational e.g. $\pi/2$); integral representations have been given by Babich *et al* (2000, 2004).

4.2. Including curvature: Shells

Shells are important in many civil applications serving as structural elements in cars and aeroplanes. Shell theory started with the building of domes and with the attempt to understand spectra of church bells (Rayleigh 1890). Shells in architecture are often designed to have wide span and to be of small mass but also to be sufficiently strong. For an introduction into the acoustic properties of bells, see Rossing (1984).

In shell theory the dimensionality of the problem is reduced by considering the field only on the curved two-dimensional middle section of the shell and not in the full three-dimensional volume. There is a large literature on governing equations for shells, see the monographs of Gol'denveizer (1961) and Flügge (1972) as well as a recent article by Søndergaard (2007) for a mathematical introduction. The simplest form of a shell theory by Kirchoff–Love is a curved formulation of the theory for plates. To leading order, the flexural vibrations obey a biharmonic wave equation (section 1.2.2) whereas the in-plane modes follow conventional two-dimensional vectorial elasticity (section 1.2.3) with the use of covariant derivatives to include curvature. Thus, in principle the same questions and methods of wave chaos can be applied to the spectral theory of shells.

Kirchoff–Love's shell theory is known to be less accurate for higher modes, that is, in the high-frequency limit where the bulk properties of the shell become important. A ray description is expected to work for the intermediate part of the spectrum, where the wavelengths are much larger than the thickness. Rays are replaced by *geodesics* (Gol'denveizer 1961, Safarov and Vasil'ev 1992); at sufficiently small wavelengths—which yet are larger than the thickness of the shell—conventional WKB analysis yields that wave splitting occurs only among the

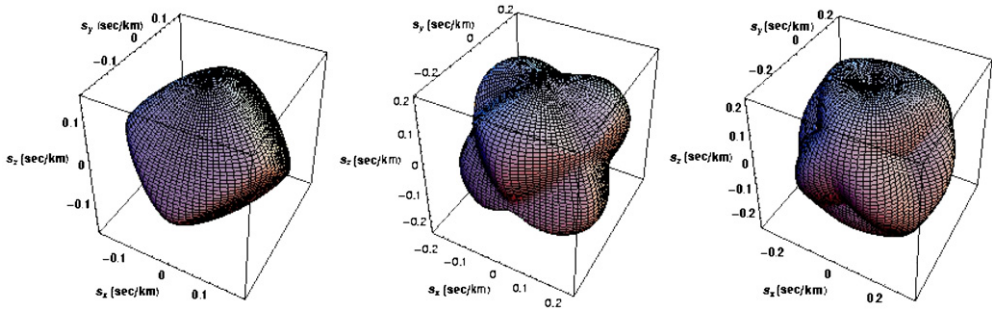

Figure 21. The three slowness sheets of anisotropic quartz (Søndergaard *et al* 2004).

in-plane vibrations and that the trace formula for the density of states can be separated into in-plane and flexural contributions.

New effects enter when the wavelengths become comparable to the radii of curvature as discussed by Pierce (1991) and Norris and Rebinsky (1994). The bi-characteristics are no longer geodesics but are also influenced by a potential. This potential depends on the position but also on the direction of the momentum. Although this result was found for the particular simple Donnel shell theory, see Flügge (1972), similar effects are expected to occur for other shell theories.

4.3. Anisotropic elastic resonators

The review has focused on isotropic elastic materials, so far. However, some of the best resonators are made of anisotropic single crystals. It is therefore of interest to extend the discussion to three-dimensional anisotropic media.

4.3.1. Background. Elastic anisotropy (Landau and Lifshitz 1959) manifests itself in a more general elasticity tensor obeying the symmetries

$$c_{ijkl} = c_{jikl} = c_{ijlk} = c_{klij} \tag{93}$$

corresponding to at most 21 elastic constants. The stress tensor becomes

$$\sigma_{ij} = c_{ijkl} u_{kl} \qquad \text{with} \qquad u_{kl} = \frac{1}{2}\left(\frac{\partial u_k}{\partial x_l} + \frac{\partial u_l}{\partial x_k}\right) \tag{94}$$

and the elastic wave equation (14) takes on the form

$$c_{ijkl}\frac{\partial^2 u_l}{\partial x_j \partial x_k} + \rho\omega^2 u_i = 0. \tag{95}$$

The free boundary conditions can be written as in equation (21).

In k-space the corresponding wave vectors depend linearly on the given angular velocity ω. In elastodynamics, this has lead to the introduction of a conveniently scaled momentum

$$\mathbf{s} = \mathbf{k}/\omega, \tag{96}$$

the so-called *slowness*. The strongly anisotropic behaviour of the slowness is shown in figure 21.

4.3.2. Smooth counting function. In section 2.2.1, we discussed Weyl theory in the isotropic case. In the anisotropic case governed by equation (95), the notation of 'phase space' has to

be modified. A derivation of the leading term in the Weyl formula for anisotropic media has been given by Søndergaard *et al* (2004) and the result has been compared with experimental data of measured resonances of a single-crystal quartz sphere. In that experiment, a sphere of the size of a small grape fruit was excited by various transducers. The resonance positions were extracted using an advanced filtering and fitting algorithm based on maximum entropy methods. Using this method, approximately 40 000 resonances could be isolated.

The wave equation (95) does not admit closed form solutions even for spherical symmetries. The leading Weyl term was calculated using a suitable representation of the Green function via the Radon transform following the work of Burridge (1967) and Wang *et al* (1995). After taking the trace, the leading term in the counting function of eigenmodes could be determined, which is—like in the isotropic case—given by the available phase-space volume (Søndergaard *et al* 2004). In the anisotropic case this volume has a more complicated shape than in the isotropic case: it consists of three sheets and is a so-called sextic algebraic surface whose volume V_s must be calculated numerically. That volume together with the physical volume of the resonator V_x determines the counting function if the material properties are assumed constant within the resonator. Thus the number of states as a function of frequency f goes to leading order as

$$\overline{N}(f) = V_x V_s f^3. \tag{97}$$

4.3.3. Evolution of open rays. Presently there are no discussions of closed orbits and trace formulae in the literature in the anisotropic case. However, there exists a body of work on the ray dynamics associated with anisotropy. In the anisotropic case, there is a discrepancy in direction between the wave vector and the group velocity, referred to as 'extraordinary refraction' (Musgrave 1970, Auld 1973). Hence, increments in configuration space are no longer parallel with the momentum but the group velocity. Nevertheless, the tangential momentum is still conserved at impact with boundaries. Thus, the tangential part of the wave vector remains unchanged as in the isotropic case. The dispersion surface is no longer simple, so the normal wave vector of a reflected wave can be quite different from that of the incoming wave. In particular, orbits as seen in configuration space only, may no longer seem to fulfil the law of reflection even if mode conversion does not occur. In conclusion, ray trajectories in an anisotropic resonator are very different from those of an isotropic cavity. Regarding the evolution of the amplitude of wave packets, there are particular directions in the crystal where decay is considerably weaker than $(kr)^{-1}$ (Musgrave 1970). This has been observed experimentally by Wichard and Dietsche (1992) and Schwab *et al* (2000) for heat transport in crystals and is called phonon-focusing.

5. Summary and conclusions

The review aims at describing wave phenomena in acoustics and elastodynamics by relating them to an underlying classical ray dynamics. This has been done in section 2 by making explicit connections between Green functions and related functions to ray trajectories using semiclassical or short-wavelength asymptotics. In a second part, in section 3, we discussed statistical approaches based mainly on the observation that statistical properties of 'typical' wave systems coincide with that of ensembles of random matrices. The universalities observed are related to universality in the underlying ray dynamics for chaotic systems such as ergodicity and exponential decay of correlations; the long time dynamics of chaotic systems looks alike on scales small compared to the system size.

The way of thinking advocated in this review has enormous potential and *predictive value*. Small wavelength asymptotics can reach frequency regimes outside the range of direct numerical solution methods keeping at the same time some of the details of the system which get lost in purely statistical approaches. In the universal regime, statistical distributions can be obtained analytically using RMT techniques. Deviations from universal behaviour can be predicted whenever the underlying ray dynamics shows 'non-chaotic' features.

Wave chaos methods have so far not had a larger impact on applications in an engineering context. This is the more surprising as wave chaos techniques are much easier to apply and to implement in a controlled way in an acoustics setting than in, for example, quantum systems. We hope that the present review will help to make wave chaos ideas more widely known and accepted also among engineers, and to test the full potential of these approaches by applying them to theories such as SEA. In fact, scattering on irregular structures producing 'diffusive' wave fields as considered in SEA has been studied in great detail in, for example, disordered system theory. Many of the sophisticated methods used in this field such as supersymmetric techniques have by now found a place in elastodynamics as described in section 3.2.4. Remarkably, the best experimental verification of the supersymmetric prediction of the correlation function, equation (82), has been carried out in an elastic resonators, see section 3.2.3.

There are a wide variety of other open questions touched on in this review which deserve mentioning. Among them are higher order corrections to Weyl's law in elasticity, especially for anisotropic elastic bodies or shells. Likewise, the ray dynamics including effects of ray splitting and mode conversion have not been studied systematically. They become important when considering the counting function on a finer scale such as in generalizations of Gutzwiller's trace formula introduced in section 2.2. Ray splitting adds new features to a dynamical system rendering, for example, rectangular geometries non-integrable. The actual nature of the dynamics and its influence on the eigenspectra and wavefunctions is still an open problem. A semiclassical ray theory for anisotropic media or curved surfaces is largely missing.

The connection between RMT statistics and chaos will help to reshape some of the statistical assumptions made with respect to the diffusivity of wave fields or the distribution of eigenfrequencies and resonance widths. We have stressed throughout the review that the RMT assumption only holds when the underlying ray dynamics is chaotic. This assumption may, however, often not be fulfilled for structures relevant in an engineering context; build-up structures may consist of different, weakly coupled elements such as plates connected to frames, plate stiffeners, shells or rods fixed to plates and walls. Thus, wave chaos methods will need to deal with coupled and strongly non-uniformly hyperbolic systems in general; in addition, each of the elements may have quite regular features such as straight edges or polygonal boundaries. A future task will be to use wave chaos ideas to characterize these intermediate regimes between order and chaos; it will also be important when considering wave effects caused by the non-diffusive part of the wave field. Such features introduce non-universal effects, which can not be described in an RMT analysis alone. Combining statistical tools with ray methods for a wave analysis may lead to extensions of existing SEA theories towards a global description of wave problems in the mid-frequency regime.

Acknowledgments

We would like to thank Steve Tomsovic, Robin Langley and Brian Mace for reading parts of the manuscript and Predrag Cvitanović for getting us both interested in this subject many years ago. GT thanks the EPSRC for support and NS thanks the Swedish Research Council.

References

Achenbach J D, Gautesen A K and McMaken H 1982 *Ray Methods for Waves in Elastic Solids* (Boston: Pitman)
Akolzin A and Weaver R L 2004 *Phys. Rev.* E **70** 046212
Andersen A, Ellegaard C, Jackson A D and Schaadt K 2001 *Phys. Rev.* E **63** 066204
Artuso R, Aurell E and Cvitanović P 1990 *Nonlinearity* **3** 325, 361
Auld B A 1973 *Acoustic Fields and Waves in Solids: 1, 2* (New York: Wiley)
Aurich R, Sieber M and Steiner F 1988 *Phys. Rev. Lett.* **61** 483
Babich V M, Borovikov V A, Fradkin L J, Gridin D, Kamotski V and Snyshlyaev V M 2000 Diffraction coefficients for tilted surface-breaking cracks *Diffraction and Scattering in Fluid Mechanics and Elasticity* ed I D Abrahams, P A Martin and M J Simon (Dordrecht: Kluwer) p 209
Babich V M, Borovikov V A, Fradkin L J, Kamotski V and Samokish B A 2004 *NDT & E Int.* **37** 105
Bäcker A and Schubert R 1999 *J. Phys. A: Math. Gen.* **32** 4795
Balian R and Bloch C 1970 *Ann. Phys., NY* **60** 401
Baltes H P and Hilf E R 1976 *Specta of Finite Systems* (Mannheim: Bibliographisches Institut)
Barth M, Kuhl U and Stöckmann H J 1999a *Phys. Rev. Lett.* **82** 2026
Barth M, Kuhl U and Stöckmann H J 1999b *Ann. Phys., Lpz.* **8** 733
Bauch Sz, Bledowski A, Sirko L, Koch P M and Blümel R 1998 *Phys. Rev.* E **57** 304
Bayer G and Niederdränk T 1993 *Phys. Rev. Lett.* **70** 3884
Bedford A and Drumheller D S 1994 *Introduction to Elastic Wave Propagation* (New York: Wiley)
Beenakker C W J 1997 *Rev. Mod. Phys.* **69** 731
Benettin G and Strelcyn J M 1978 *Phys. Rev.* A **17** 773
Bergmann G 1984 *Phys. Rep.* **107** 1
Berkolaiko G, Schanz H and Whitney R S 2002 *Phys. Rev. Lett.* **88** 104101
Berkolaiko G, Schanz H and Whitney R S 2003 *J. Phys. A: Math. Gen.* **36** 8373
Beron-Vera F J, Brown M G, Colosi J A, Tomsovic S, Virovlyansky A L, Wolfson M A and Zaslavsky G M 2003 *J. Acoust. Soc. Am.* **113** 1226
Berry M V 1975 *J. Phys. A: Math. Gen.* **8** 1952
Berry M V 1977a *Phil. Trans. R. Soc.* A **287** 237
Berry M V 1977b *J. Phys. A: Math. Gen.* **10** 2083
Berry M V 2002 *J. Phys. A: Math. Gen.* **35** 3025
Berry M V 1981 *Ann. Phys., USA* **131** 163
Berry M V 1985 *Proc. R. Soc.* A **400** 229
Berry M V 1986 Quantum chaos and statistical nuclear physics *Lecture Notes in Physics* vol 263 ed T H Seligmann and H Nishioka (Berlin: Springer) p 1
Berry M V 1987 *Proc. R. Soc.* A **413** 183
Berry M V 1989 *Phys. Scr.* **40** 335
Berry M V and Howls C J 1994 *Proc. R. Soc.* A **447** 527
Berry M V and Keating J P 1990 *J. Phys. A: Math. Gen.* **23** 4839
Berry M V and Tabor M 1976 *Proc. R. Soc.* A **349** 101
Berry M V and Tabor M 1977a *J. Phys. A: Math. Gen.* **10** 371
Berry M V and Tabor M 1977b *Proc. R. Soc.* A **356** 375
Bertelsen P, Ellegaard C, Guhr T, Oxborrow M and Schaadt K 1999 *Phys. Rev. Lett.* **83** 2171
Bertelsen P, Ellegaard C and Hugues E 2000 *Eur. J. Phys.* B **15** 87
Bies W E, Lepore N and Heller E J 2003 *J. Phys. A: Math. Gen.* **36** 1605
Biswas D 1996 *Phys. Rev.* E **54** 1232
Blümel R and Smilansky U 1988 *Phys. Rev. Lett.* **60** 477
Blümel R, Antonsen T M Jr, Georgeot B, Ott E and Prange R E 1996a *Phys. Rev. Lett.* **76** 2467
Blümel R, Antonsen T M Jr, Georgeot B, Ott E and Prange R E 1996b *Phys. Rev.* E **53** 3284
Bodlund K 1987 *J. Sound Vib.* **73** 19
Bogomolny E B 1992 *Nonlinearity* **5** 805
Bogomolny E and Hugues E 1998 *Phys. Rev.* E **57** 5404
Bogomolny E Gerland U and Schmitt C 1999 *Phys. Rev.* E **57** R1315
Bogomolny E and Schmitt C 2004 *Phys. Rev. Lett.* **92** 244102
Bogomolny E, Pavloff N and Schmit C 2000 *Phys. Rev. Lett.* **85** 2486
Bohigas O, Giannoni M J and Schmit C 1984 *Phys. Rev. Lett.* **52** 1
Bohigas O, Legrand O, Schmit C and Sornette D 1991 *J. Acoust. Soc. Am.* **89** 1456
Bolt R H 1946a *J. Acoust. Soc. Am.* **18** 130

Bolt R H 1946b *J. Acoust. Soc. Am.* **19** 79
Bonnet M 1995 *Boundary Integral Equation Methods for Solids and Fluids* (New York: Wiley)
Bothelho L C L and Vilhena R 1994 *Phys. Rev.* E **49** R1003
Brack M and Bhaduri R K 1997 *Semiclassical Physics* (Reading, MA: Addison-Wesley)
Brechovskich L M 1980 *Waves in Layered Media* 2nd edn (New York: Academic)
Briggs G A 1992 *Acoustic Microscopy (Monographs on the Physics and Chemistry of Materials* vol 47) (New York: Oxford University Press)
Brodier O, Neicu T and Kudrolli A 2001 *Eur. J. Phys.* **23** 365
Brown M G, Colosi J A, Tomsovic S, Virovlyansky A L, Wolfson M A and Zaslavsky G M 2003 *J. Acoust. Soc. Am.* **113** 2533
Bruus H, Lewenkopf C H and Mucciolo E R 1996 *Phys. Rev.* B **53** 9968
Burkhardt J and Weaver R L 1996a *J. Sound Vib.* **196** 147
Burkhardt J and Weaver R L 1996b *J. Acoust. Soc. Am.* **100** 320
Burkhardt J and Weaver R L 1996c *J. Acoust. Soc. Am.* **100** 327
Burkhardt J 1997 *J. Acoust. Soc. Am.* **102** 2113
Burkhardt J 1998 *Ultrasonics* **36** 471
Burridge R 1967 *Q. J. Mech. Appl. Math.* **20** 41
Campillo M and Paul A 2003 *Science* **299** 547
Casati G, Valz-Gris F and Guarnieri I 1980 *Lett. Nuovo Cimento* **28** 279
Castor K, Gerstoft P, Roux P and Kuperman W A 2004 *J. Acoust. Soc. Am.* **116** 2004
Cerruti N R and Tomsovic S 2002 *Phys. Rev. Lett.* **88** 054103
Cervený V 1985 *Seismic Shear Waves: part A. Theory* ed G Dohr (London: Geophysical Press) p 1–124
Chabanov A A and Genack A Z 2001 *Phys. Rev. Lett.* **87** 233903
Chabanov A A, Hu G and Genack A Z 2004 *Phys. Rev. Lett.* **93** 123901
Chinnery P H and Humphrey V F 1996 *Phys. Rev.* E **53** 272
Chirikov B 1979 *Phys. Rep.* **52** 263
Clausius R 1889 *Die kinetische Theorie der Gase* (Braunschweig: Vieweg)
Colin de Verdière Y 1985 *Commun. Math. Phys.* **102** 497
Colin de Verdière Y 2006 *Preprints* math-ph/0610043, math-ph/0610044
Collins M D and Kuperman W A 1994 *J. Acoust. Soc. Am.* **95** 3167
Colosi J A and Brown M G 1998 *J. Acoust. Soc. Am.* **103** 2232
Colosi J A *et al* 1999 *J. Acoust. Soc. Am.* **105** 3202
Cotoni V, Langley R S and Kidner M R F 2005 *J. Sound Vib.* **288** 701
Couchman L, Ott E and Antonsen T M Jr 1992 *Phys. Rev.* A **46** 6193
Couchmann (née Schuetz) L S 1991 *PhD Thesis* University of Maryland
Craik R J M 1996 *Sound Transmission through Buildings: Using Statistical Energy Analysis* (Hampshire: Gower)
Creagh S C, Robbins J M and Littlejohn R G 1990 *Phys. Rev.* A **42** 1907
Creagh S C 1996 *Ann. Phys.* **248** 60
Cvitanović P 1988 *Phys. Rev. Lett.* **61** 2729
Cvitanović P and Eckhardt B 1989 *Phys. Rev. Lett.* **63** 823
Cvitanović P and Eckhardt B 1991 *J. Phys. A: Math. Gen.* **24** L237
Cvitanović P, Artuso R, Mainieri R, Tanner G and Vattay G 2006 *Classical and Quantum Chaos* (Copenhagen: Niels Bohr Institute) www.nbi.dk/ChaosBook/
Czuber E 1884 *Silzungsber. Math. Classe Akad. Wiss. Wien Math.* **90** 719
Dabaghian Y, Jensen R V and Blümel R 2001 *Phys. Rev.* E **63** 066201
Dacol D K 1994 *Waves Random Media* **4** 117
Dashen R 1979 *J. Math. Phys.* **20** 894
Davy J L 1981 *J. Sound Vib.* **77** 455
Davy J L 1987 *J. Sound Vib.* **115** 145
Décanini Y and Folacci A 2003 *Phys. Rev.* E **68** 046204
Delande D, Sornette D and Weaver R L 1994 *J. Acoust. Soc. Am.* **96** 1873
Delande D and Sornette D 1997 *J. Acoust. Soc. Am.* **101** 1793
Derode A, Larose E, Campillo M and Fink M 2003a *Appl. Phys. Lett.* **83** 3054
Derode A, Larose E, Tanter M, de Rosny J, Tourin A, Campillo M and Fink M 2003b *J. Acoust. Soc.* **113** 2973
Derode A, Roux P and Fink M 1995 *Phys. Rev. Lett.* **75** 23
Derode A, Tourin A and Fink M 1998 *Ultrasonics* **36** 443
Derode A, Tourin A and Fink M 1999 *J. Appl. Phys.* **85** 6343
Derode A, Tourin A and Fink M 2001 *Phys. Rev.* E **64** 036606

Derode A, Tourin A, de Rosny J, Tanter M, Yon S and Fink M 2003c *Phys. Rev. Lett.* **90** 014301
de Rosny J, Tourin A and Fink M 2000 *Phys. Rev. Lett.* **84** 1693
de Rosny J, Tourin A and Fink M 2001 *Phys. Rev.* E **64** 066604
de Rosny J and Fink M 2002 *Phys. Rev. Lett.* **89** 124301
de Rosny J, Tourin A, Derode A, van Tiggelen B and Fink M 2004 *Phys. Rev.* E **70** 046601
de Rosny J, Tourin A, Derode A, Roux P and Fink M 2005 *Phys. Rev. Lett.* **95** 074301
Dietz B and Smilansky U 1993 *Chaos Solitons Fractals* **3** 581
Dong W G, Huang X Y and Wu Q L 2001 *J. Acoust. Soc. Am.* **110** 120
Doolittle R D and Überall H 1968 *J. Acoust. Soc. Am.* **43** 1
Doron E, Smilansky U and Frenkel A 1990 *Phys. Rev. Lett.* **65** 3072
Doron E, Smilansky U and Frenkel A 1991 *Physica* D **50** 367
Doron E and Smilansky U 1992 *Nonlinearity* **5** 1055
Draeger C, Cassereau D and Fink M 1997 *J. Acoust. Soc. Am.* **102** 1289
Draeger C and Fink M 1997 *Phys. Rev. Lett.* **79** 407
Draeger C and Fink M 1999 *J. Acoust. Soc. Am.* **105** 611
Draeger C, Aime J-C and Fink M 1999 *J. Acoust. Soc. Am.* **105** 618
Dupuis M, Mazo R and Onsager L 1960 *J. Chem. Phys.* **33** 1452
Duvall T L Jr, Jeffferies S M, Harvey J M and Pomerantz M A 1993 *Nature* **362** 430
Eckhardt B and Aurell E 1989 *Europhys. Lett.* **9** 509
Eckhardt E, Dörr U, Kuhl U and Stöckmann H-J 1999 *Europhys. Lett.* **46** 134
Efetov K 1997 *Supersymmetry in Disorder and Chaos* (Cambridge: Cambridge University Press)
Ellegaard C, Guhr T Lindemann K, Lorensen H Q, Nygård J and Oxborrow M 1995 *Phys. Rev. Lett.* **75** 1546
Ellegaard C, Guhr T Lindemann K, Nygård J and Oxborrow M 1996 *Phys. Rev. Lett.* **77** 4918
Ellegaard C, Schaadt K and Bertelsen B 2001 *Phys. Scr.* T **90** 223
Ergün G and Fyodorov Y V 2003 *Phys. Rev.* E **68** 046124
Ericson T 1960 *Phys. Rev. Lett.* **5** 430
Ericson T 1963 *Ann. Phys.* **23** 390
Ewing W M and Worzel J L 1948 *Geol. Soc. Am. Mem.* **27** part 3rd 1
Ewing W M, Jardetzky W S and Press F 1957 *Elastic Waves in Layered Media* (New York: McGraw-Hill)
Eyring C F 1930 *J. Acoust. Soc. Am.* **1** 217
Ezra G S, Richter K, Tanner G and Wintgen D 1991 *J. Phys. B: At. Mol. Opt. Phys.* **24** L413
Feynman R P and Hibbs A R 1965 *Quantum Mechanics and Path Integrals* (New York: McGraw-Hill)
Fink M 1997 *Phys. Today* **50** 34
Fink M, Cassereau D, Derode A, Prada C, Roux P, Tanter M, Thomas J-L and Wu F 2000 *Rep. Prog. Phys.* **63** 1933
Fink M *et al* 2002 Imaging of complex media with acoustic and seismic waves *Topics in Applied Physics* **48** (Berlin Springer)
Flügge W 1972 *Tensor Analysis and Continuum Mechanics* (Berlin: Springer)
Fokker A D 1924 *Physica* **4** 262
Forrester P J, Snaith N C and Verbaarschot J J M 2004 *J. Phys. A: Math. Gen.* R **36** 1 (No 12: special issue: Random Matrix Theor.)
Franz W 1954 *Z. Naturf.* **9a** 705
Fyodorov Y and Sommer H-J 1995 *Z. Phys.* B **99** 123
Fjodorov Y V and Sommers H-J 1997 *J. Math. Phys.* **38** 1918
Fjodorov Y V, Savin D V and Sommers H-J 2005 *J. Phys. A: Math. Gen.* **38** 10731
Flatté S M, Dashen R, Munk W H, Watson K M and Zachariasen F 1979 *Sound Transmission Through a Fluctuating Ocean* (Cambridge: Cambridge University Press)
Fujisaka Y and Tohyama M 2003 *J. Sound Vib.* **267** 867
Gnutzmann S and Altland A 2004 *Phys. Rev. Lett.* **93** 194101
Gnutzmann S and Altland A 2005 *Phys. Rev.* E **72** 056215
Gonyi I V and Mirlin A D 2002 *Phys. Rev.* E **65** 025202R
Gol'denveizer A L 1961 *Theory of Elastic Thin Shells* (New York: Pergamon)
Gorin T, Seligman T H and Weaver R L 2006 *Phys. Rev.* A **73** 015202
Gorman D J 1978 *J. Sound Vib.* **57** 437
Gorman D J 1982 *Free Vibration Analysis of Rectangular Plates* (New York: Elsevier)
Gough D O, Leibacher J W, Scherrer P H and Toomre J 1996 *Science* **272** 1281
Grammaticos B and Voros A 1979 *Ann. Phys.* **123** 359
Gregory R D 1971 *Proc. Camb. Phil. Soc.* **70** 103
Grönqvist J and Guhr T 2005 *Phys. Rev.* E **71** 036214

Guhr T and Weidenmüller H A 1990 *Ann. Phys., NY* **199** 412
Guhr T, Müller-Groeling A and Weidenmüller H A 1998 *Phys. Rep.* **299** 189
Gutzwiller M C 1971 *J. Math. Phys.* **12** 343
Gutzwiller M C 1990 *Chaos in Classical and Quantum Mechanics* (New York: Springer)
Haake F 2001 *Quantum Signatures of Chaos* (New York: Springer)
Hamilton M F and Bladstock D T 1998 *Nonlinear Acoustics* (New York: Academic)
Hannay J H and Ozorio de Almeida A M 1984 *J. Phys. A: Math. Gen.* **17** 3420
Hegewisch K C, Cerruti N R and Tomsovic S 2005 *J. Acoust. Soc. Am.* **117** 1582
Heller E J 1984 *Phys. Rev. Lett.* **53** 1515
Heinemann M G, Larraza A and Smith K B 2002 *Appl. Phys. Lett.* **80** 694
Hennino R, Trégourès N, Shapiro N M, Margerin L, Campillo M, van Tiggelen B A and Weaver R L 2001 *Phys. Rev. Lett.* **86** 3447
Hensel J C and Dynes R C 1977 *Phys. Rev. Lett.* **39** 969
Heusler S, Müller S, Braun P and Haake F 2004 *J. Phys. A: Math. Gen.* **37** L31
Heusler S, Müller S, Altland A, Braun P and Haake F 2007 *Phys. Rev. Lett.* **98** 044103
Hlushchuk Y, Kohler A, Bauch Sz, Blümel R, Barth M and Stöckmann H-J 2000 *Phys. Rev.* E **61** 366
Hodge C H and Woodhouse J 1984 *Rep. Prog. Phys.* **49** 107
Hortikar S and Srednicki M 1998a *Phys. Rev. Lett.* **80** 1646
Hortikar S and Srednicki M 1998b *Phys. Rev.* E **57** 7313
Hudson J A 1980 *The Excitation and Propagation of Elastic Waves* (Cambridge: Cambridge University Press)
Hussein M S, Malta C P, Pato M P and Tufaile A P B 2002 *Phys. Rev.* E **65** 057203
Izbicki J L, Conoir J M and Veksler N 1998 *Wave Motion* **28** 277
Jacquod P, Silvestrov P G and Beenakker C W J 2001 *Phys. Rev.* E **64** 055203
Jalabert R A and Pastawski H M 2001 *Phys. Rev. Lett.* **86** 2490
Joyce W B 1975 *J. Acoust. Soc. Am.* **58** 643
Kadanoff L and Tang C 1984 *Proc. Natl. Acad. Sci. USA* **81** 1276
Kaplan L 1999 *Nonlinearity* **12** R1
Kawakami K and Yamiguchi K 1986 *J. Acoust. Soc. Am.* **80** 543
Keane A J and Price W G 1994 *Statistical Energy Analysis* (Cambridge: Cambridge University Press)
Keller J B and Karal F C Jr 1960 *J. Appl. Phys.* **31** 1039
Keller J B 1962 *J. Opt. Soc. Am.* **52** 116
Keller J B and Karal F C Jr 1964 *J. Acoust. Soc. Am.* **36** 32
Kinsler L E, Frey A E and Coppens A B Sanders J V 1999 *Fundamentals of Acoustics* 4th edn (New York: Wiley)
Kohler A, Killesreiter G H M and Blümel R 1997 *Phys. Rev.* E **56** 2691
Kohler A and Blümel R 1998a *Phys. Lett.* **247** 87
Kohler A and Blümel R 1998b *Ann. Phys.* **267** 249
Kohler A and Blümel R 1999 *Phys. Rev.* E **59** 7228
Kottos T and Smilansky U 1997 *Phys. Rev. Lett.* **79** 4794
Kottos T and Smilansky U 1999 *Ann. Phys.* **274** 76
Krein M 1953 *Mat. Sb.* **33** 597 (For a more recent discussion see also Faulkner J S 1977 *J. Phys. C: Solid State Phys.* **10** 4661)
Kuperman W A and Jackson D R 2002 Imaging of complex media with acoustic and seismic waves *Topics in Applied Physics* vol 48 (Berlin: Springer) p 43
Kuhl U, Stöckmann H J and Weaver R 2005 *J. Phys. A: Math. Gen.* **38** 10433
Kuttruff H 1970 *Acoustica* **23** 238
Kuttruff H 1971 *Acoustica* **24** 356
Lai Y-C, Blümel R, Ott E and Grebogi C 1992 *Phys. Rev. Lett.* **68** 3491
Landau L D and Lifshitz E M 1959 *Theory of Elasticity* (Oxford: Pergamon)
Langley R S 1990 *J. Sound Vib.* **141** 207
Langley R S 1999 *Proc. R. Soc.* A **455** 3325–49
Langley R S and Bremner P 1999 *J. Acoust. Soc. Am.* **105** 1657
Langley R S and Brown A W M 2004a *J. Sound Vib.* **275** 823
Langley R S and Brown A W M 2004b *J. Sound Vib.* **275** 847
Langley R S and Cotoni V 2004 *J. Acoust. Soc. Am.* **115** 706
Langley R S and Cotoni V 2005 *J. Acoust. Soc. Am.* **118** 3064
Larose E, Margerin L, van Tiggelen B A and Campillo M 2004 *Phys. Rev. Lett.* **93** 048501
Larose E, Lobkis O I and Weaver R L 2006 *Europhys. Lett.* **76** 422

Larose E, Margerin L, Derode A, van Tiggelen B A, Campillo M, Shapiro N, Paul A, Stehly L and Tanter M 2006 *Geophysics* **71** SI11–SI21
Lauterborn W and Cramer E 1981 *Phys. Rev. Lett.* **47** 1445
Lauterborn W and Holzfuss J 1991 *Int. J. Bifurcation* **1** 13
Lee H W 1995 *Phys. Rep.* **259** 147
Legrand O and Sornette D 1990 *J. Acoust. Soc. Am.* **88** 865
Legrand O, Schmitt C and Sornette D 1992 *Europhys. Lett.* **18** 101
Legrand O, Mortessagne F and Sornette D 1995 *J. Phys.* I **5** 1003
Leitner D M 1997 *Phys. Rev.* E **56** 4890
Lewenkopf C H and Weidenmüller H A 1991 *Ann. Phys.* **212** 53
Lobkis O I and Weaver R L 2000 *J. Acoust. Soc. Am.* **108** 1480
Lobkis O I, Weaver R L and Rozhkov I 2000 *J. Sound Vib.* **237** 281
Lobkis O I and Weaver R L 2001a *J. Acoust. Soc. Am.* **109** 2636
Lobkis O I and Weaver R L 2001b *J. Acoust. Soc. Am.* **110** 3011
Lobkis O I and Weaver R L 2003 *Phys. Rev. Lett.* **90** 254302
Lobkis O I, Rozhkov I S and Weaver R L 2003 *Phys. Rev. Lett.* **91** 194101
Lotfi K 1995 *PhD thesis* Université Paris-Sud
Love A E H 1944 *A Treatise on the Mathematical Theory of Elasticity* (New York: Dover)
Lyon R H 1969 *J. Acoust. Soc. Am.* **45** 545
Lyon R H and DeJong R G 1995 *Theory and Application of Statistical Energy Analysis* 2nd edn (Boston, MA: Butterworth-Heinemann)
MacDonald B E and Kuperman W A 1987 *J. Acoust. Soc. Am.* **81** 1406
Mace B and Shorter P J 2000 *J. Sound Vib.* **233** 369–89
Mace B 2003 *J. Sound Vib.* **264** 391
Mace B 2005 *J. Sound Vib.* **279** 141
Malcolm A E, Scales J A and van Tiggelen B A 2004 *Phys. Rev.* E **70** 015601(R)
Marchetti F M, Smolyarenko I E and Simons B D 2003 *Phys. Rev.* E **68** 036217
Margerin L, Campillo M and van Tiggelen B A 2001 *Geophys J. Int.* **145** 593
Mazur M A and Gilbert K E 1997 *J. Acoust. Soc. Am.* **101** 174 and 184
McDonald S W and Kaufman A K 1979 *Phys. Rev. Lett.* **42** 1189
McDonald S W and Kaufman A K 1988 *Phys. Rev.* A **37** 3067
Mehta M L 1991 *Random Matrices* 2nd edn (New York: Academic)
Miklowitz J 1978 *Elastic Waves and Waveguides* (Amsterdam: North Holland)
Morse P M and Bolt R H 1944 *Rev. Mod. Phys.* **16** 69
Mortessagne F, Legrand O and Sornette D 1992 *Europhys. Lett.* **20** 287
Mortessagne F, Legrand O and Sornette D 1993 *J. Acoust. Soc. Am.* **94** 154
Müller S, Heusler S, Braun P, Haake F and Altland A 2004 *Phys. Rev. Lett.* **93** 014103
Müller S, Heusler S, Braun P, Haake F and Altland A 2005 *Phys. Rev.* E **72** 046207
Musgrave M J P 1970 *Crystal Acoustics* (San Fransisco: Holden-Day)
Neicu T, Schaadt K and Kudrolli A 2001 *Phys. Rev.* E **63** 026206
Neicu T and Kudrolli A 2002 *Europhys. Lett.* **57** 341
Nöckel J U and Stone A D 1997 *Nature* **385** 6611
Norris A N and Rebinsky D A 1994 *J. Vib. Acoust.* **116** 457
Northrop G A and Wolfe J P 1979 *Phys. Rev. Lett.* **43** 1424
Oertner R N, Ott E, Antonsen T M Jr and So P 1996 *Phys. Lett.* A **216** 59
Ozorio de Almeida A M and Hannay J H 1983 *Ann. Phys.* **145** 100
Pance K, Lu W and Sridhar S 2000 *Phys. Rev. Lett.* **85** 2737
Pao Y H and Mow C C 1971 *Diffraction of Elastic Waves and Dynamic Stress Concentrations* (New York: Rand Corporation)
Peres A 1984 *Phys. Rev.* A **30** 1610
Pierce A D 1991 NCA-vol 12/AMD-vol 128, Structural Acoustics, ASME 195
Popovski K, Wysocki B J and Wysocki T A 2007 EURASIP article ID: 71610
Porter C E and Thomas R G 1956 *Phys. Rev.* **104** 483
Porter C E 1965 *Statistical Theory of Spectra: Fluctuations* (New York: Academic)
Prange R E, Ott E, Antonsen T M Jr, Georgeot B and Blümel R 1996 *Phys. Rev.* E **53** 207
Prigodin V N, Altshuler B L, Efetov K B and Iida S 1994 *Phys. Rev. Lett.* **72** 546
Prosen T 1994 *J. Phys. A: Math. Gen.* **27** L709
Prosen T 1995 *J. Phys. A: Math. Gen.* **28** 4133

Prosen T 1996 *Physica* D **91** 244
Prosen T and Znidaric M 2002 *J. Phys. A: Math. Gen.* **35** 1455
Prosen T, Seligman T H and Znidaric M 2003 *Prog. Theor. Phys. Suppl.* **150** 200
Rayleigh Lord 1890 *Lond. Edinburgh Dublin Phil. Mag. J. Sci.* **29** (fifth series) pp 1–17
Reed M and Simon B 1972a *Methods of Modern Mathematical Physics* vol 1 (New York: Academic) chapter 6
Reed M and Simon B 1972b *Methods of Modern Mathematical Physics* vol 4 (New York: Academic) chapter 13
Ribay G, de Rosny J and Fink M 2005 *J. Acoust. Soc. Am.* **117** 2866
Richens P J and Berry M V 1981 *Physica* D **1** 495
Ricket J and Claerbout J 1999 *The Leading Edge* **18** 957
Robbins J M 1991 *Nonlinearity* **4** 343
Rossing T D 1984 *Acoustics of Bells* (Princeton, NJ: Van Nostrand Reinhold)
Rouvinez C and Smilansky U 1995 *J. Phys. A: Math. Gen.* **28** 77
Roux P and Fink M 2000 *J. Acoust. Soc. Am.* **107** 2418
Roux P and Fink M 2003 *J. Acoust. Soc. Am.* **113** 1406
Roux P, Kupermann W A and Group the NPAL 2004 *J. Acoust. Soc. Am.* **116** 1995
Roux P and Kupermann W A 2005 *J. Acoust. Soc. Am.* **117** 131
Roux P, Sabra K G, Kupermann W A and Roux A 2005 *J. Acoust. Soc. Am.* **117** 79
Rozhkov I, Fyodorov Y V and Weaver R L 2003 *Phys. Rev.* E **68** 016204
Rozhkov I, Fyodorov Y V and Weaver R L 2004 *Phys. Rev.* E **69** 036206
Rulf B 1969 *J. Acoust. Soc. Am.* **45** 493
Sabine W C 1922 *Collected Papers on Acoustics* (Cambridge, MA: Harvard University Press)
Sabine W C 1964 *Collected Papers on Acoustics* (New York: Dover) (reprinted)
Sabra K G, Roux P and Kupermann W A 2005 *J. Acoust. Soc. Am.* **117** 164
Safarov Y and Vasil'ev D G 1992 *Spectral Theory of Operators (American Mathematical Society Translations* vol 150) ed S Gindikin (Princeton, NJ: American Mathematical Society)
Sakai K, Yamamoto K and Takagi K 1997 *Phys. Rev.* B **56** 10930
Savytskyy N, Kohler A, Bauch Sz, Blümel R and Sirko L 2000 *Phys. Rev.* E **64** 036211
Schaadt K and Kudrolli A 1999 *Phys. Rev.* E **60** R3479
Schaadt K 2001 Experiments on acoustic chaology and statistical elastodynamics *PhD Thesis* Copenhagen University, http://www.nbi.dk/schaadt/publications.html
Schaadt K, Simon G and Ellegaard C 2001 *Phys. Scr.* **T90** 231
Schaadt K, Tufaile A P B and Ellegaard C 2003a *Phys. Rev.* E **67** 026213
Schaadt K, Guhr T, Ellegaard C and Oxborrow M 2003b *Phys. Rev.* E **68** 036205
Schäfer R, Stöckmann H-J, Gorin T and Seligman T H 2005 *Phys. Rev. Lett.* **95** 184102
Schäfer R, Kuhl U, Barth M and Stöckmann H-J 2001 *Found. Phys.* **31** 475
Schanze H, Alves E R P, Lewenkopf C H and Stöckmann H-J 2001 *Phys. Rev.* E **64** 065201(R)
Schomerus H and Sieber M 1997 *J. Phys. A: Math. Gen.* **30** 4537
Schomerus H, van Bemmel K J H and Beenakker C W J 2000 *Eur. Phys. Lett.* **52** 518
Schomerus H, van Bemmel K J H and Beenakker C W J 2001 *Phys. Rev.* E **63** 026605
Schröder M R 1954a *Acustica* **4** 594 (1987 *J. Audio Eng. Soc.* **35** 299 (reprinted in English))
Schröder M R 1954b *Acustica* **4** 456 (1987 *J. Audio Eng. Soc.* **35** 307 (reprinted in English))
Schröder M R 1959 *J. Acoust. Soc. Am.* **31** 1407
Schröder M R 1962 *J. Acoust. Soc. Am.* **34** 1819
Schröder M R 1965 *Proc. 5th Int. Congress on Acoustics* Liege G31 1
Schulman L S 1981 *Techniques and Application of Path Integration* (New York: Wiley) chapter 20
Schuster K and Waetzmann E 1929 *Ann. Phys. Lpz.* 1
Schwab K, Henriksen E A, Worlock J M and Roukes M L 2000 *Nature* **404** 974
Sebbah P 2001 *Waves and Imaging through Complex Media* (Dordrecht: Kluwer)
Sepúlveda M-A, Tomsovic S and Heller E J 1992 *Phys. Rev. Lett.* **69** 402
Shapiro N M and Campillo M 2004 *Geophys. Res. Lett.* **31** L07614
Shapiro N M, Campillo M, Stehly L and Ritzwoller M H 2005 *Science* **307** 1615
Shnirelman A I 1974 *Usp. Mat. Nauk.* **29** 181
Shorter P J and Langley R S 2005 *J. Sound Vib.* **288** 669–99
Sieber M 2002 *J. Phys. A: Math. Gen.* **35** L613
Sieber M and Richter K 2001 *Phys. Scr.* T **90** 128
Sieber M and Steiner F 1990 *Phys. Lett.* A **144** 159
Sieber M, Smilansky U, Creagh S C and Littlejohn R G 1993 *J. Phys. A: Math. Gen.* **26** 6217
Sieber M, Primack H, Smilansky U, Ussishkin I and Schanz H 1995 *J. Phys. A: Math. Gen.* **28** 5041

Simons B D and Altshuler B L 1993 *Phys. Rev.* B **48** 5422
Sirko L, Koch P M and Blümel R 1997 *Phys. Rev. Lett.* **78** 2940
Skipetrov S E and van Tiggelen B A 2006 *Phys. Rev. Lett.* **96** 043902
Smilansky U 1994 *Les-Houches Summer School on Mesoscopic Quantum Physics* ed E Akkermans *et al* (Amsterdam: North-Holland) 373
Smilansky U and Ussishkin I 1996 *J. Phys. A: Math. Gen.* **29** 2587
Smirnov I P, Virovlyansky A L and Zaslavsky G M 2001 *Phys. Rev.* E **64** 036221
Smirnov I P, Virovlyansky A L, Edelman M and Zaslavsky G M 2005 *Phys. Rev.* E **72** 026206
Smith F T 1960 *Phys. Rev.* **118** 349
Smith K B, Brown M G and Tappert F D 1992 *J. Acoust. Soc. Am.* **91** 1939, 1950
Snieder R K and Scales J A 1998 *Phys. Rev.* A **58** 5668
Snieder R, Gret A, Douma H and Scales J 2002 *Science* **295** 2253
Snieder R 2004 *Phys. Rev.* E **69** 046610
Soize C 1993 *J. Acoust. Soc. Am.* **94** 849–65
Soize C 2003 *J. Sound Vib.* **263** 893
Soize C 2005 *Comput. Methods Appl. Mech. Eng.* **194** 1333
Søndergaard N 2001 Wave chaos in elastodynamic scattering *Thesis* Northwestern University, www.nbi.dk/~nsonderg
Søndergaard N and Tanner G 2002 *Phys. Rev.* E **66** 066211
Søndergaard N, Guhr T, Oxborrow M, Schaadt K and Ellegaard C 2004 *Phys. Rev.* E **70** 036206
Søndergaard N 2007 *J. Phys. A: Math. Theor.* **40** 5067
Stewartson K and Waechter R T 1971 *Proc. Camb. Phil. Soc.* **69** 353
Stoffregen U, Stein J, Stöckmann H J, Kuś M and Haake F 1995 *Phys. Rev. Lett.* **74** 2666
Stöckmann H J 1999 *Quantum Chaos: An Introduction* (Cambridge: Cambridge University Press)
Strohmer T, Emami M, Hansen J, Paparicolaou G and Paulraj A J 2004 Application of time-reversal with MMSE equalizer to UWB communications *Proc. Global Telecommunications Conference 2004 (GLOBECOM04)* (Piscalaway, NJ: IEEE) vol 5 pp 3123–7
Sunaram B and Zaslavsky G M 1999 *Chaos* **9** 483
Sutin A M, TenCate J A and Johnson P A 2004 *J. Acoust. Soc. Am.* **116** 2779
Szafer A and Altshuler B L 1993 *Phys. Rev. Lett.* **70** 587
Takahashi K and Saito N 1985 *Phys. Rev. Lett.* **55** 645
Takami T and Hasegawa H 1992 *Phys. Rev. Lett.* **68** 419
Tanner G, Scherer P, Bogomolny E B, Eckhardt B and Wintgen D 1991 *Phys. Rev. Lett.* **67** 2410
Tanner G and Wintgen D 1995 *Phys. Rev. Lett.* **75** 2928
Tanner G, Hansen K and Main J 1996 *Nonlinearity* **9** 1641
Tanner G 1997 *J. Phys. A: Math. Gen.* **30** 2863
Tanner G, Richter K and Rost J M 2000 *Rev. Mod. Phys.* **72** 497
Tanner G 2001 *J. Phys. A: Math. Gen.* **34** 8485
Tanner G and Søndergaard N 2007 *Phys. Rev.* E **75** 036607
Tappert F D and Brown M G 1996 *J. Acoust. Soc. Am.* **99** 1405
Teitsworth S W 2000 *Proc. 16th Sitges Conf. on Stat. Mech.* ed D Reguerra, G Platero and L L Bonilla (Berlin: Springer) 62
Temkin S 1981 *Elements of Acoustics* (New York: Wiley)
Titchmarsh E C 1986 *The Theory of the Riemann Zeta Function* (Oxford: Clarendon)
Titov M and Beenakker C W J 2000 *Phys. Rev. Lett.* **85** 3388
Tomsovic S and Heller E J 1993 *Phys. Rev.* E **47** 282
Tourin A, Derode A, Roux P, vann Tiggelen B A and Fink M 1997 *Phys. Rev. Lett.* **79** 3637
Tourin A, Van Der Biest F and Fink M 2006 *Phys. Rev. Lett.* **96** 104301
Tsang L and Ishimaru A 1984 *J. Opt. Soc. Am.* **1** 836
Tulino A M and Verdú S 2004 Random matrix theory and wireless communication *Found. Trends Commun. Inf. Theor.* **1** 1 http://www.nowpublishers.com/cit/
Tworzydlo J and Beenakker C W J 2000 *Phys. Rev. Lett.* **85** 674
Urbina J D and Richter K 2003 *J. Phys. A: Math. Gen.* **36** L495
Urbina J D and Richter K 2004 *Phys. Rev.* E **70** 015201(R)
Urbina J D and Richter K 2006 *Phys. Rev. Lett* **97** 214101
Vaa C, Koch P M and Blümel R 2003 *Phys. Rev. Lett.* **90** 194102
Van Albada M P and Lagendijk A 1985 *Phys. Rev. Lett.* **55** 2692
van Tiggelen B A 2003 *Phys. Rev. Lett.* **91** 243904

van Tiggelen B A, Margerin L and Campillo M 2001 *J. Acoust. Soc. Am.* **110** 1291
Vasil'ev D G 1987 *Trans. Moscov Math. Soc.* **49** 173
Vattay G, Wirzba A and Rosenqvist P E 1994 *Phys. Rev. Lett.* **73** 2304
Verbaarschot J M, Weidenmüller H A and Zirnbauer M R 1985 *Phys. Rep.* **129** 367
Viktorov I A 1967 *Rayleigh and Lamb Waves* (New York: Plenum)
Virovlyansky A L and Zaslavsky G M 1999 *Phys. Rev.* E **59** 1656
Virovlyansky A L 2000 *J. Acoust. Soc. Am.* **108** 84
von Oppen F 1994 *Phys. Rev. Lett.* **73** 798
von Oppen F 1995 *Phys. Rev.* E **51** 2647
Wang C Y, Saez A and Achenbach J D 1995 3d elastodynamic Green's functions for BEM applications to anisotropic solids *IUTAM Symposium on Anisotropy, Inhomogeneity and Nonlinearity in Solid Mechanics* ed D F Parker and A H England 307
Weaver R L 1982 *J. Acoust. Soc. Am.* **71** 1608
Weaver R L 1989a *J. Acoust. Soc. Am.* **85** 1005
Weaver R L 1989b *J. Sound Vib.* **130** 487
Weaver R L and Burkhardt J L 1994 *J. Acoust. Soc. Am.* **96** 3186
Weaver R L and Burkhardt J L 2000 *Chaos Solitons Fractals* **11** 1611
Weaver R L and Lobkis O I 2000a *Phys. Rev. Lett.* **84** 4942
Weaver R L and Lobkis O I 2000b *J. Sound Vib.* **231** 1111
Weaver R L and Lobkis O I 2001 *Phys. Rev. Lett.* **87** 134301
Weaver R L and Lobkis O I 2002 *Ultrasonics* **40** 435
Weaver R L and Lobkis O I 2003 *J. Acoust. Soc.* **113** 2611
Weaver R L 2001 *Waves and Imaging through Complex Media* ed P Sebbah (Dordrecht: Kluwer) p 141
Weaver R L and Lobkis O I 2004 *J. Acoust. Soc. Am.* **116** 2731
Weaver R L and Lobkis O I 2005a *J. Acoust. Soc. Am.* **117** 3432
Weaver R L and Lobkis O I 2005b *J. Acoust. Soc. Am.* **118** 3447
Weyl H 1912 *Mathematische Annalen* **71** 441 (1968 *Gesammelte Abhandlungen* (Berlin: Springer) (reprinted in English))
Wheeler C T 2005 *J. Phys. A: Math. Gen.* **38** 1491
Whelan N D 1996 *Phys. Rev. Lett.* **76** 2605
Wichard R and Dietsche W 1992 *Phys. Rev.* B **45** 9705
Wigner E P 1955 *Phys. Rev.* **98** 145
Wirzba A 1992 *Chaos Solitons Fractals* **2** 77
Wirzba A and Rosenqvist P E 1996 *Phys. Rev.* A **54** 2745
Wirzba A 1999 *Phys. Rep.* **309** 1
Wirzba A, Søndergaard N and Cvitanović P 2005 *Europhys. Lett.* **72** 534
Wishart J 1928 *Biometrica* A **20** 32
Wolf P-E and Maret G 1985 *Phys. Rev. Lett.* **55** 2696
Wolfson M A and Tomsovic S 2001 *J. Acoust. Soc. Am.* **109** 2693
Worcester P F *et al* 1999 *J. Acoust. Soc. Am.* **105** 3185
Zakrzewski J and Delande D 1993 *Phys. Rev.* E **47** 1650
Zelditch S 1987 *Duke Math. J.* **55** 919